Active Structural Acoustic Control of Aircraft Interior Flow Noise Via the Use of Active Trim Panels

by

Brian W. Mahnken

Thesis Submitted to the Faculty of Virginia Polytechnic Institute and State University in Partial Fulfillment of the Requirements for the Degree of

Master of Science

in Mechanical Engineering

APPROVED:

Dr. C.R. Fuller, Chair

Dr. H.H. Cudney

Dr. R.A. Burdisso

February 1996

Blacksburg, Virginia

Keywords: ASAC, Aircraft, Noise, Control, Active, Panel

LD
5655
V855
1996
M346
c.2

Active Structural Acoustic Control of Aircraft Interior Flow Noise Via the Use of Active Trim Panels

By

Brian W. Mahnken

Committee Chair: Chris R. Fuller

Abstract

Modern jet aircraft interior noise can be categorized into two main types: tonal noise caused by engine imbalance or blade passage, and mid frequency broadband noise resulting from turbulent flow. This project addresses aircraft interior flow noise caused by a flow separation over the crown of the aircraft. The noise control approach is to mount piezoelectric actuators to the aircraft interior cockpit crown trim panel and use them to actively control aircraft interior noise with feed-forward adaptive LMS control algorithms. The experiments were performed on a Cessna Citation III fuselage with the production crown interior trim panel in place. Flow noise was simulated by three speakers mounted above the crown of the aircraft producing random noise with a frequency range of 500-

1000 Hz. Several piezoelectric (PZT) actuators were mounted on the interior crown trim panel as control outputs. Sixteen microphones served as error/global attenuation sensors. Microphones and PZTs were selected from off-line optimizations. The control reference signal was obtained from either an accelerometer mounted on the skin of the aircraft or from the signal generator itself. Control was executed on a personal computer digital signal processing. Single frequency control experiments were performed to judge the feasibility of control. The main broadband tests were performed with a variety of controller configurations. The results using the active panel are compared with more traditional acoustic control utilizing speakers as control actuators instead of PZT's. The project concludes that a 2 dB reduction over the frequency range is obtainable at the pilot's ears in a 2I2O configuration with an accelerometer reference signal. Acausality and slow controller speeds were found to be the main causes which limit further reduction.

Acknowledgments

In order for me to reach this point of presenting my thesis, there are many people that deserve to be thanked. Topping the list are my parents. I would like to thank them for providing me with a proper start in life, and supporting my undergraduate and graduate careers.

I would also like to thank all my undergraduate professors at Michigan Tech for taking the time to teach me well, giving me my Mechanical Engineering undergraduate basis. Of these professors, I would particularly like to thank Mohan Rao and Harold Evenson who initially sparked my interest in Vibrations and Acoustics.

Additionally, thanks are in order for Chris Fuller for selecting me as a graduate student and supporting me as an advisor. I'd like to thank Cessna Aircraft Corporation and NASA-Langley for providing the research grants which have supported me.

Also, I would like to thank everyone else who has helped me here on my project and elsewhere. Including Jamie Carneal, Jerome Smith, and Mari Willcockson for help with editing of this thesis, and Richard Wright for his help with experiments during the summer that he worked in the Cessna Lab.

Table of Contents

List of Figures.....viii

List of Tables.....xii

List of Symbols.....xiv

1. Introduction 1

1.1 Current Active Noise Reduction Technology 2

1.2 Applications 5

1.3 Problem Statement 9

1.4 Thesis Outline 12

2. Experimental Design and System Identification 15

2.1 Fuselage and Trim Panels 15

2.2 Data Acquisition..... 18

2.3 Microphones and Actuators..... 19

2.4 The Disturbance 22

2.5 Control Reference Signal and Controller Format..... 24

3. Single Frequency Experiments 29

3.1 System Identification 29

3.2 Initial Single Frequency Tests 33

3.2.1 Controller Comparison 40

3.2.2 System Analysis and Modifications 43

3.3 Optimized Single Frequency Tests 48

3.3.1 Error Microphone Optimization 51

3.3.2 Global Microphone Optimization 58

3.3.3 Actuator Grouping Optimization 63

3.4 Speaker Comparison Tests 68

4. Broadband Control Experiments 74

4.1 Introduction to Broadband Experiments 74

4.2 SISO Controller Parametric Studies 78

4.3 Causality Analysis 90

4.4 SISO Experiments 94

4.4.1 SISO Tests With Internal Delayed Reference Signal 94

4.4.2 SISO with External Reference Accelerometer 101

4.5 Two Input-Two Output Broadband Tests 104

4.5.1 2I2O Tests With Varying Microphone Positions 104

4.5.2 2I2O Tests With Varying Actuators 105

4.5.3 2I2O Tests With Off-Line Optimization 109

4.5.4 Reduction Zone Mapping 110

4.6 Three Input-Three Output Broadband Tests 118

5. Discussion of Results 121

6. Conclusions and Recommendations 126

Appendix: Comparison of Removable and Permanent PZT Actuators 130

References 135

Vita 140

List of Figures

Figure 1-1, Turbulence Over the Crown of the Aircraft 10

Figure 1-2, Cessna Flight Test, Cockpit Located Microphone 10

Figure 1-3, Cessna Flight Test, Rear Cabin Located Microphone 11

Figure 2-1, View of the Front of the Aircraft from Top Indicating Crown Trim Panel Mounting Location 17

Figure 2-2, Trim Panel Composite Sectional View 18

Figure 2-3, Microphone Locations 19

Figure 2-4, Impact Hammer Average Response 21

Figure 2-5, PZT Location and Numbering 22

Figure 2-6, Diagram Indicating Position of Reference Accelerometer and Disturbance Speakers 23

Figure 2-7, Typical Filtered-X LMS Control Algorithm 25

Figure 2-8, MIMO Filtered-X LMS Controller Block Diagram 26

Figure 2-9, General Control Schematic 28

Figure 3-1, Cabin Spatially Averaged FRF, Shaker Excitation 30

Figure 3-2, Cabin Spatially Averaged FRF, Speaker Excitation 31

Figure 3-3, Cockpit Spatially Averaged Sum FRF 32

Figure 3-4, 4I4O Control Schematic 35

Figure 3-5, Single Frequency Experimental Setup 36

Figure 3-6, Control to Spillover Ratios for Controller Comparison Tests 43

Figure 3-7, Speaker Enclosure 45

Figure 3-8, Intensity Scan Paths 46

Figure 3-9, Longitudinal and Horizontal Sum Intensity Scans, 500-1000 Hz 48

Figure 3-10, Single Frequency Control, 900 Hz, Case #2, Error Microphones 57

Figure 3-11, Single Frequency Control, 900 Hz, Case #2, Global Microphones 57

Figure 3-12, Global Non-Error Sensor Optimization, 508.75 Hz, Case #3, Error Microphones 62

Figure 3-13, Global Non-Error Sensor Optimization, 508.75 Hz, Case #3, Global Microphones 63

Figure 3-14, Control Speaker Locations 68

Figure 4-1, Controller Signal Paths 76

Figure 4-2, Number of FIR Filters SISO Parametric Study 80

Figure 4-3, Filter Number Parametric Study, FIR Filter Values for 255 Coefficients 81

Figure 4-4, Filter Number Parametric Study, FIR Filter Values for 50 Coefficients 82

Figure 4-5, Controller A/D Sampling Parametric Study 83

Figure 4-6, Sampling Rate Parametric Study, FIR Filter Coefficients for 5000 Hz Sampling Rate 84

Figure 4-7, Sampling Rate Parametric Study, FIR Filter Coefficients for 2000 Hz Sampling Rate 85

Figure 4-8, Reference Signal Parametric Tests 88

Figure 4-9, FIR Control Coefficients, Internal Reference Delayed 20 Samples 89

Figure 4-10, FIR Control Coefficients External Accelerometer Reference 90

Figure 4-11, Coherence and FRF of Roof Accelerometer Signal to Microphone #7 91

Figure 4-12, SISO Broadband Tests, Internal Ref Sig, Error Mic 3, 13.6 dB Reduction. 98

Figure 4-13, SISO Broadband Tests, Internal Ref Sig, Error Mic 7, 23.2 dB Reduction. 99

Figure 4-14, SISO Broadband Tests, Internal Ref Sig, Error Mic 8, 14.1 dB Reduction. 99

Figure 4-15, SISO Broadband Tests, Internal Ref Sig, Error Mic 14, 3.6 dB Reduction 100

Figure 4-16, SISO Broadband Tests, Internal Ref Sig, Global Mic #15 Spectrum, (Error Mic #8) 100

Figure 4-17, Reference Accelerometer Location 102

Figure 4-18, Spectrum Responses of SISO Tests with Accelerometer Reference Signal 103

Figure 4-19, Spectrum Responses of Mirophones 7 and 8 with Broadband Control with External Accelerometer Reference 108

Figure 4-20, Microphone Array 111

Figure 4-21, Contour Test #1, PZT Actuation, External Reference Signal 115

Figure 4-22, Contour Test #2, PZT Actuation, Internal Reference Signal 116

Figure 4-23, Contour Test #3, Speaker Actuation, Internal Reference Signal 117

Figure A-1, Removable PZT Actuator 131

Figure A-2, Permanent and Removable Comparison PZT Locations 132

List of Tables

Table 3-1, Series I 4I4O Initial Single Frequency Test 38

Table 3-2, Series II 6I4O Initial Single Frequency Tests 40

Table 3-3, Controller Comparison Test Results 42

Table 3-4, Single Frequency Off-Line Error Sensor Optimization 52

Table 3-5, Single Frequency Error Sensor Reduction Optimization, 508.75 Hz. 53

Table 3-6, Single Frequency Error Sensor Reduction Optimization, 710 Hz. 53

Table 3-7, Single Frequency Error Sensor Reduction Optimization, 900 Hz. 54

Table 3-8, Single Frequency, Off-Line, Global Non-Error Sensor Optimization 59

Table 3-9, Single Frequency Global Non-Error Sensor Reduction Experiment Results, 508.75 Hz. 60

Table 3-10, Single Frequency Gloabl Non-Error Sensor Reduction Experiment Results, 900 Hz. 61

Table 3-11, Single Frequency Actuator Grouping, 508.75 Hz 65

Table 3-12, Single Frequency Actuator Grouping, 710 Hz 65

Table 3-13, Single Frequency Actuator Grouping, 900 Hz 66

Table 3-14, Single Frequency Off-Line Speaker/Error Sensor Optimization 70

Table 3-15, Single Frequency Optimal Speaker/PZT Analysis, 508.75 Hz. 72

Table 3-16, Single Frequency Optimal Speaker/PZT Analysis, 710 Hz. 72

Table 3-17, Single Frequency Optimal Speaker/PZT Analysis, 900 Hz. 73

Table 4-18, System Causality Analysis 92

Table 4-1, SISO Broadband Tests, Delayed Reference Signal 96

Table 4-2, SISO Control Tests, External Accelerometer Reference 103

Table 4-3, 2I2O Broadband Test Results, Microphone Location Varied 105

Table 4-4, 2I2O Broadband Test Results, PZT Actuators Varied 106

Table 4-5, 2I2O Broadband Test Results, Accelerometer External Reference Signal, Error Mics 7&8 107

Table 4-6, 2I2O Broadband Optimizations With Error Microphones #7 & #8 110

Table 4-7, 2I2O Broadband Reduction Contour Zone Mapping Configurations and Control Levels 112

Table 4-8, Initial 3I3O Broadband Results 119

Table 4-9, 3I3O Broadband Optimizations 120

Table A-1, SISO Permanent Verses Removable PZT Control Comparison Tests 133

Table A-2, 2I2O Permanent Verses Removable PZT Control Comparison Tests 133

List of Symbols

$\vec{D}$	primary disturbance response
e_k	error sensor microphone
$\vec{P}$	microphone pressure response
$\vec{T}$	transfer functions of each control output to error microphone
u_k	control signal time sequence
$\vec{V}$	complex actuator voltage.
$W_{(z)}$	FIR filter coefficient
x_k	disturbance signal
y_k	output sequence
Φ	cost function

1. Introduction

It is the role of the modern engineer to introduce seen and unseen technologies into the lives of everyday people. These technologies may be as prominent as adding airbags to cars which will lead to more saved lives or as inconspicuous as creating a new manufacturing technique that will make a product more inexpensive to manufacture. Noise control technology is one type of technology that is more obscure than prominent. However, noise control can contribute to a product's higher perceived quality, lessen operator fatigue, and even reduce hearing loss. The work presented here is a step in developing active noise control technology. It works towards creating a system to actively control flow noise in the interior of a business jet with active trim panels.

1.1 Current Active Noise Reduction Technology

Active noise control has progressed greatly since its first conception with the idea of canceling noise with noise. In 1934, the early work of Paul Lueg[1], a German Physicist, outlined the basic philosophy of active noise control in ducts and free space. The overall idea is simple: create a signal (such as a sine wave) that is equal in amplitude and opposite in phase with the noise which is desired to be reduced. This signals will then combine with and cancel the offending noise. This is referred to as destructive interference.

Although the underlining theory of active noise control is simple, the practical execution of the technique is not. It has usually been much simpler and more cost effective to implement passive measures such as adding acoustic foam or creating a noise barrier to achieve the desired noise reduction than to implement active noise reduction techniques. However, there are cases where passive solutions do not always achieve the desired results. Such is the case with low frequency or lightweight applications. It is well known that the lower the frequency, the longer the acoustic wavelength is, and the thicker, stronger, or larger the passive implementation has to be. However, absorptive materials and acoustic barriers have weight, which is undesirable in certain applications such as automobiles or especially airplanes. With active noise control, the heavy and bulky

acoustic foams and barriers are replaced with lighter sensors and actuators. The premise of actively canceling noise can be a more effective solution at lower frequencies.

Nonetheless, Lueg's ideas took time to develop. In 1953 Harry Olson[2] identified the possible application of this technology to controlling noise in cars and aircrafts. Soon afterwards, in 1956, William Conover[3] performed the first practical application of active noise control by attempting to reduce transformer noise. He placed a loudspeaker near a transformer and located a microphone further out. He varied the amplitude and phase of a harmonic signal to the transformer until he was able to achieve a noise reduction of 6 dB over a large radial distance. However complete continuous cancellation was not achieved due to the angular variation in noise pattern of the transformer and the need for a continuous self adjusting system.

Other early work has been devoted to the problem of controlling noise in ducts. In these applications at low frequencies, the sound waves can be reasonably modeled as plane waves in one dimension. In France, Jessel[4] gave a theoretical approach of active absorption of noise in air ducts. Soon there after Swinebanks[5] developed a method of attenuating propagating waves in a duct by actively operated sources mounted in the walls of the duct. The technique was then successfully applied to ducted one dimensional sound fields[6,7].

Typically noise fields are much more complicated than one dimensional ducts. Such examples would be the interiors of an auditorium, automobile, or aircraft. Here the interior noise fields are quite complicated due to irregular geometry and noise reflections. In order to achieve global noise attenuation, the created anti-noise field would have to be equally complicated. In complex cases like these, active noise control often requires many acoustic control sources to achieve proper attenuation[8]. Again, this poses practical concerns because of the number of sensors and actuators required by the system.

This dilemma sparked the idea of directly attacking the noise source. Noise is often caused by a vibrating structure. For example, a musical cymbal struck with a drumstick vibrates. The vibrating structure of the cymbal causes the surrounding air molecules to move which creates sound. Therefore, if it is possible to reduce the structural vibration that causes noise then the problem of reproducing a complex noise field with multiple speakers can be avoided. Thus began the study of Active Structural Acoustic Control (ASAC)[9], first demonstrated by Fuller[10,11,12,13]. The process involves structurally controlling the vibrational response of the noise-radiating structure to reduce only the vibration modes which transmit acoustic energy. The technique of ASAC involves the implementation of "secondary" external (control) input forces to a structure vibrating under the excitement of a "primary" disturbance force input so that the noise source is reduced. This differs from traditional Active Noise Control (ANC) which allows the offending structure to vibrate and radiate noise but attempts to attack this resulting

noise field by recreating an equal and opposite anti-noise field with loudspeakers. Hansen, Snyder and Fuller[14] performed a study which compared ASAC to active noise control for a rectangular plate with harmonic disturbances and found that ASAC was more effective for reducing the radiated sound power.

Originally, the implementation of ASAC usually required large and heavy shaker force actuators. The advent of small and lightweight piezoelectric actuators provided an effective unobtrusive actuator for use with ASAC[15]. The piezoelectric (PZT) actuators can be mounted directly on the structure itself eliminating the need for bulky shakers. Another major contribution to current ASAC technology continued controller development, especially with the broadband controller.[16] Smith[17] showed that a multi-channel broadband controller could be utilized for ASAC by using a multi-channel broadband controller with PZT actuators mounted on a simply supported plate with a shaker force disturbance. The results yielded total SPL reductions ranging from 10-14 dB at points in the far-field for a disturbance bandwidth of 0-400 Hz.

1.2 Applications

With the theory and potential of active structural acoustic control developed and proven by others, it becomes obvious that such technology must be applied to real

applications. One of the major areas for application of this technology is controlling airplane interior noise.

Anyone who has ridden in a plane can probably recall the dominant low frequency drones of the engines. This is mainly due to the low blade pass frequencies of turbo-prop planes and low primary frequency imbalances of jet engines which can excite low frequency cabin acoustic modes. These low frequency noises are difficult to control with passive means, making active noise reduction techniques worth examining.

Recently, progress has been made in active noise reduction with experiments on cylinders, simulated aircraft fuselages, and actual aircraft structures. Early cylinder active noise control models showed that it was theoretically possible to obtain 20-25 dB noise reductions over a cross sectional region at typical turbo-prop blade passage frequencies and harmonics with only a few monopole control sources[18]. Additionally, Fuller *et al.*[19] have shown that a simplified analytical structural acoustic model of a propeller aircraft can achieve noise reductions of the order of 6-10 dB with globally detuned vibration absorbers at blade passage frequencies.

Other more recent cylinder experiments have accomplished significant noise reductions. Fuller and Jones[20] have shown that with a finite unstiffened aluminum cylinder representative of a simplified aircraft fuselage, noise reductions on the order of 10-20 dB

can be achieved with a single shaker actuator and an incident exterior acoustic disturbance. Similar experiments with PZT actuation on a cylinder model aircraft fuselage with an single tone external noise disturbance have been performed by Fuller and Silcox[21]. The results achieved a global interior noise attenuation of 10-15 dB with a single channel controller.

More realistic tests have also been successfully completed using more representative models than just cylinders. Silcox *et al.*[22] have performed experiments on a composite model of a commuter aircraft. Control was demonstrated for tonal excitation with a maximum of 4 actuator channels and 6 error channels. Actuation was provided by frame and skin mounted piezoceremic actuators with results of global reductions on the order of 9-12 dB.

In 1989 ASAC experiments were performed at the Douglas Aircraft Company Fuselage Acoustic Research Facility using a 50 foot (15 M) aft section of a fully furnished DC-9 Aircraft[23]. Disturbance shakers were attached to the engine pylons to simulate engine vibrations causing the fuselage to vibrate and produce noise. Control forces provided by shakers located in the aircraft interior connecting to the fuselage structure achieved global reductions on the order of 13 dB. Additionally, a broader European aircraft interior noise study showed that a noise reduction potential of about 15 to 20 dB

on the first propeller tone was possible using a multitude of cabin speakers as actuators in flight and ground tests[24].

However, many of the above mentioned experiments have inherent impracticalities. The shakers used by some of the ASAC systems are heavy and bulky and the multitude of control speakers used in the ANC experiments can hardly be described as lightweight. Weight is a key issue with aerospace technologies. Another important consideration of aircraft ASAC systems is the problem of fatiguing the fuselage. Force actuators such as shakers or PZT actuators, impart a cycling localized strain on the structure which may result in premature catastrophic failure of the aircraft fuselage.

Since most aircraft have an outer structural skin and an interior trim, a solution to these fatiguing problems is to mount the actuators directly to the interior trim. Thus no abnormal strain is imparted to the aircraft structure, yet the vibration at the walls of the acoustic volume can be modified in a way that yields noise reduction. This creates a double panel system which has been investigated by Carneal[25]. He mounted two plates in a transmission loss facility and showed that by applying control to the radiating panel transmission lose could be improved 5 dB verses applying control on the incident panel. Applying this double panel system to a real aircraft warrants serious consideration as an practical active noise reduction approach.

1.3 Problem Statement

Most interior noise in modern jet aircraft can be categorized into two types: low frequency tonal sounds resulting from engine imbalance (or blade passage), and mid frequency broadband flow noises caused by turbulent air flow towards the front of the aircraft (see Figure 1-1). This broadband flow noise is believed to be caused primarily by a flow separation over the crown of the aircraft and is most prominent in the mid frequency range. The noise source is located directly over the heads of the pilot and copilot. Two typical noise spectras obtained from Cessna Aircraft Corporation in a Citation VII flying at Mach 0.81 are shown in Figure 1-2 and Figure 1-3. A comparison of the noise spectra from the front and rear of the aircraft indicates the two types of noise mentioned above in a mid-size business jet. Cockpit flow noise can have critical negative affects in speech interference between pilot and copilot, and greatly adds to mental fatigue of the pilots. Until now no one has approached these mid frequency noise problems with any type of active solutions.

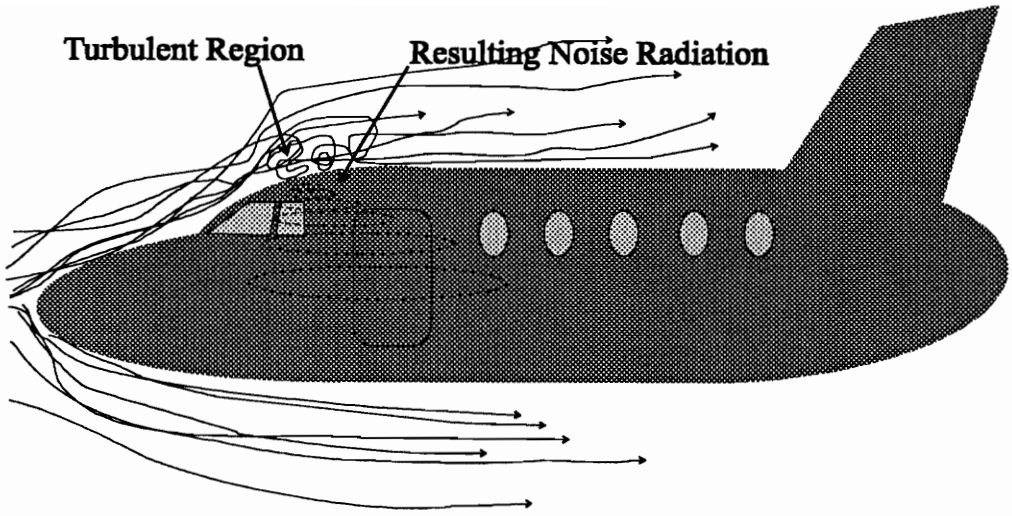

Figure 1-1, Turbulence Over the Crown of the Aircraft

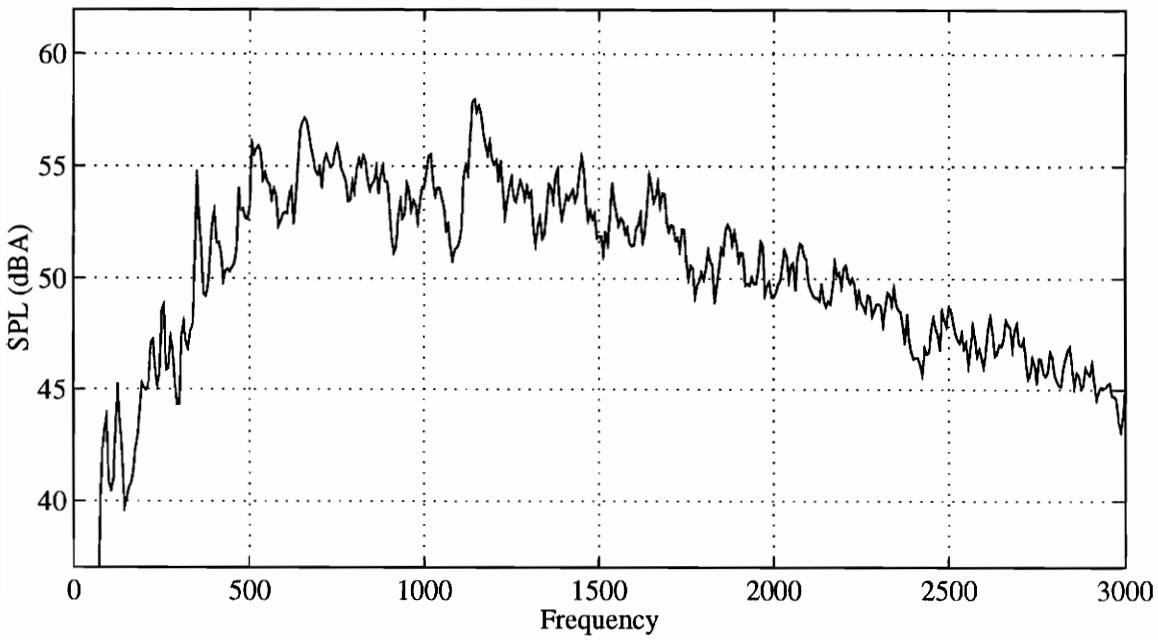

Figure 1-2, Cessna Flight Test, Cockpit Located Microphone

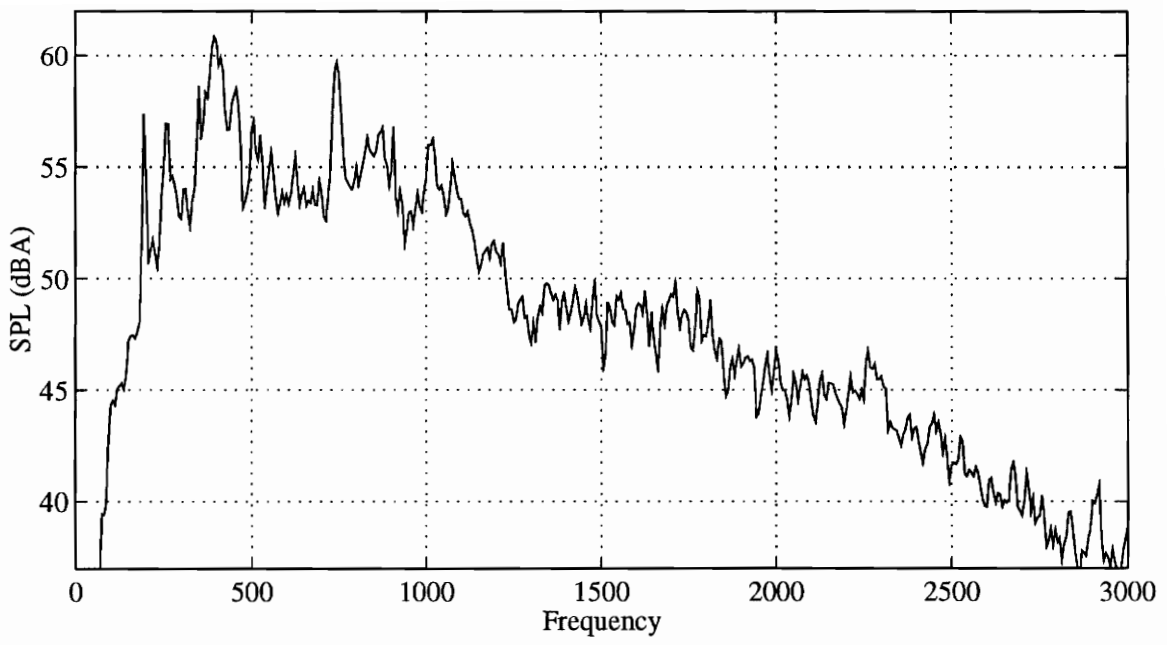

Figure 1-3, Cessna Flight Test, Rear Cabin Located Microphone

This work attempts to experimentally solve the problem of mid frequency cockpit noise on a full-size Cessna Citation III business jet fuselage located at Virginia Polytechnic Institute and State University. The approach is to actively control the vibration of the interior crown trim panel in a attempt to achieve local and global attenuation of a 500-1000 Hz disturbance signal simulating flow separation over the crown of the aircraft. Initial experiments will determine the feasibility of obtaining global interior noise reductions throughout the cockpit and cabin while later tests will focus on achieving local regions of reduction around the pilot's head.

Three speakers mounted above the crown of the aircraft will create the disturbance signal while microphone error sensors scattered throughout the fuselage will provide control input. Output from the controller will be trim panel mounted PZT actuators while the controller reference signal will either be tapped internally from the signal generator or acquired from an accelerometer located on the skin of the aircraft. Control is to be implemented with multiple input, multiple output filtered-X LMS single frequency and broadband controllers which will minimize the noise at the error sensor microphones.

1.4 Thesis Outline

This project is an experimental study into the potential of controlling mid range (500-1000 Hz) acoustic radiation with active trim panels inside an airplane using adaptive feedforward control approaches. The objective of this work is to further current ASAC technology by applying ASAC toward a common noise problem. This project attempts to answer the following questions:

- Can global interior noise reduction of broadband flow noise on a real aircraft fuselage be achieved with current technology by controlling the vibration of the interior crown panel?
- How effective would it be to use the same techniques to create strategic localized zones of noise reduction at the pilot's ears?

- What are some of the optimum controller configurations for producing the greatest noise reduction?
- What are the best ways of choosing actuator and sensor locations for a complex system such as a business jet?
- Can an effective control reference signal be acquired from the outer skin of the aircraft?
- What are the best compromises of controller speed and number of input/output channels that yields the greatest noise reduction?
- How does ASAC compare against traditional active noise control techniques for controlling mid-frequency flow noise in an aircraft?
- Can this problem be practically solved in a way that could be implemented by industry?

The rest of the thesis will be as follows: Chapter 2 begins by discussing in detail the experimental design and optimization algorithms. It describes the equipment used, the aircraft fuselage, and the experimental setup. It also explains the optimization algorithms utilized to chose the best actuators and sensors. Chapter 3 begins with system identification and controller background descriptions and then leads to a multitude of single frequency experiments. Chapter 4 then describes the broadband experiments, beginning with some parametric studies and then ending with a variety of broadband tests.

Chapter 5 discusses the final results and Chapter 6 ends with conclusions and recommendations.

2. Experimental Design and System Identification

This section of the thesis discusses the details of the experimental design. It fully describes the Cessna fuselage, the testing equipment, and explains the testing procedure. It also briefly introduces some of the fundamental system identification tests that help quantify the dynamics of the Cessna fuselage system and guide the location of some of the actuators and sensors.

2.1 Fuselage and Trim Panels

All the experiments listed in this thesis were performed at the Cessna Lab facility of the Vibration and Acoustics Laboratory of Virginia Polytechnic Institute and State

University's Mechanical Engineering Department. The facility is designed to promote the research and development of modern noise control systems for aircraft.

The heart of the facility is a Cessna Citation III business jet fuselage. The fuselage is an actual six passenger business jet fuselage which was once slated for production. For the following tests the production crown trim panel was installed in the cockpit ceiling. During the initial signal frequency tests, the interior was comprised of only the bare aluminum interior in a "green" configuration with production windows and replica doors. However, for the majority of the experiments the production interior trim, acoustic foam, and carpet were installed in the cockpit and cabin. This trim installation reduced the reverberant characteristics of the "green" interior to the damped acoustic characteristics of a real business jet. To reproduce realistic cockpit acoustic properties, two aircraft seats were placed in the cockpit and replica cockpit/cabin divider walls were constructed. It should be noted that this model of aircraft has no door sealing the cockpit from the cabin. Thus much of the flow noise originating from the cockpit reaches the cabin and hence motivated the initial investigation into the achievablity of a global noise reduction

The crown trim panel is a Cessna production part and covers the area above the pilot/copilot's head from the windshield back to the cabin/cockpit divider wall (Figure 2-1). It is constructed from sandwiching American Cyamid Prepeg Cycom on both sides of an one-eighth inch (3.1mm) thick foam core layer of American Klegecell (Figure 2-2). The

composite panel is 'D' shaped; and is cupped to follow the interior contour of the crown of the aircraft. Mounting is accomplished with 15 screws along the front and side edges. The back edge of the panel was acoustically sealed with tape and putty since the bordering panel was not initially in place.

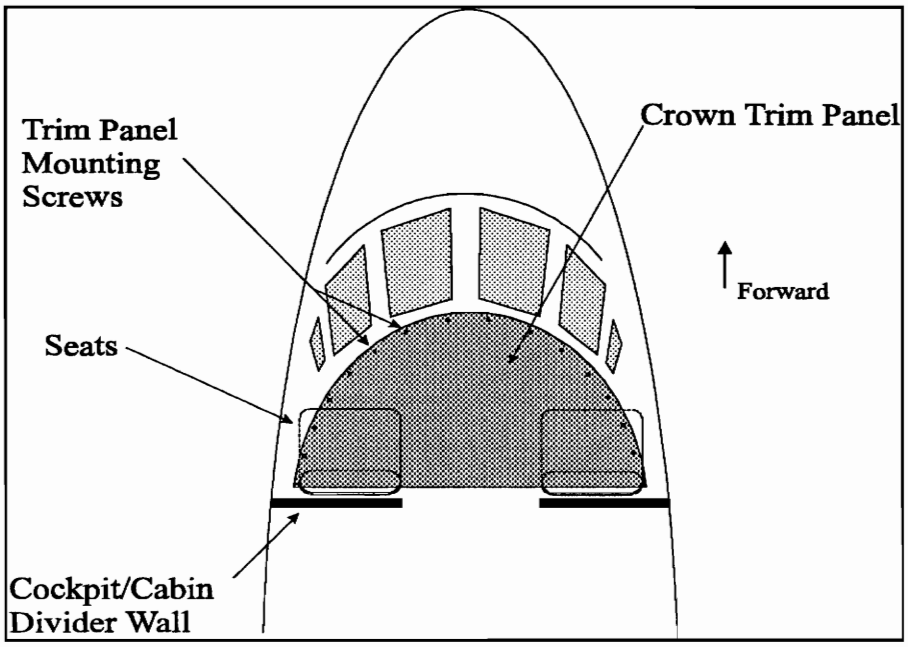

Figure 2-1, View of the Front of the Aircraft from Top Indicating Crown Trim Panel Mounting Location

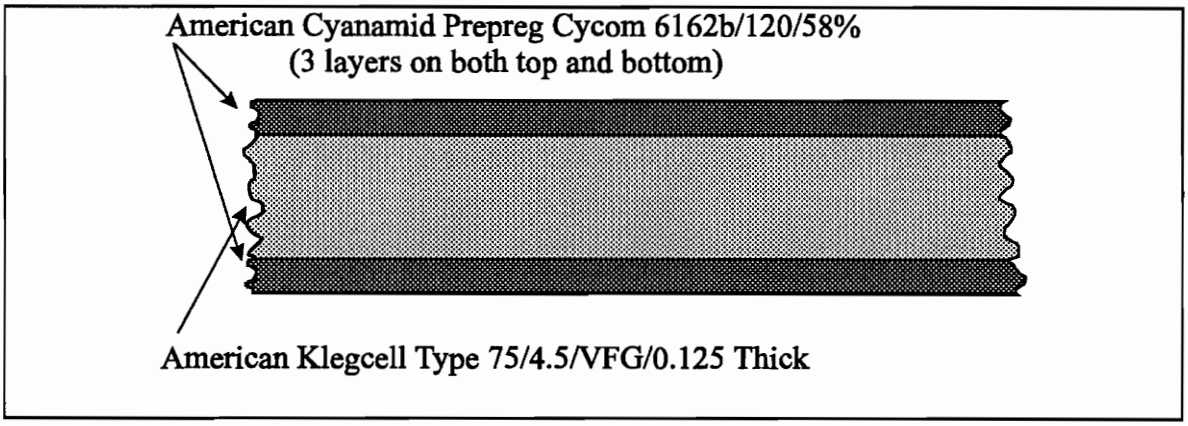

Figure 2-2, Trim Panel Composite Sectional View

2.2 Data Acquisition

The noise measurements presented in this work were acquired with a Macintosh based Zonic WCA 16 channel analyzer. The Zonic analyzer makes it possible to take 16 channels of data simultaneously, providing the ability to measure error and global microphones at the same time. The data acquisition programs were written in the base Zonic Zeta language to semi-automate the process. These Zeta programs allow for the autoranging of the analyzer, acquiring of 16 channels of data, and saving of the data to hard drive with the press of one button. For all test cases, data was taken before and after control and the spectrums were saved for further analysis.

2.3 Microphones and Actuators

The microphones utilized for the following experiments were two sets of sixteen channels PCB Acousticel microphones. Sixteen microphones were scattered throughout the fuselage in strategic locations to serve as error and global non-error sensors (Figure 2-3). The other sixteen microphones were aligned and mounted in a row for measuring the zones of reduction around the error microphones. Error microphone signals are used for control while global microphones are not. The global microphones are used to help judge if a global noise reduction is being achieved away from the error microphones. Two of the 16 error/global microphones were located at the pilot's left and right ear (microphone #7 and #8). All microphones were calibrated using a B&K pistonphone calibrator prior to testing and the calibration factor was entered into the analyzer so that proper calibrated noise levels would be outputted.

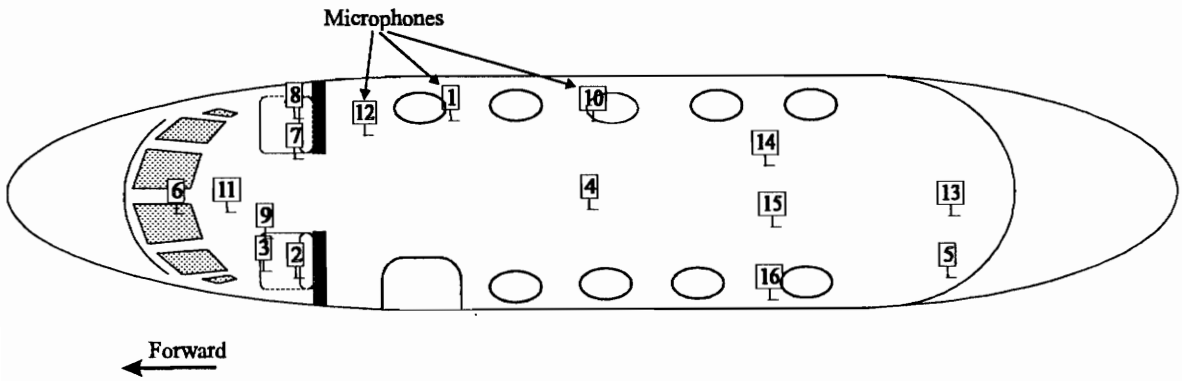

Figure 2-3, Microphone Locations

The actuators used for all these ASAC experiments were G1195 piezoelectric patches of dimensions 3.81 cm x 6.35 cm x 0.254 mm. Fifteen of these actuators were mounted on the crown trim panel in a removable mounting format. Removable PZT's are created by permanently gluing a PZT to a thin aluminum shim which is in turn mounted to the desired structure with accelerometer wax. McCray and Cudney[26] have proven the validity of the removable PZT's on a clamped-free beam. Their tests showed only an average of 6 dB (G's/Volt) loss of authority on modes 2-6 at resonance. Validation of the removable PZT's on the crown panel of the Cessna were performed using SISO and 2I2O broadband control cases (see Appendix). These tests were performed with three pairs of permanent and removable PZT's mounted next to each other on the crown trim panel. The tests indicate that similar noise reductions were obtained with either the removable or permanent PZT actuation.

Fifteen PZT actuators were mounted on the crown panel. To try to approximate the proper mounting locations, an impact hammer test was performed on the mounted panel. Data points were taken every 4 inches (0.1 m) for a total of 79 points. The sum response from 500-1000 Hz was plotted and the actuators were positioned around the peaks of this plot (Figure 2-4) and the plots of the 3 frequencies chosen for single frequency tests (see Chapter 3.1). Figure 2-5 shows the numbering and location of each PZT.

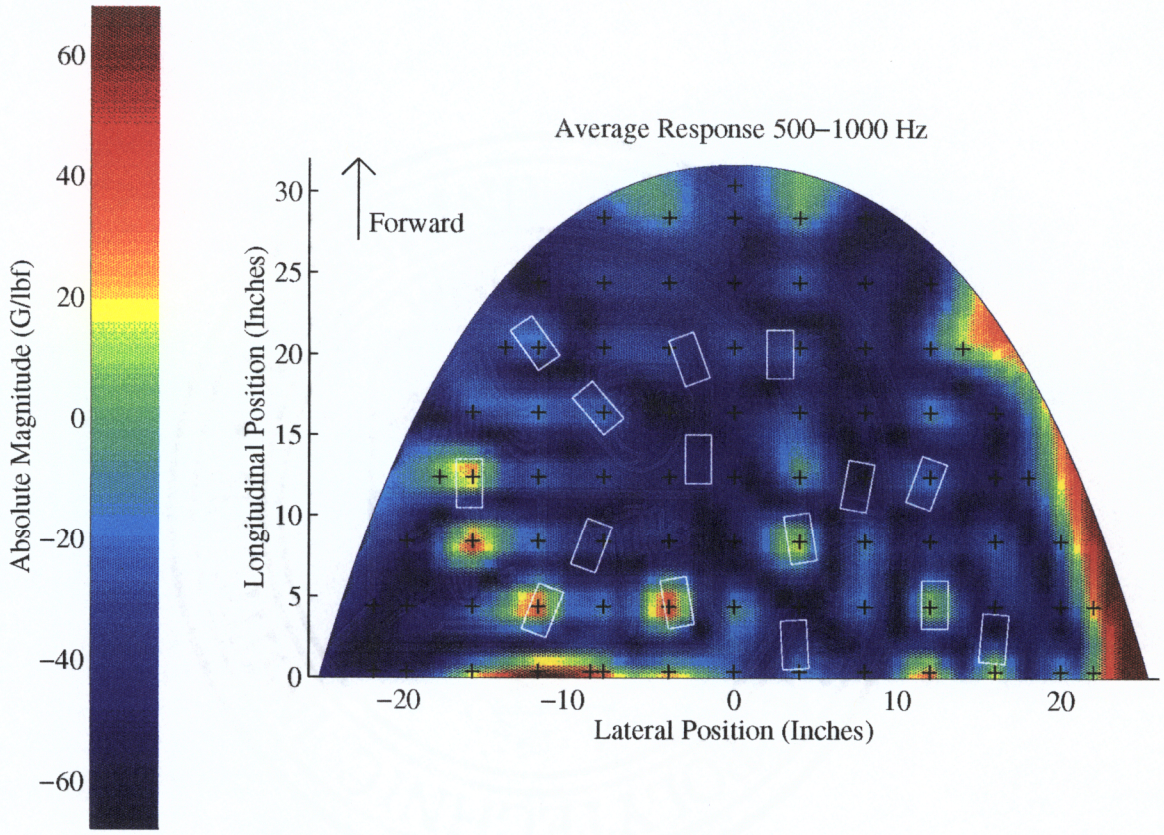

Figure 2-4, Impact Hammer Average Response

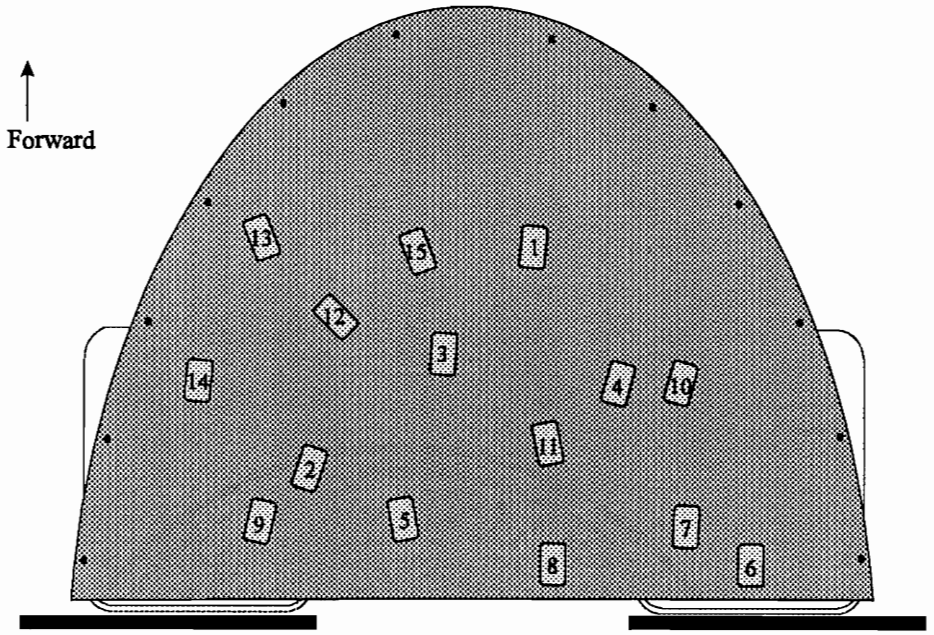

Figure 2-5, PZT Location and Numbering

2.4 The Disturbance

To simulate the flow noise disturbance, three 5 inch (127 mm) ported speakers were mounted over the crown of the aircraft (Figure 2-6). They were suspended from the ceiling of the laboratory and externally located one inch above the centerline of the fuselage's crown. Later tests include an enclosure built around the speakers to better focus the acoustic energy at the crown of the aircraft. (see Chapter 3.3.3). The speakers were connected in phase with two speakers connected in series with each other and in

parallel with the third to better match the impedance of the power amplifier. Thus the same sound levels were generated by each speaker. These speakers are used in all the control cases to serve as the disturbance input.

The three speaker disturbance was designed to better distribute the acoustic energy over the area of the crown as would a real flow disturbance. Wiring the three speakers together caused a fully coherent disturbance. Although an incoherent disturbance is more realistic, it is beyond the scope of this project and this is left for future work.

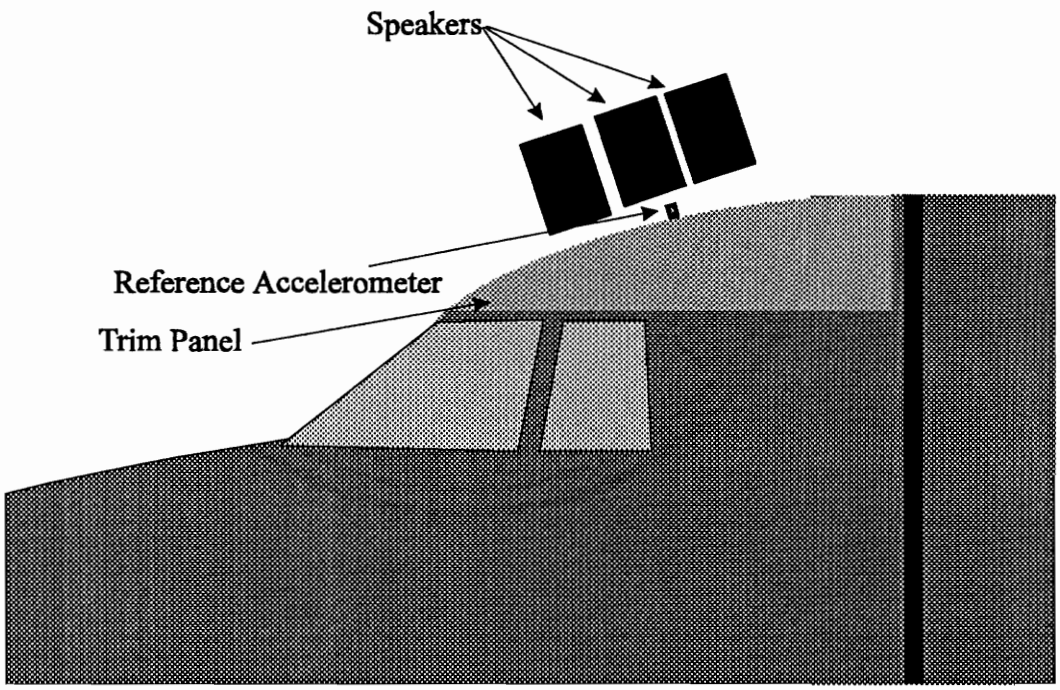

Figure 2-6, Diagram Indicating Position of Reference Accelerometer and Disturbance Speakers

2.5 Control Reference Signal and Controller Format

In recent years the advances in high speed digital signal processors have made practical application of digital control realizable for many applications. The ability of adaptive control systems to "adapt" or change in their environment makes them useful for a wide range of applications which necessitate a robust control system.

The controller design used with these experiments is the feedforward filtered-X least means squared algorithm with adaptive finite impulse response (FIR) filters. Since the transfer function of a FIR filter contains only zeros and no poles, the FIR filter is inherently stable[27,28]. The disadvantage of using a FIR filter is the inability of the FIR filter to individually model sharp residences or other pole characteristics. Since the system frequencies at hand are very modally dense and are well damped (with trim installed), this should not cause a problem.

Briefly stated, the feedforward control approach works by sensing the incoming disturbance with a reference signal. Knowing the relationship between the control output and error sensor response from the system identification, and assuming coherence between the reference signal and error sensor, the controller is able to adapt the actuator output for a given reference signal in such a way that minimizes noise at the error sensor microphones.

A single-input single-output filtered-X LMS typical block diagram[2,29] is shown in Figure 2-7. The plant output is the error signal which is denoted by e_k. It is a linear combination of the response of the disturbance input x_k and the control output u_k. For most of the experiments discussed in this thesis a multiple input multiple output (MIMO) filtered-X LMS controller was used. The MIMO controller is a simple extension of the SISO controller except with more degrees of freedom. A diagram of a three-input three-output MIMO filtered-X LMS controller can be seen in Figure 2-8. For the sake of brevity, the full details of the filtered-X LMS controller are not presented here. For more information the reader is referred to references [28,29,31,&32].

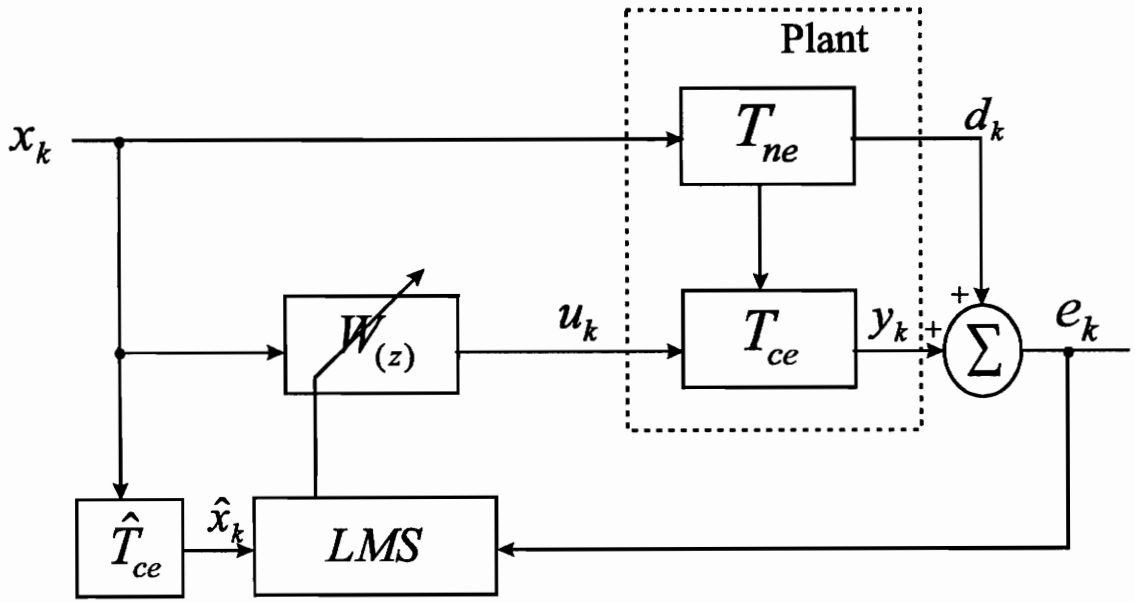

Figure 2-7, Typical Filtered-X LMS Control Algorithm

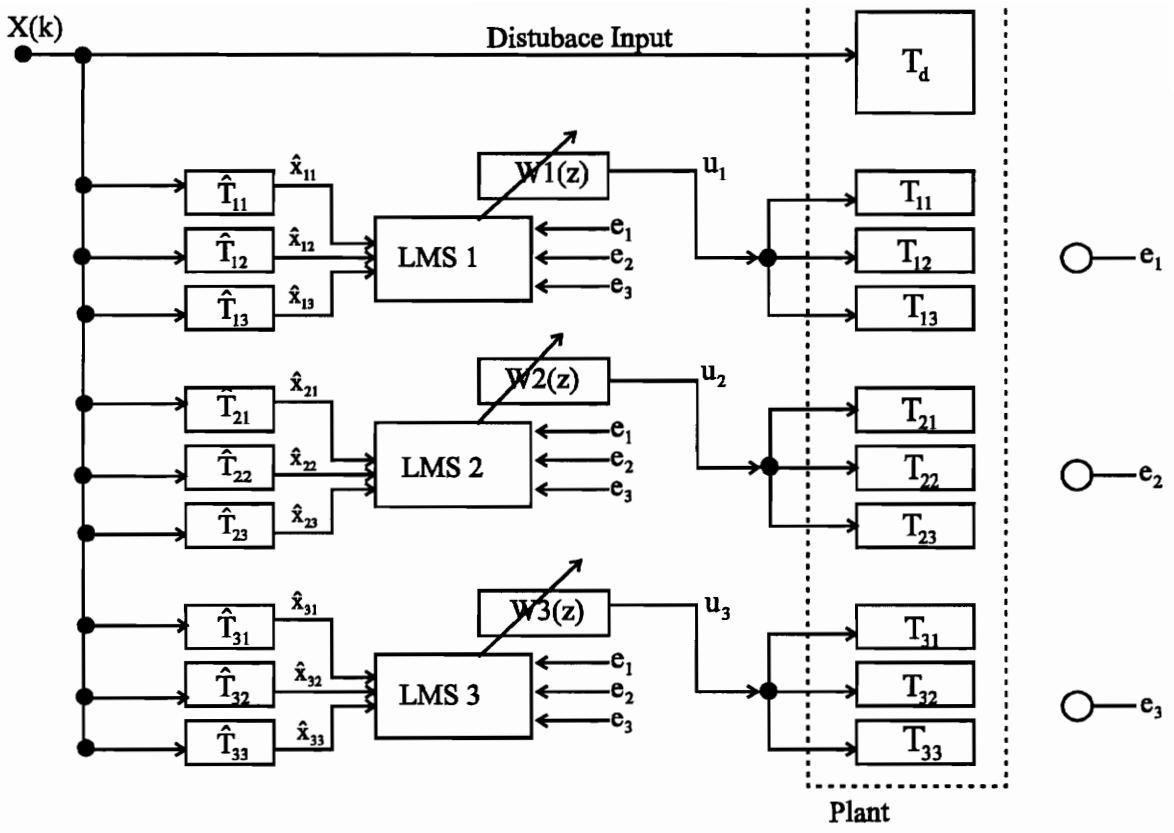

Figure 2-8, MIMO Filtered-X LMS Controller Block Diagram

However, in order to successfully implement feedforward control, a reference signal which is coherent to the error sensor signal must be obtained. Therefore it is necessary to accurately sense the disturbance signal. For realistic applications towards the aircraft flow noise problem this is accomplished by sensing the vibrations on the outer crown skin of the aircraft with an accelerometer or PVDF film. For these experiments an

accelerometer was mounted on the skin (Figure 2-6). The accelerometer is a small lightweight PCB unit mounted directly underneath the disturbance speakers.

The use of the accelerometer reference signal however brings up the issue of causality. For single frequency control experiments, the disturbance noise can be described as deterministic. This means that assuming steady state conditions knowing the frequency and amplitude of the disturbance signal, it is possible to predict what the disturbance signal will be at some time in the future. Unfortunately broadband flow noise is not deterministic and therefore it is not possible to predict what the future noise will be. Thus the controller must be able to receive the disturbance reference signal and produce the appropriate control output to the active panel before the disturbance noise propagates from the outer skin of the fuselage past the crown trim panel. Because the broadband controller used in these experiments was not always able to react fast enough to avoid the ill affects of causality, many tests were performed with the reference signal being acquired from the signal generator itself with a delay in the signal disturbance path. This delay was artificially introduced to provide the controller more time to react. This factors out the ill effects of causality from the tests.

ASAC has been demonstrated using adaptive feedforward control for single frequency disturbances.[30] The feedforward filtered-x LMS control algorithm has also been successfully applied to the control of broadband structural vibration[31,32] and acoustic

radiation[33]. The control algorithms used in the following experiments were implemented on a Texas Instruments TMS320C30 digital signal processing (DSP) board which was resident in a IBM 486 host personal computer (PC). DSP Expansion boards were installed so that multiple-input, multiple-output control cases could be executed with as many as 16 inputs and outputs. A diagram of the general control schematic can be seen in Figure 2-9.

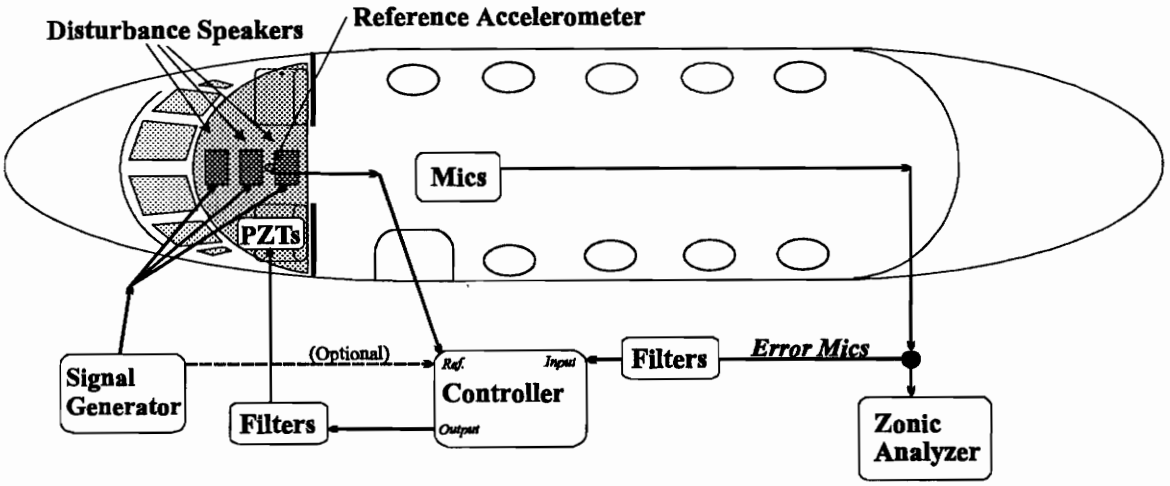

Figure 2-9, General Control Schematic

3. Single Frequency Experiments

This chapter discusses all of the single frequency experiments which are a prelude to the broadband tests. The single frequency tests serve as a preliminary feasibility study towards the applicability of ASAC to this noise problem, and will provide an indication of the maximum achievable performance of the broadband controller. The single frequency controller is faster than the broadband controller and avoids the issue of causality since single frequency noise is deterministic. This chapter begins with system identification tests designed to help locate actuators and choose frequencies for analysis. It then continues to discuss all the other single frequency experiments with full detailed analysis.

3.1 System Identification

In 1994 a full aircraft system identification of the structural-acoustic behavior of the Citation III fuselage was performed by Gibbs, Mahnken and Fuller[34] for Cessna

Aircraft Corporation. In this project a 2700 point interior acoustic survey was performed twice: once with structural excitation consisting of a shaker mounted radially on the aft left engine mount, and once with an interior acoustic excitation resulting from a speaker located in the front center of the plane. For the analysis a 90 microphone flight ready traverse was designed and built. The traverse spanned the cross-section of the aircraft and moved longitudinally up and down the cabin. Tests were performed and analyzed from 0-400 Hz with an automated data acquisition system. A sample of the averaged sum of the absolute values of the frequency response functions for both the speaker and shaker excitation are detailed in Figure 3-1 and Figure 3-2.

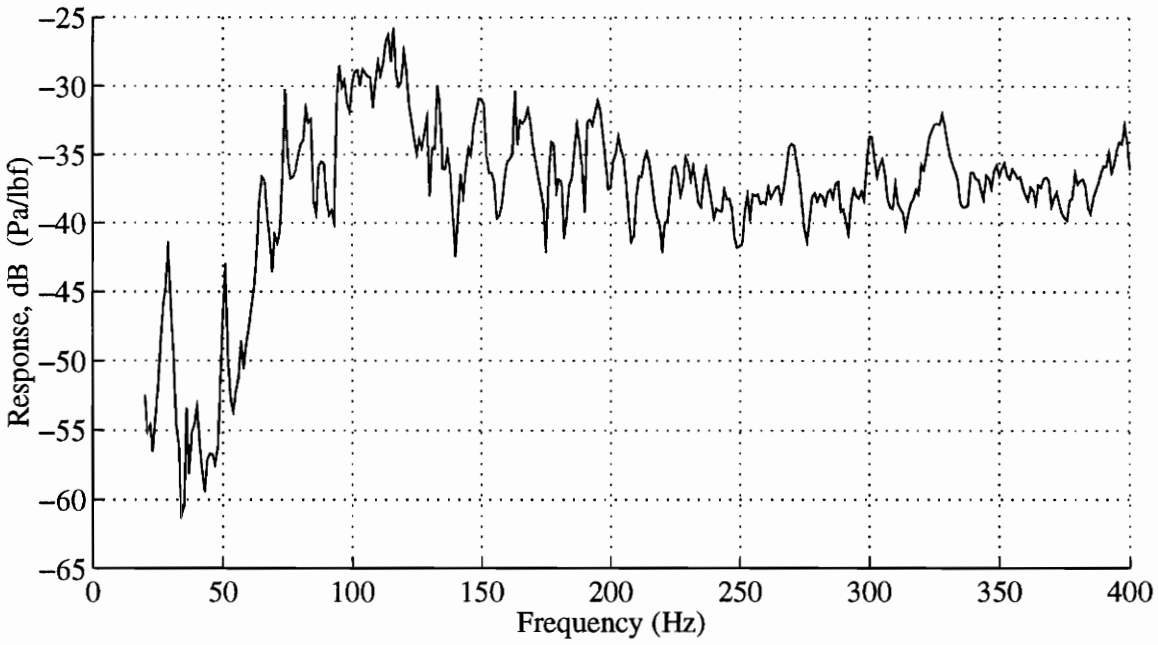

Figure 3-1, Cabin Spatially Averaged FRF, Shaker Excitation

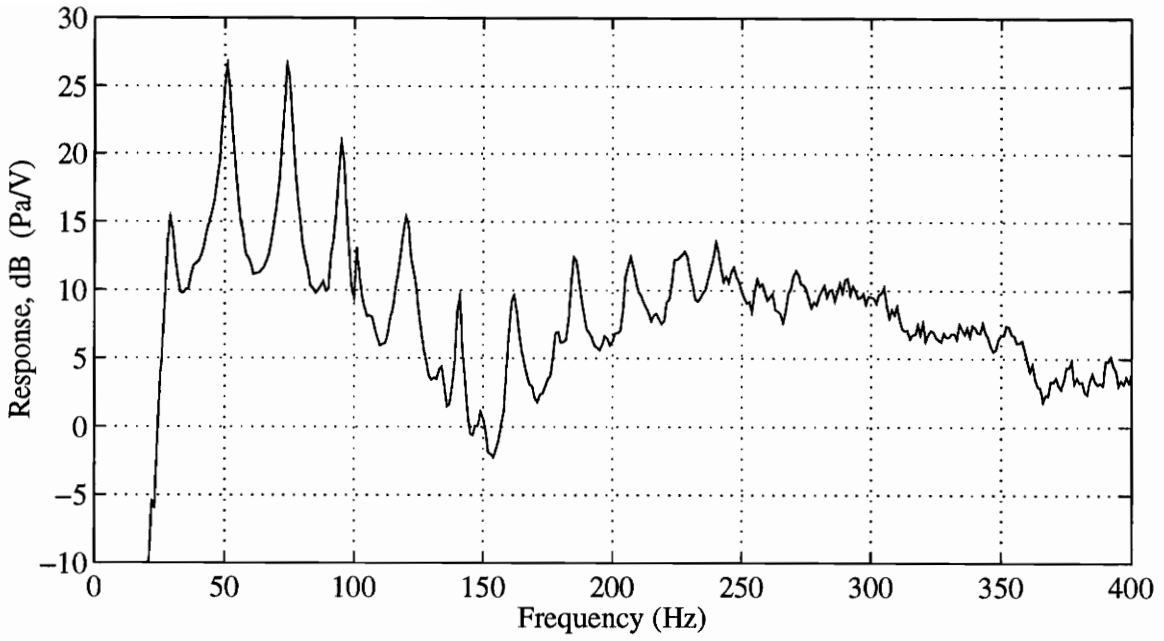

Figure 3-2, Cabin Spatially Averaged FRF, Speaker Excitation

Figure 3-1 and Figure 3-2 reveal that the interior acoustic system is very modally dense in the region above 300 Hertz. The modes are too close together to distinguish individually. This makes active control more difficult because the controller can not eliminate a few simple modes with an easy to identify pattern but rather has to cancel a multitude of complicated modes.

To better identify the acoustic field of the cockpit (as opposed to the previously mentioned 2700 point test that scanned the cabin) a similar type test was performed on the cockpit of the aircraft with 15 phase calibrated microphones located on a microphone stand. Again, two excitation sources were used. The first being an acoustical excitation

consisting of three disturbance speakers mounted above the plane to simulate the crown flow noise phenomenon. The second excitation source was a speaker located on the floor in the front left-hand side of the cockpit interior. The purpose of doing these tests twice with different excitations was to distinguish between the structural coupled acoustic modes and the pure acoustic modes of the cockpit. The spatially averaged sum frequency response plots of both excitations can be seen in Figure 3-3. It is shown that the responses are very modally dense in the 500-1000 range, there are few tonal resonance peaks, and the acoustic field can be described as disperse. These tests were perfomed to chose the three frequencies for the single frequency control tests.

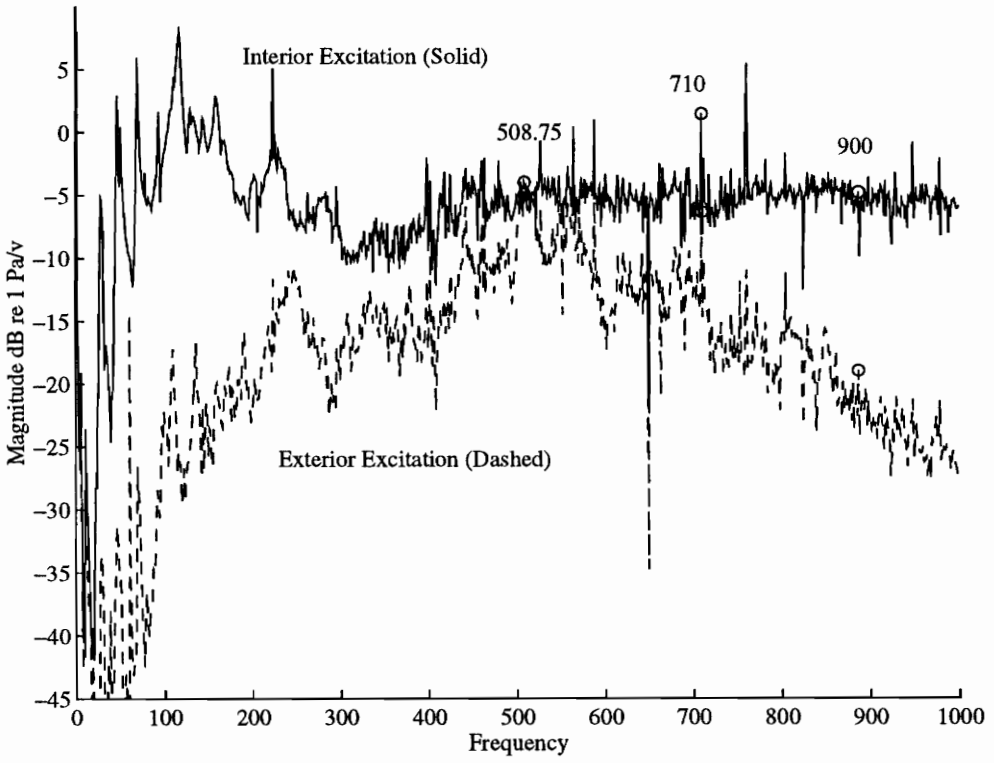

Figure 3-3, Cockpit Spatially Averaged Sum FRF

From the sum FRFs in Figure 3-3, three frequencies in the 500-1000 Hz range were chosen for the single frequency control analysis. They are the frequencies of 508.75, 710 and 900 Hz. The frequency of 508.75 Hz represents a fuselage structural resonance, 710 Hz represents both a fuselage structural and a cockpit acoustical resonance, and 900 Hz is off resonance both acoustically and structurally. The frequencies were chosen to cover various on/off resonance cases over the wide 500-1000 Hz frequency range. Each of these frequencies is indicated by a circle at the representative locations along the sum FRF curves of Figure 3-3.

3.2 Initial Single Frequency Tests

Although the main purpose of this project is to practically reduce interior broadband noise it is helpful to perform some single frequency control experiments to test the feasibility of broadband control and to measure the maximum achievable control performance. For example, if a single frequency control setup has performance difficulties, then a similar broadband setup would contain all those problems plus others inherent to broadband control. These broadband inherent difficulties are causality (being able to receive a disturbance reference signal and produce the appropriate control output

before the disturbance propagates past the actuators) and lack of FIR filter coefficient resolution (broadband controllers require more coefficients to cover a frequency span).

Another justification for performing the single frequency experiments is that single frequency control is better developed than broadband control. Thus optimization programs are more available and developed for single frequency applications than broadband applications. Since single frequency controllers are much quicker in terms of sampling rate and number of input/output channels, it is easier to judge how a faster sampling rate and more input/output channels might affect overall performance of a broadband system given the eventual availability of faster digital signal processing capabilities.

Initial single frequency tests were performed before the cabin was trimmed. Since the Cessna Citations does not separate the cockpit from the cabin with a door, without trim, the interior acoustics of both the cabin and cockpit are much more reverberant than is a normal plane. (Later tests, however, do include full trim). The initial tests were designed to gain an overall feeling for the success of control and to develop testing configurations for future experiments.

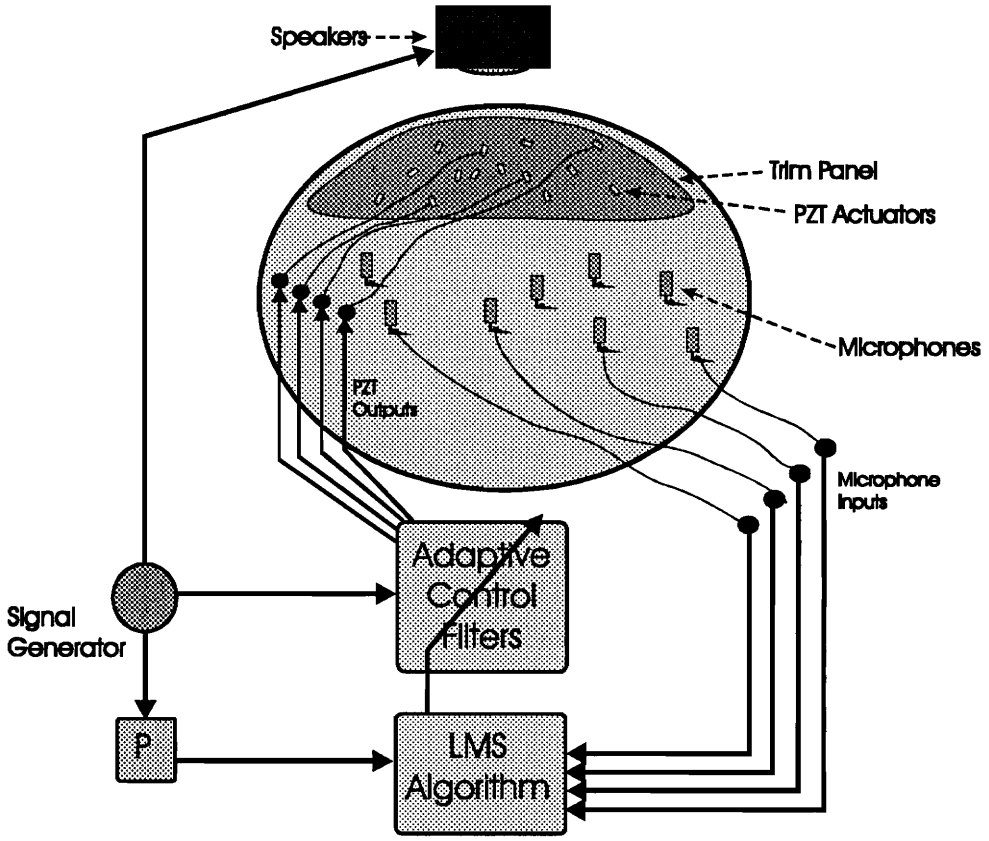

Figure 3-4, 4I4O Control Schematic

Thirty-six tests were performed for this initial single frequncy study. They consisted of thirteen separate setups of varying error sensor and actuator configurations run at the three standard frequencies of 508.75, 710 and 900 Hertz. Four of these test sets were performed with a 4I4O filtered-X LMS control setup (Figure 3-4) in which the microphone locations were varied. The microphone locations were altered to determine if the microphones should be located in the cockpit or scattered throughout the fuselage. The number of cockpit located microphones varied from 4 to 1. The second series of test

repeated the first set of experiments except with a 6I4O controller. Diagrams of the general control schematic and experimental setups are shown in Figure 3-4 and Figure 3-5.

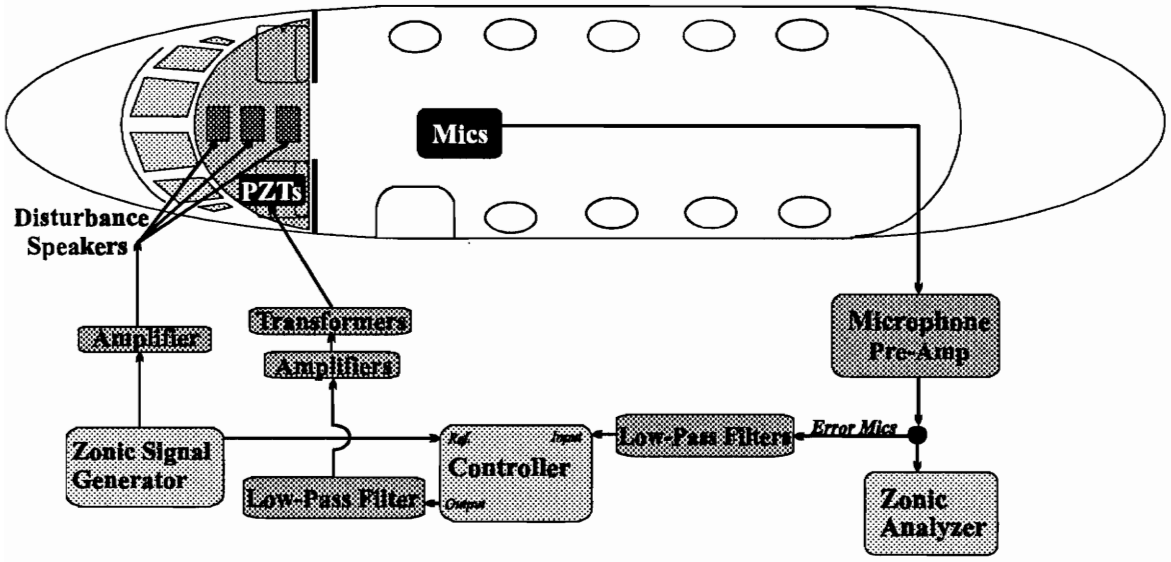

Figure 3-5, Single Frequency Experimental Setup

The first series of tests were performed to determine the initial feasibility of the 4I4O controller and to determine the effects of microphone placement. The tests were performed at interior noise levels of 80 dB with the controller sampling at 5000 Hz. The signals going into and out of the controller were all filtered with Frequency Device low-pass filters set at or above the nearest 100 Hz of the disturbance frequency. This filtering reduced noise of the error sensor inputs and rounds off the control output square waves (reducing unwanted harmonics).

The results of these tests can be summarized with two numbers: average noise reduction of the error sensor microphones and average noise reduction of the global microphones. The error microphone reduction is defined as the average sound pressure level reduction, in Decibels (dB), of the control error microphones. The average global microphone response is similar except that it is the average output of all of the microphones which are excluded from control. It is important to note that a positive reduction value is a net noise reduction, while a negative value is a net noise increase.

The microphones and PZT's used for each test set configuration is listed at the bottom of each column. Please refer to Figure 2-3 for the placement of each microphone and Figure 2-5 for location of each PZT actuator. Looking at the results of the first series of 4I4O single frequency tests, the first revelation is the shear magnitude of localized reduction. Most reduction levels averaged in the 30-50 dB range. This contrasts with no net reduction at the global microphones. In fact the typical noise levels of the global microphones tend to increase from 1-9 dB with the exception of one case where a 1.6 dB attenuation was obtained. The controller lowers error microphone noise to levels that would be well below the noise floor in any real aircraft application. Meanwhile noise levels increase at locations away from the error microphones.

Table 3-1, Series I 4I4O Initial Single Frequency Test

	4I4O Microphone Locations							
	4 Cockpit, 0 Cabin Mics		3 Cockpit, 1 Cabin Mics		2 Cockpit, 2 Cabin Mics		1 Cockpit, 3 Cabin Mics	
Frequency	Error Mics Reduct (dB)	Global Mics Reduct (dB)	Error Mics Reduct (dB)	Global Mics Reduct (dB)	Error Mics Reduct (dB)	Global Mics Reduct (dB)	Error Mics Reduct (dB)	Global Mics Reduct (dB)
508.75 Hz	50.8	-1.1	50.8	-3.1	47.3	-4.5	46.9	-9.5
710 Hz	53.6	-6.6	57.8	-6.1	14.9	-3.1	27.7	-3.7
900 Hz	56.2	-1.6	36.2	+1.6	8.3	-1.1	47.4	-3.2
Sensors	*Mics:2,7,8,11*		*Mics:2,4,7,8*		*Mics:2,4,5,8*		*Mics:1,4,5,8*	
Actuators	*PZT's:2,3,4,5*		*PZT's:2,3,4,5*		*PZT's:2,3,4,5*		*PZT's:2,3,4,5*	

Another observation to be drawn from the data is the variation in reduction levels between differing testing configurations. The error microphone reductions range from 8.3 dB to 57.8 dB while the global microphones attentions range from a reduction of 1.6 dB to an increases of 9.5 dB. This may be a result of the modal sound field changing between tests due to different disturbance frequencies or different error microphones. These changes alters whether the error sensors are at resonance or anti-resonance. If all error microphones are at resonance then there is great potential for large noise reductions while if the error microphones are at nodes, then obtaining a sizable attenuation is difficult.

Finally, looking at the trend of reduction levels verses microphone positions it seems that greater error microphone reductions occur with 3-4 microphones in the cockpit. This suggests that it is better to locate the error microphones closer to the control outputs verses placing them in the far-field away towards the back of the plane.

However, back to the issue of error microphone and global microphone magnitudes of reduction. It may be beneficial to try to sacrifice some of the control authority at the error microphones for lesser noise level increases at the global microphones. This can be accomplished by creating an overdetermined system with more error sensors than actuators. Since there are more error sensors than actuators, the exact control solution can not be mathematically reached Therefore the PZT's control authority is spread over more microphones creating more zones of less reduction than a properly determined system with equal numbers of actuators and error sensors.

The next series of tests were performed with a 6I4O (6 error microphone and 4 actuators) overdetermined configuration as shown in Table 3-2. However, the results are disappointing. The control levels diminished from 30-50 dB of control at error sensors with the 4I4O system to only 3-12 dB reductions with the 6I4O configuration. Meanwhile the global microphone spillover level do not improve with the 6I4O configurations. During experiments, the 6I4O actuator voltages has a periodic tendency to "drift" and

occasionally become unstable. This indicates that collinearity of the output signals was a problem with the PZT output signals fighting each other.

Table 3-2, Series II 6I4O Initial Single Frequency Tests

	6I4O Microphone Locations									
	6 Cockpit Mics		**5 Cockpit, 1 Cabin Mics**		**4 Cockpit, 2 Cabin Mics**		**3 Cockpit, 3 Cabin Mics**		**2 Cockpit, 4 Cabin Mics**	
Frequency	Error Mics Reduc (dB)	Global Mics Reduc (dB)	Error Mics Reduc (dB)	Global Mics Reduc (dB)	Error Mics Reduc (dB)	Global Mics Reduc (dB)	Error Mics Reduc (dB)	Global Mics Reduc (dB)	Error Mics Reduc (dB)	Global Mics Reduc (dB)
508.75 Hz	3.4	2.9	9.2	-1.1	7.2	-3.4	6.9	-1.8	4.4	-5.2
710 Hz	6.1	-5	2.6	-6.8	3.4	-4.5	4.8	-3.0	10.3	-4.3
900 Hz	6.8	-1.0	6.2	-3.2	6.2	-3.5	6.1	-3.2	12.3	-12.1
Sensors	*Mics: 2,6,7,8,9,11*		*Mics: 2,4,6,7,8,9*		*Mics: 2,4,5,7,8,9*		*Mics: 1,2,4,5,7,8*		*Mics: 2,5,8,14,15*	
Actuators	*PZT's: 2,3,4,5*		*PZT's: 2,3,4,5*		*PZT's: 2,3,4,5*		*PZT's: 2,3,4,5*		*PZT's: 2,3,4,5*	

3.2.1 Controller Comparison

The previous poor 4I4O and 6I4O results with too much reduction at the error microphones and collinierity concerns suggests that the MIMO filtered-X LMS controller might not be the most appropriate controller for this system. These difficulties may improve by trying a differing control approach. To investigate this a controller

comparison was performed at the three standard test frequencies (508.75, 710 & 900 Hz). The controllers evaluated were the standard filtered-X LMS, time averaged gradient LMS (TAG-LMS), and three variants of the biologically inspired hierarchical (bio) controller[35]: the phase variation bio controller, the adaptive magnitude bio controller and the adaptive phase bio controller. The three bio controllers vary the outputs of slave actuators relative to one master actuator. The phase variation bio controller varies the slaves output to either in phase, out of phase or off relative to the master. The adaptive magnitude bio controller changes the magnitude of the slave output verses the master's output, while the adaptive phase bio controller alters the slave actuators phase. Since the master-slave arrangement of the bio controllers are better designed for a multitude of actuators they were implemented in a 4I8O arrangement while the filtered-X LMS controller was used at 4I4O. The TAG-LMS controller was run at both 4I4O and 4I8O. The microphones and actuators that provided the strongest response were selected for control at these frequencies. The results of these comparisons appear in Table 3-3.

The results show that overall the filtered-X LMS controller was the most powerful in terms of error sensor attenuation. It provided the most reduction with 21-33 dB of control. It also only displayed the 3rd worst noise level spillover at the global microphones. In fact, what maybe a better measure of controller performance is the control to spillover ratio. The ratio is defined as the error microphone reduction levels divided by the levels of increase at the global microphones. The Filtered-X LMS

controller showed an average control to spillover ratio of 7.9:1 (Figure 3-6). The next closest performer, the amplitude modulation bio controller, has a control to spillover ratio of 5.5. From the results of these test comparisons it could be safely concluded that of the controllers tested, the filtered-X LMS controller is the best one for this application and that there would be no decisive gain from switching to another control strategy.

Table 3-3, Controller Comparison Test Results

	Frequency					
	508.75 Hz		**710 Hz**		**900 Hz**	
Controller	Error Mics Reduc (dB)	Global Mics Reduc (dB)	Error Mics Reduc (dB)	Global Mics Reduc (dB)	Error Mics Reduc (dB)	Global Mics Reduc (dB)
4I4O Fx-LMS	33.1	-4.1	31.8	-0.4	20.9	-4.7
4I4O TAG-LMS	8.6	-0.4	13.2	-1.2	8.0	-4.3
4I8O TAG-LMS	13.1	-5.6	12.7	0.1	12.1	-3.6
4I8O Bio PV	8.9	-2.5	13.7	-2.0	5.9	-3.3
4I8O Bio AM	7.0	-0.3	10.6	-0.2	10.9	-5.2
4I8O Bio AP	11.0	-2.3	14.4	-4.0	13.1	-5.4
Microphones	1,3,6,7		3,6,8,9		2,3,6,11	
4I4O Actuators	2,4,9,14		4,5,11,12		4,7,11,14	
4I8O Actuators	2,4,6,8,9,11,12,14		2,4,5,8,9,11,12,14		2,4,7,9,10,11,12,14	

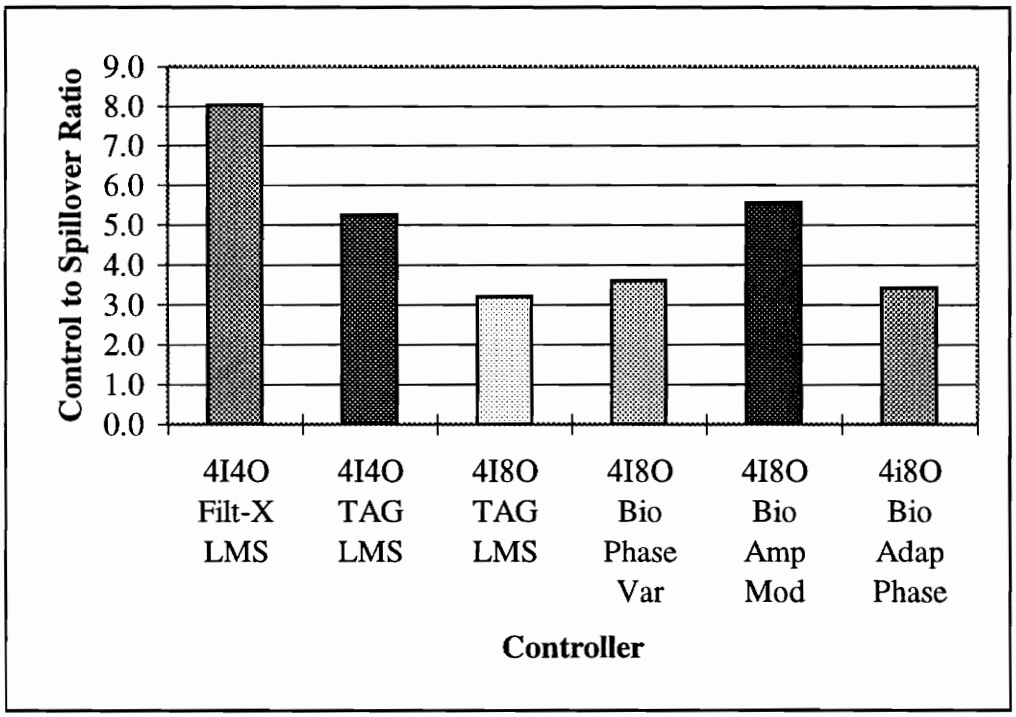

Figure 3-6, Control to Spillover Ratios for Controller Comparison Tests

3.2.2 System Analysis and Modifications

Since the filtered-X LMS control approach has been proven valid for this application, the next most logical step is to investigate whether the noise is flanking around the trim panel and entering into the interior where it can not be controlled. As mentioned earlier the first control tests were performed without any interior trim or

acoustic foam (except for the active crown panel). Also the roof mounted disturbance speakers were not enclosed. This allows the disturbance noise to reverberate around the lab and to enter back into the fuselage away from the crown. Because for the initial single frequency experiments the only panel inside the plane was the crown panel, the disturbance has a tendency to bypass the controlled crown trim panel and enter in other locations.

In an attempt to reduce this flanking, the cabin of the plane was fully trimmed with actual Cessna production interior trim, and the disturbance speakers were enclosed. The interior trim panels, foam, carpet and carpet padding of an current Cessna Citation were installed throughout the cabin and cockpit. This dramatically alters the acoustic properties of the interior allowing more realistic acoustic damping levels.

To more accurately focus the disturbance noise to the crown of the aircraft an enclosure made of ¾ inch (19 mm) thick wooden press-board was constructed around the disturbance speakers. The enclosure reaches from the front of the windshield back to the cockpit divider wall. The enclosure rests on the fuselage and is sealed with thick foam along its edges. A picture of the enclosure is included in Figure 3-7. The disturbance speaker enclosure and interior trim remained installed for the remainder of the single frequency and all of the broadband experiments.

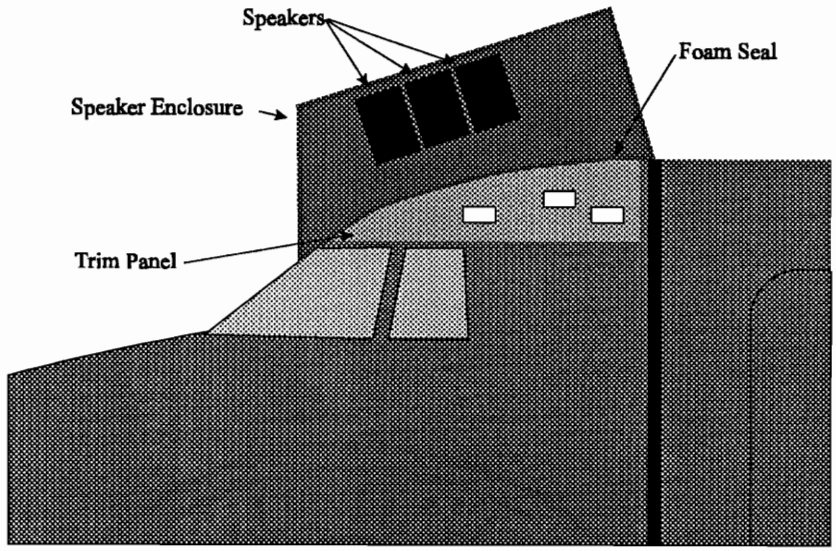

Figure 3-7, Speaker Enclosure

To objectively judge if sufficient disturbance noise is being directed through the trim panel and not around it, an intensity study was performed with the enclosure in place but without the full interior trim. For the study the disturbance was turned on and a calibrated B&K intensity probe was used to run two scans at intervals of 1 inch (25.4 mm). Intensity was measured from the interior of the aircraft with a B&K intensity probe by examining the cross-power spectrum between each microphone[36].

The two intensity scans were performed in the longitudinal and horizontal directions (Figure 3-8). The longitudinal scan was offset 4 inches (102 mm) to the left of centerline of the aircraft. It began 12 inches (0.3 m) below the edge of the windshield and finished 30 inches (0.76 m) beyond the back edge of the crown trim panel. The 4 inch

(102 mm) offset was to avoid measuring directly at the centerline fuselage longitudinal reinforcing rib. The total longitudinal scan was 84 points over 84 inches (2.13 m). To compliment the longitudinal scan, a horizontal scan was also performed. It covers 54 points at 1 inch (25.4 mm) spacing and runs from the top center of the aircraft to roughly 90 degrees down on the left hand side. The paths of both scans can be seen in Figure 3-8.

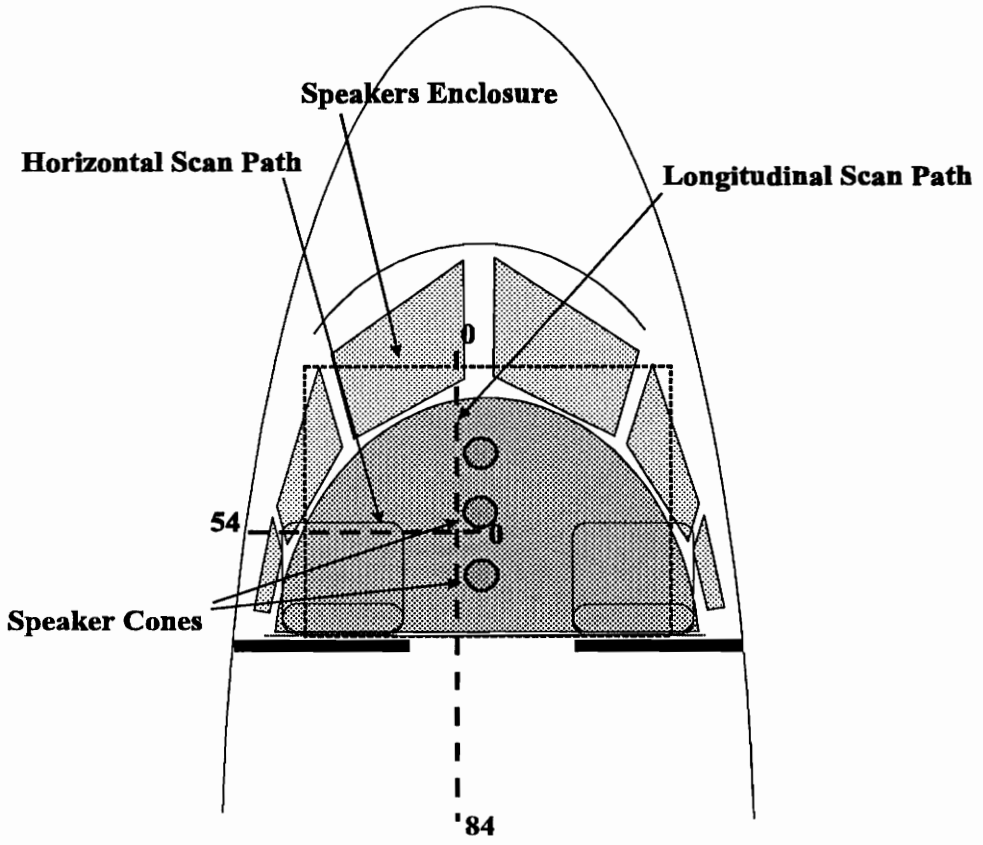

Figure 3-8, Intensity Scan Paths

The results of the intensity scans can be seen in Figure 3-9. In this figure the single frequency intensities are integrated over the 500-1000 Hz range at 1.25 Hz. bin spacings. The longitudinal intensity scan shows that most of the incoming sound is contained within the region covered by the panel. This area is denoted as between the two vertical lines at 13 and 45. There is a strong cutoff at 43 inches (1.09 m) which is approximately the back edge of the speaker enclosure. Nonetheless behind the panel in the 50-80 inch (1.27-2.03 m) range there does seem to be some slight flanking of the incoming noise where the crown panel stops and there is only bare aluminum. A re-measurement of sound intensity in this are with the full interior trim installed shows that the addition of trim has dramatically reduced the flanking in this area.

The horizontal intensity scan is also displayed in Figure 3-9. In this graph it is evident that the incoming noise flow cuts off sharply and even starts to flow out of the plane after the trim panel edge. Thus it is safely concluded that no noise is flanking around the sides of the panel.

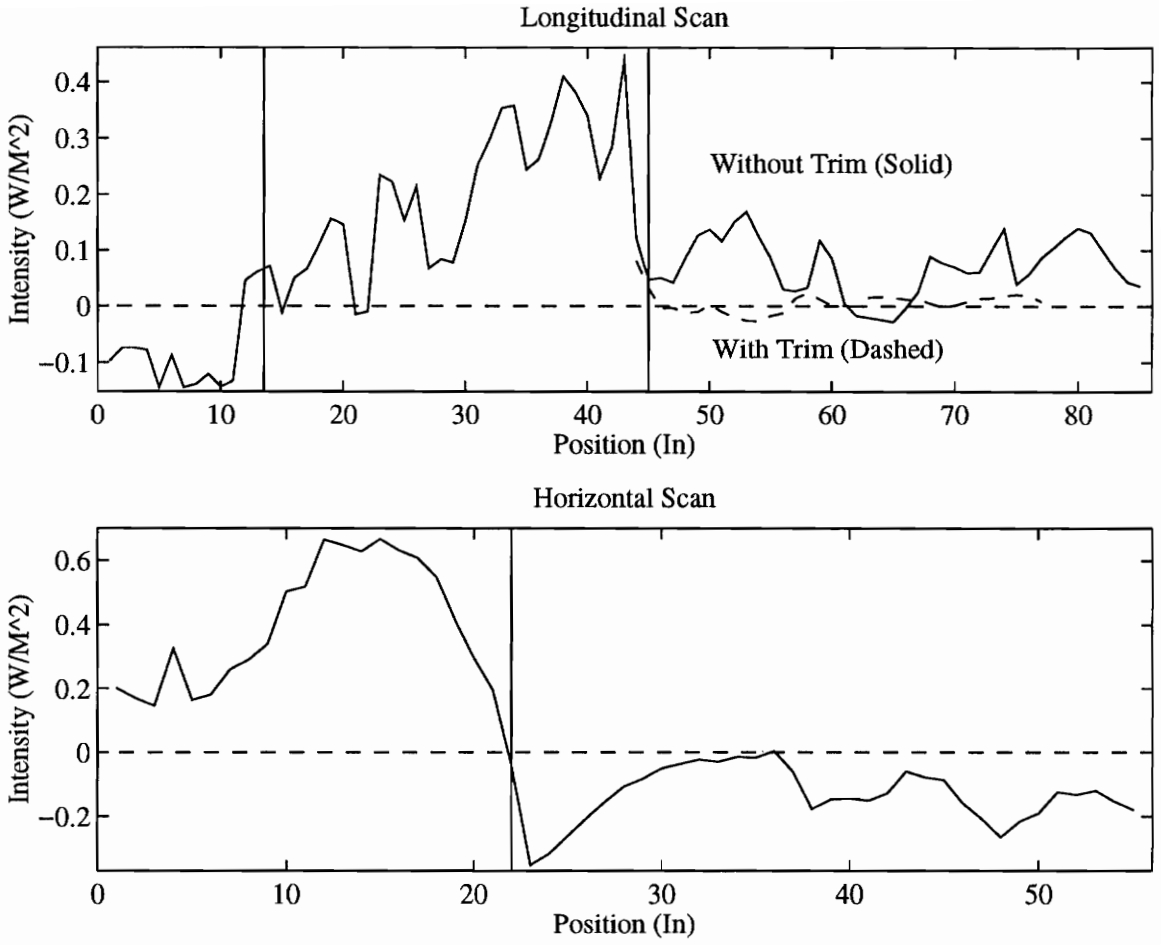

Figure 3-9, Longitudinal and Horizontal Sum Intensity Scans, 500-1000 Hz

3.3 Optimized Single Frequency Tests

Once the speaker enclosure and trim were installed, the next step was to perform more single frequency experiments in an effort to try to determine if there were any improvements in the control system performance. To factor out one test variable in what is already an extremely complex system, the controller parameters were fixed at 6I3O with

a sampling rate of 5000 Hz. This setting allows for a large enough number of error sensors while allowing the system to be simple enough for future off-line optimizations. The 6I3O configuration with only 3 verses the previous 4 output channels also helps reduce the chances of the PZT's fighting each other.

The excitation frequencies tested were the standard three: 508.75, 710 and 900 Hz with the control reference signal being drawn directly from the signal generator. All tests were performed with cockpit interior noise levels in the 70 dB range. Microphone measurements were taken before and after control for each test individually. The control schematic is the same as shown in Figure 2-9. Controller input and output signals were low pass filtered with Frequency Device filters to eliminate high frequency noise on the input and harmonics on the output. All noise measurements were taken with the calibrated PCB microphones in their standard test configurations (Figure 2-3).

Since earlier tests have displayed sensitivity to actuator and sensor locations an off-line optimization algorithm was implemented to choose the optimal PZT's and microphones for each frequency control case. Three types of optimizations are to be performed: Error Microphone Optimizations, which select the best microphones and actuators that reduce noise at the error microphones; Global Optimizations, which select the best error sensors and actuators which minimize noise globally; and Actuator

Grouping Optimizations which group all the actuators into control channels which provide the greatest attenuation at the error sensors.

These optimizations were performed by acquiring all the transfer functions from the disturbance and actuators to each microphone and then iterating through possible microphones and PZT control configurations while calculating the control attenuation at each iteration. The equation used for the off-line control optimization was:

$$\{\vec{P}\} = [\vec{T}]\{\vec{V}\} + \{\vec{D}\} \tag{5}$$

Where $\vec{P}$ represents a complex vector of microphone pressure response, $\vec{D}$ is the complex vector of microphone response due to the primary disturbance, $\vec{T}$ is a matrix of transfer functions relating applied actuator voltages to the microphone pressure responses, and finally, $\vec{V}$ is the complex actuator voltage. From equation (5) $\vec{T}$ and $\vec{D}$ are known quantities measured experimentally from transfer functions. $\vec{P}$ is the microphone response which is to be minimized in a least squared approach. This is accomplished by varying the actuator voltages $\vec{V}$.

To solve (5) mathmatically, a cost function needs to be defined. The typical cost function for LMS control is the sum of the squared error microphone pressure responses. This is denoted by Φ:

$$\Phi = \vec{P}^{*}\vec{P} \tag{6}$$

Omitting the math, the solution for the voltages $\vec{V}$ that minimizes the sum of the squared pressure response becomes:

$$\vec{V} = -\{\vec{T}^*\vec{T}\}^{-1}(\vec{T}^*\vec{D}) \tag{7}$$

Once the voltages have been calculated, they can be reinserted into the original equation (5) to acquire the individual microphone pressure responses with control on.

3.3.1 Error Microphone Optimization

To perform the error microphone optimization scheme as described above, the transfer functions between the disturbance and 9 PZT's actuators to the first 15 microphones were measured (analyzer channel 16 was used as an output voltage reference). These transfer functions were then inserted into a Matlab program that solved equation (7) for every possible combination of a 6I3O system. The 10 best 6I3O combinations that provided the biggest error sensor reductions were saved for each of the three frequency cases. Theoretical voltages and cost function reductions were also stored along with the microphone and actuator selected.

This optimization was performed for all three frequencies to find the configurations yielding the best error sensor reductions. The results of the error sensor optimizations for all three frequencies is shown in Table 3-4. The reduction of the error sensor cost function is given in dB, along with non-dimensionalized voltages and the

selected actuators and sensors. The voltages are non-dimensionalized by dividing the voltage of each PZT's by the average voltages of all three output PZT's of each case. This is performed because the disturbance output levels were not equalized between the FRF acquisition and control experiments due to the time lapse between the two tests.

The cases listed in Table 3-4 were then performed experimentally. The results of these tests can be seen in Table 3-5 Table 3-6, and Table 3-7. For comparison, all actuator output levels and microphone input levels were equalized into and out of the controller. This was acomplished by setting the PZT output amplifier levels equally and by equalizing the microphone gains into the controller.

Table 3-4, Single Frequency Off-Line Error Sensor Optimization

Freq. (Hz.)	Case	Reduct (dB)	Voltages (non-dim.)			PZT's			Microphones					
508.75	1	32.8	0.39	1.61	1.00	1	2	11	3	4	5	8	14	15
	2	30.5	0.93	1.03	1.04	2	8	9	5	6	10	11	12	13
	3	30.4	0.91	0.69	1.41	1	10	11	3	4	5	6	10	13
710	1	32.5	0.82	1.65	0.53	1	7	10	1	5	7	10	14	15
	2	30.5	0.77	0.48	1.76	1	7	12	4	5	7	9	12	13
	3	30.0	0.77	0.50	1.73	3	7	11	2	3	5	7	12	14
900	1	38.6	0.39	1.61	1.00	1	7	10	1	4	6	7	13	15
	2	35.8	0.93	1.03	1.04	2	3	12	5	6	7	8	10	15
	3	34.4	0.91	0.69	1.41	3	7	9	5	7	11	12	14	15

Table 3-5, Single Frequency Error Sensor Reduction Optimization, 508.75 Hz.

Frequency: 508.75 Hz.									
Case	Theor-etical Error Reduct (dB)	Actual Error Reduct (dB)	Actual Global Reduct (dB)	Theoretical Voltages			Actual Voltages		
1	32.8	-11.5	-8.3	0.39	1.61	1.00	0.44	0.95	1.62
2	30.5	10.1	-5.7	0.93	1.03	1.04	1.16	0.83	1.00
3	30.4	20.3	-3.4	0.91	0.69	1.41	0.28	1.58	1.14

Table 3-6, Single Frequency Error Sensor Reduction Optimization, 710 Hz.

Frequency: 710 Hz.									
Case	Theor-etical Error Reduct (dB)	Actual Error Reduct (dB)	Actual Global Reduct (dB)	Theoretical Voltages			Actual Voltages		
1	32.5	22.0	-8.3	0.82	1.65	0.53	0.65	0.68	1.67
2	30.5	19.1	-3.9	0.77	0.48	1.76	0.58	0.55	1.87
3	30.0	21.2	-4.7	0.77	0.50	1.73	0.80	1.38	0.83

Table 3-7, Single Frequency Error Sensor Reduction Optimization, 900 Hz.

Frequency: 900 Hz.									
Case	**Theor-etical Error Reduct (dB)**	**Actual Error Reduct (dB)**	**Actual Global Reduct (dB)**	**Theoretical Voltages**			**Actual Voltages**		
1	38.6	19.1	0.3	0.39	1.61	1.00	0.77	0.75	1.48
2	35.8	21.4	-3.3	0.93	1.03	1.04	0.38	0.86	1.77
3	34.4	1.2	-10.2	0.91	0.69	1.41	0.46	1.27	1.28

The theoretical analysis predicts reduction levels in the 30-35 dB range while the actual reductions obtained peaked in the lower twenties. The full potential reduction of the off-line theoretical control was never realized. This is because theoretical numbers are an exact mathematical solution without any sampling errors, noise, or controller inability to converge on the exact solution. The theoretical solution also assumes complete linearity, which is not necessarily true. The control output is not analog and thus the dynamic range of the DSP limits reduction. In addition, the FRFs for the off-line analysis were taken at a different period of time than the actual experiments. Thus environmental factors may have changed or the microphones may have been bumped out of position making the "optimal solution" less than optimal. Also, even though the microphones were not intentionally moved during the period of time between FRF acquisition and experiments, is possible that some of the microphones may have been bumped slightly out of position.

However, it should be noted that there is a typical lack of consistency in the experimental attenuations. For example, the 900 Hz cases obtained reductions of 19.1, 21.4 and 1.2 dB. Clearly the third case with only a 1.2 dB reduction is out of place. This 1.2 dB reduction at the error sensors was coupled with a 10.2 increase at the global microphones. Although the PZT output voltages did stabilize for this case, it can be assumed that there are collinearity problems. The three PZT's don't have distinct enough transfer functions to the error microphones resulting in the PZT's conflicting with each other. This hinders proper control. This effect can also be observed in case #1 and in case #2 of the 508.75 Hz experiments.

When comparing the absolute voltage levels of the experimental and theoretical reductions it is difficult to draw a correlation between the two. It can be said that case #2 for both the 710 and 508.75 Hz test sets displays similarities between the predicted and measured voltage levels, but considering that none of the other cases exhibit any such similarities this is believed to be coincidental. Also, it is important to note that the experimental actuator phases were not measured. Therefore an actuator phase comparison (which should complement the voltage magnitude comparison) can not be performed.

And finally, a few comments should be made about reductions at the global microphones. It seems that with the configurations that give error sensor reductions of 19-22 dB, the other global microphones tend to become 3-8 dB louder. Only the 900 Hz case #1 showed any significant control (19.1 dB) without any increase at the global microphones. In fact, the global microphones in that test showed a decreased noise level, but by only 0.3 dB.

Microphone by microphone reductions for a typical case are shown in Figure 3-10 and Figure 3-11. This is the 900 Hz case #2 which achieved an error sensor reduction averaging 21.4 dB with the global microphones rising an average of 3.3 dB. The error sensor microphones (Figure 3-10) all seem to show reductions, though their reductions vary significantly from 2.2 dB at microphone #5 to a reduction of 40.9 dB at microphone #8. Coincidentally, the largest reductions are found at microphones #7 & #8 which happen to be the microphones placed at the pilot's left and right ears. Since the microphones are about 12 inches (0.3 m) apart, the reduction zone from #7 might be assisting the reduction at microphone #8 and vice versa.

As for the global microphones, (Figure 3-11) it can be seen that all except one of the microphones increase in SPL level. This increase ranges from 2.4 dB at microphone #11 to 12.9 dB for microphone #1. All the other microphones whose values increased went up between 4-8 dB. The one global microphone that displayed a noise reduction

was microphone #12 which decreased 13.8 dB. However, generally the global microphones showed a fairly consistent gain of 3.3 dB.

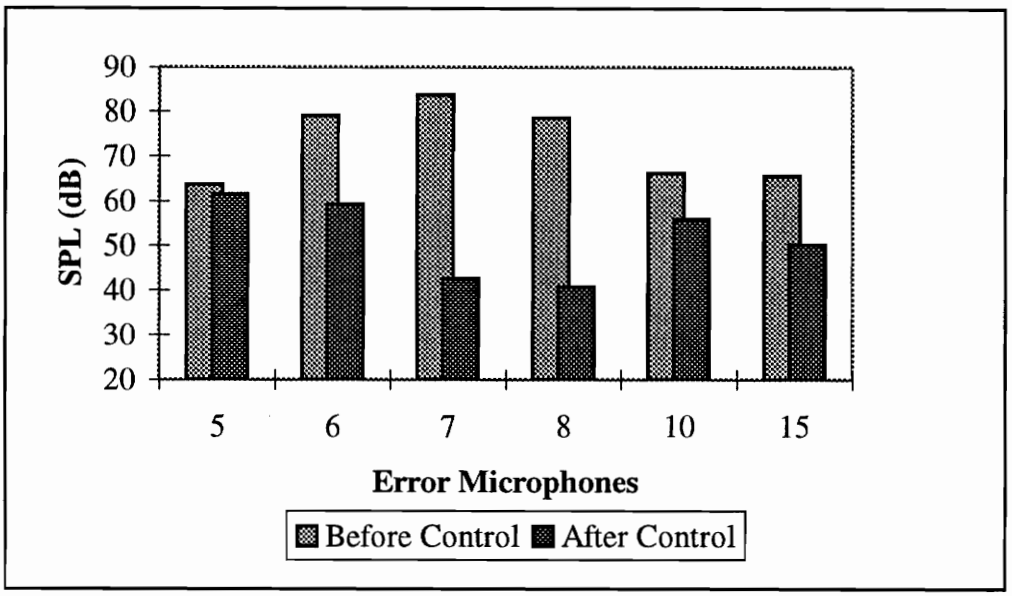

Figure 3-10, Single Frequency Control, 900 Hz, Case #2, Error Microphones

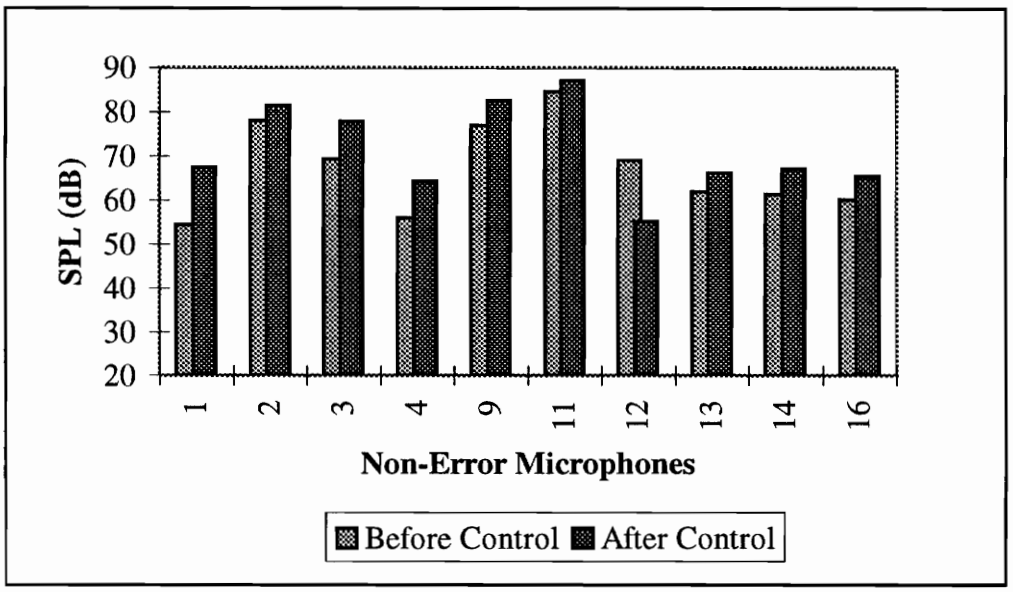

Figure 3-11, Single Frequency Control, 900 Hz, Case #2, Global Microphones

3.3.2 Global Microphone Optimization

Once the error sensor optimizations and corresponding experiments were completed, it became evident that the hopes for global reductions at the global microphones were not evolving. The global microphone levels were still increasing despite the speaker enclosure, interior trim, and off-line optimizations. The next step to try to remedy this situation was to rewrite the optimization code. A similar global microphone optimization routine was performed. This time instead of solving for the configurations that best reduced noise at the error sensors, the configurations that seem to achieve the best reduction of the global microphones were saved. Due to the computational complexity of iterating through every possible combination of microphone and PZT, this analysis was only performed on the 508.75 and 900 Hz frequencies. The results of the off-line analysis can be seen in Table 3-8 with the reduction column being defined as the averaged reduction of the 12 global non-error sensor microphones.

These results show that the theoretical global microphone reductions for the best three configurations for both frequency sets range from 7.4 to 11.0 dB. The 508.75 Hz cases all chose the same actuators while the microphone selections seemed to vary widely.

Since the actuator configurations remain consistent, the voltages to each of the PZT's remains fairly similar throughout the cases.

The 900 Hz cases also shows similar PZT selections with cases 1 and 3 having the same attenuation. It also shows similar microphone selections that only vary by one or two microphones between each case. It is interesting to note that the only difference between the 900 Hz case 1 and case 3 is that for case 3 microphone 14 (located in the middle of the cabin) replaces microphone 2 (located at copilot's head). Amazingly, this one microphone substitution causes the global non-error sensor overall theoretical reduction to drop from 11.0 to 7.4 dB. This exemplifies how sensitive system performance is to the slightest changes.

Table 3-8, Single Frequency, Off-Line, Global Non-Error Sensor Optimization

Freq. (Hz.)	Case	Global Mic Reduct (dB)	Voltages (non-dim.)			PZT's			Microphones					
508.75	1	9.2	1.01	0.68	1.31	2	3	10	3	4	5	8	14	15
	2	8.6	0.98	0.78	1.24	2	3	10	5	6	10	11	12	13
	3	8.5	0.99	0.76	1.25	2	3	10	3	4	5	6	10	13
900	1	11.0	1.07	1.02	0.92	3	7	9	2	3	6	8	9	11
	2	7.9	1.25	1.22	0.53	8	10	12	2	3	6	8	11	12
	3	7.4	1.14	0.86	1.00	3	7	9	3	6	8	9	11	14

The controller configurations from these off-line global microphone optimizations were performed experimentally. The results can be seen in Table 3-9 and Table 3-10. The results seem to vary signifigantly between frequency cases. The 508.75 Hz cases performed well, with overall reductions of 3.9, 4.4, and 5.8 dB at the global microphones while the error microphones showed a similar reduction of 3.2-3.5 dB.

Conversely, the 900 Hz case (Table 3-10) show discouraging results. Reduction is only obtained for one of the 3 cases at the global microphones while the error microphones show a net increase in noise levels with every case. The probable cause is that either the system has changed, disallowing the predicted control, or that this experimental configuration encounters some collinearity problems not accounted for in the off-line analysis.

Table 3-9, Single Frequency Global Non-Error Sensor Reduction Experiment Results, 508.75 Hz.

Frequency: 508.75 Hz.									
Case	**Theoretical Global Mic Reduction (dB)**	**Measured Error Mic Reduction (dB)**	**Measured Global Mic Reduction (dB)**	**Theoretical Voltages**			**Measured Voltages**		
1	9.2	3.2	3.9	1.01	0.68	1.31	N/A	N/A	N/A
2	8.6	3.5	4.4	0.98	0.78	1.24	0.85	1.33	0.82
3	8.5	3.3	5.8	0.99	0.76	1.25	0.79	1.12	1.09

Table 3-10, Single Frequency Gloabl Non-Error Sensor Reduction Experiment Results, 900 Hz.

Frequency: 900 Hz.									
Case	**Theoretical Global Mic Reduction (dB)**	**Measured Error Mic Reduction (dB)**	**Measured Global Mic Reduction (dB)**	**Theoretical Voltages**			**Measured Voltages**		
1	11.0	-1.1	-3.1	1.07	1.02	0.92	0.74	0.78	1.48
2	7.9	-0.5	1.6	1.25	1.22	0.53	1.40	0.52	1.08
3	7.4	-5.7	-1.3	1.14	0.86	1.00	1.57	0.59	0.84

A sample of the microphone by microphone reductions of the 508.75 Hz case #3 with a 3.3 dB reduction at the error sensors and a 5.8 dB reduction at global sensors can be seen in Figure 3-12 and Figure 3-13. Figure 3-12 shows that most of the error microphones exhibit some form of reduction, but this reduction varies from 11.1 dB for microphone #6 to 0.8 dB for microphone #11. Meanwhile both microphones #7 and #10 increase slightly by 0.4 dB.

However, the real controversy is in Figure 3-13. This graph depicts the before and after control sound levels for the global microphones. The data shows that despite the 5.8 dB average reduction over the 10 microphones, only 3 microphones actually show a net

reduction in noise levels. This is because of the spatial logarithmic averaging required to average decibel values. In fact, a linear average of the reduction values show that the interior noise levels show a slight increase by 0.02 dB. This is all caused by microphone #3 having a higher before control level of around 13 decibels above the next highest microphone. This microphone experiences a reduction of 10.8 dB which (since it is the strongest microphone) skews the average. But the important factor is that a reduction in interior acoustic energy level was obtained with this single frequency actuator/sensor configuration.

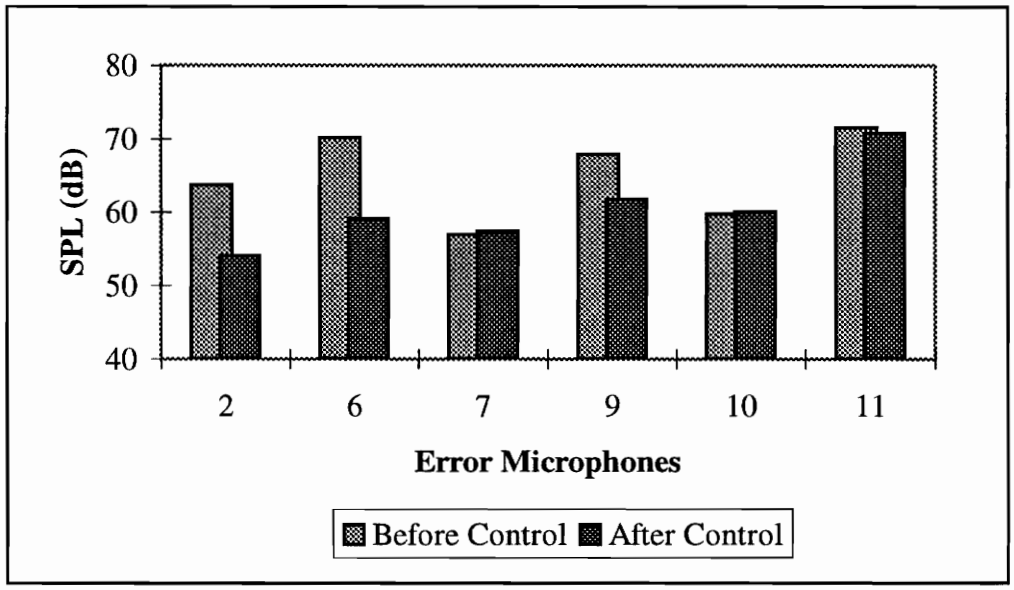

Figure 3-12, Global Non-Error Sensor Optimization, 508.75 Hz, Case #3, Error Microphones

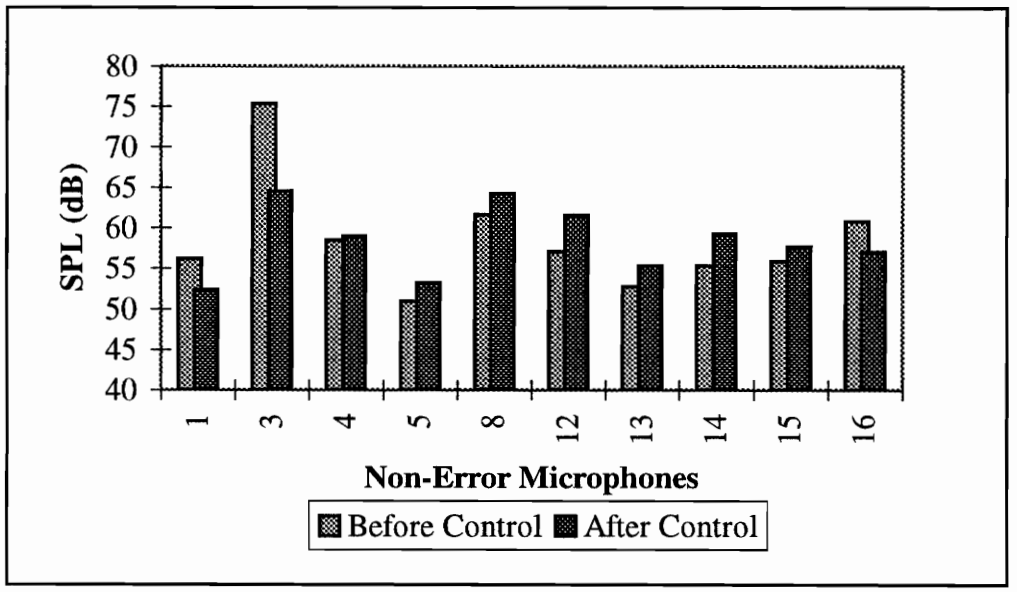

Figure 3-13, Global Non-Error Sensor Optimization, 508.75 Hz, Case #3, Global Microphones

3.3.3 Actuator Grouping Optimization

In addition to the optimizations minimizing noise at the error and the global microphones, an off-line actuator grouping optimization algorithm[37] was also applied. The actuator grouping works by tying together actuators to form a single control channel output. For example, if 9 PZT's were to be grouped into 3 control channels then each control channel may have 3 PZT's wired together. The number of actuators per control channel however is not fixed so that it is possible to have 2 PZT's as two control channels with the third control channel comprising of 7 PZT's wired together. The actuator grouping algorithm works by mathematically iterating through every possible combination

of wiring the PZT's into 3 output channels. The purpose of wiring together multiple PZT's into a single control channel is to try to obtain a more distributed actuator which will better attenuate the noise radiating modes without exciting and spilling over to other modes.

For performing this off-line grouping algorithm, the same transfer functions were used as in the previous optimizations in a two part analysis. The first optimization step was to determine the best actuator grouping for a 15I3O system using all of the microphones as error sensors. Once the actuator groupings were established, the next step was to use that grouping to determine the best six microphones in a resulting 6I3O system. This optimization was split into two parts because of the high computational time. The two part optimization iterates over 14 thousand combinations while a straight one-step exhaustive optimization would have to solve for 52.5 million combinations.

The results of the off-line groupings can be seen in Table 3-11, Table 3-12, and Table 3-13. The top three microphone configurations for the best grouping at each frequency is given. The reduction values shown in first data column of each table is the analytical error sensor noise reduction. The experimental error microphone reductions and the global microphone reductions are also shown. The bottom row of each chart shows what PZT actuators were grouped together to form each of the three output control channels.

Table 3-11, Single Frequency Actuator Grouping, 508.75 Hz

Frequency: 508.75 Hz									
Case:	**Theoretical Error Reduction (dB)**	**Measured Error Reduction (dB)**	**Measured Global Reduction (dB)**	**Microphones:**					
1	24.7	15.4	-6.2	3	5	10	11	12	13
2	24.6	4.8	1.0	1	2	3	4	5	8
3	24.5	15.1	-5.3	1	3	5	12	14	15
Actuator Groupings:				2,7		9,10,11		1,3,8,12	

Table 3-12, Single Frequency Actuator Grouping, 710 Hz

Frequency: 710 Hz									
Case:	**Theoretical Error Reduction (dB)**	**Measured Error Reduction (dB)**	**Measured Global Reduction (dB)**	**Microphones:**					
1	23.4	8.0	-15.8	1	5	6	10	13	14
2	23.2	8.9	-3.0	3	5	6	11	13	14
3	23.0	16.4	-2.1	4	5	7	12	13	14
Actuator Groupings:				1,2,7		9,10,11		3,8,12	

Table 3-13, Single Frequency Actuator Grouping, 900 Hz

Frequency: 900 Hz									
Case:	**Theoretical Error Reduction (dB)**	**Measured Error Reduction (dB)**	**Measured Global Reduction (dB)**	**Microphones:**					
1	32.6	11.4	-4.3	1	5	7	8	10	15
2	30.5	14.6	-2.4	4	5	7	8	10	15
3	29.1	13.1	-11.5	1	5	6	10	11	13
Actuator Groupings:				1,7		3,9,11		2,8,10,12	

The first observation from the tables is the similarities in actuator groupings between frequency cases. PZT #1 is always grouped with PZT #7. The same is true with PZT's #9 and #11 and also PZT's #8 and #12. This suggests that these PZT's naturally complement each other regardless of the excitation frequency.

The theoretical reductions resulting from the grouped analysis are also significantly lower than the combinations found with the previous non-grouped error microphone optimizations. The theoretical grouped reductions range from 23 to 32 dB while the non-grouped error sensor optimization reduction levels ranged from a much higher 30 to 38 dB. This is most likely not a indication of poor performance resulting from grouped

actuators, but rather result come from a less extensive optimization. While the error sensor optimization routine iterates through an exhaustive search of all possible 6I3O combinations of 9 actuators and 15 microphones (1.2 million combinations), the grouped optimization has to iterate through a two step process resulting in the evaluation of only 14.5 thousand combinations. Nonetheless it is not only the raw number of iterations that makes the difference; the way that the two step optimization first groups the actuators and then chooses the best six microphones for this grouping is not totally optimal. The best actuator grouping for a 15I3O system may not be the best actuator grouping for a 6I3O system.

Once this is understood, the reduction numbers shown in Table 3-11, Table 3-12, and Table 3-13 seem more logical. They show similar trends to the other single frequency non-grouped error microphone optimizations discussed earlier: The measured reductions are well below the theoretical ones, there tends to be significant increases in noise levels at the global microphones, and there is one "misfit" test at each frequency that does not correspond with the other tests.

Disregarding the "misfit" cases (which either show little control or extreme spillover [508.75 Hz case #1, 710 Hz case #1, and 900 Hz case #3]), overall the reductions are reasonable with an average reduction between 8-15 dB at the error microphones. The global microphones show typical increases in levels at between 2 to 6

dB. Although the response at the global microphones still showed signs of spillover, the overall grouping results are similar to the earlier optimizations except with less control and slightly less spillover.

3.4 Speaker Comparison Tests

The next and final step in the single frequency analysis is to compare the results with traditional active noise control to justify that the active panels are a better control solution than ANC. For this, 10 speakers were scattered throughout the cockpit and cabin of the aircraft and the transfer functions between the speakers and the microphones were taken for off-line analysis. The locations of the control speakers can be seen in Figure 3-14.

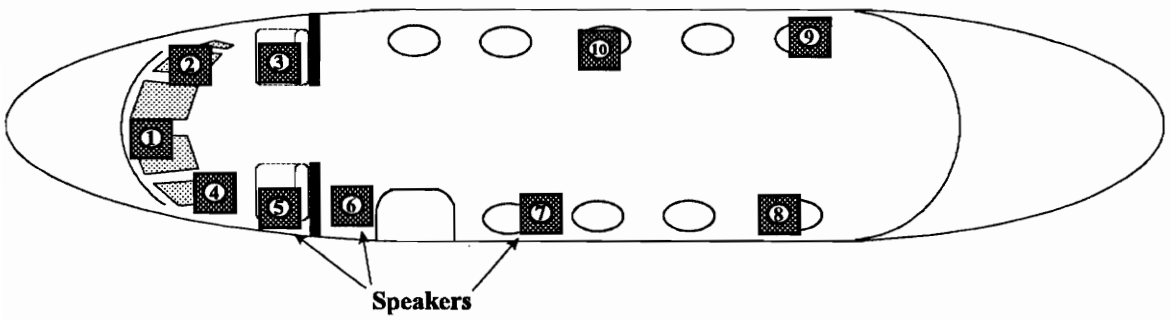

Figure 3-14, Control Speaker Locations

From the transfer functions between the speakers and microphones, error microphone off-line optimizations selecting the optimal combinations of speakers and microphones for control were performed. Again, here the objective was to solve for the best 6I3O combination of speakers and microphones that yielded the greatest error sensor attenuations. The results of the analysis can be seen in Table 3-14. The voltage comparison between theoretical and actual voltages has been omitted since two different types of control speakers were used. These speakers have differing radiation efficiencies which would make a voltage comparison invalid.

The optimization chose microphones that were scattered through out the plane without any perceivable pattern. However, with there being an equal number of cabin and cockpit speakers, the optimization seem to favor speakers located in the cockpit, rather than the cabin by an overall ratio of 20 to 7. This is a result of the control output having to align with the disturbance. This requires the speakers output waves to better match the disturbance's and hence be located nearer to the disturbance. It should be noticed that the error microphone reduction levels are lower than the comparable PZT optimization. The PZT optimizations show maximum reductions of 32.8, 32.5 and 38.6 dB while the speaker optimizations show maximum reductions of 31.1, 23.4 and 29.2 dB for each frequency case.

Table 3-14, Single Frequency Off-Line Speaker/Error Sensor Optimization

Freq. (Hz.)	Case	Theoro Reduct (dB)	Speakers			Microphones					
508.75	1	31.1	1	2	8	3	4	5	8	14	15
	2	27.8	2	5	6	5	6	10	11	12	13
	3	27.5	1	7	8	3	4	5	6	10	13
710	1	23.4	3	4	5	5	9	11	12	14	15
	2	22.5	1	3	9	1	4	5	11	12	15
	3	22.3	3	5	8	3	5	7	13	14	15
900	1	29.3	3	4	5	2	5	7	10	12	15
	2	26.5	2	3	5	1	5	6	8	13	15
	3	26.2	2	5	9	1	3	4	5	6	10

The experimental results of these speaker optimized configurations, along with the corresponding PZT tests (discussed earlier) are shown in Table 3-15, Table 3-16, and Table 3-17. It is evident that the speaker tests do not perform as well as the PZT tests. This is a consequence of the PZT output waves matching better with the primary disturbance waves.

The 508.75 Hz cases showed no reduction at all with speaker actuation. This is probably a result of either collinearity or a change in the system after the optimization

FRF's were acquired. However the 710 Hz and 900 Hz cases showed consistent results. The 710 Hz cases showed error microphone reduction of 11.3, 11.0, and 16.3 dB. This is in sharp contrast to the superior results of 22.0, 19.1, and 21.2 dB found using the optimized PZT actuators. Nonetheless, the PZT's better error microphone performance came at no increase at the global microphones. Overall, the global microphones showed similar increases in noise levels for both the PZT and speaker actuation.

Comparing the results of the 900 Hz cases shows that the speaker tests experiences error microphone reductions of 17.5, 13.6 and 11.5 dB. The PZT tests (discarding the case in which control was not achieved) showed reductions of 19.1 and 21.4 dB. Like the 710 Hz case, the error microphone performance for 900 Hz is much better with PZT actuation. The global microphones spillover levels are also slightly better with the 900 Hz case.

The overall conclusions from the ASAC-ANC comparison tests show that ASAC is superior. It provides better levels of control at the error microphones while spillover at the global microphones is the same as or better than the ANC case . From these tests it is proven that using active structural acoustic control on the trim panel gives better system performance than traditional active acoustic control.

Table 3-15, Single Frequency Optimal Speaker/PZT Analysis, 508.75 Hz.

Frequency: 508.75 Hz.						
Case	Speaker Theoretical Error Reduction (dB)	Speaker Actual Error Reduction (dB)	Speaker Actual Global Reduction (dB)	PZT Theoretical Error Reduction (dB)	PZT Actual Error Reduction (dB)	PZT Actual Global Reduction (dB)
1	31.1	1.8	-7.3	32.8	-11.5	-8.3
2	27.8	0.9	1.2	30.5	10.1	-5.7
3	27.5	-0.1	0.1	30.4	20.3	-3.4

Table 3-16, Single Frequency Optimal Speaker/PZT Analysis, 710 Hz.

Frequency: 710 Hz.						
Case	Speaker Theoretical Error Reduction (dB)	Speaker Actual Error Reduction (dB)	Speaker Actual Global Reduction (dB)	PZT Theoretical Error Reduction (dB)	PZT Actual Error Reduction (dB)	PZT Actual Global Reduction (dB)
1	23.4	11.3	-4.1	32.5	22.0	-8.3
2	22.5	11.0	-5.4	30.5	19.1	-3.9
3	22.3	16.3	-8.4	30.0	21.2	-4.7

Table 3-17, Single Frequency Optimal Speaker/PZT Analysis, 900 Hz.

Frequency: 900 Hz.						
Case	**Speaker Theoretical Error Reduction (dB)**	**Speaker Actual Error Reduction (dB)**	**Speaker Actual Global Reduction (dB)**	**PZT Theoretical Error Reduction (dB)**	**PZT Actual Error Reduction (dB)**	**PZT Actual Global Reduction (dB)**
1	29.3	17.5	-5.3	38.6	19.1	0.3
2	26.5	13.6	-10.4	35.8	21.4	-3.3
3	26.2	11.5	-5.6	34.4	1.2	-10.2

4. Broadband Control Experiments

Chapter 4 focuses on the broadband control experiments. The broadband controller will be briefly examined with its inherent advantages and disadvantages. Next will follow an explanation of the multiple testing configurations used to try to control the interior noise field from 500-1000 Hz.

4.1 Introduction to Broadband Experiments

The real purpose and motivation behind this project is to attempt to eliminate broadband noise radiating from the crown of the aircraft in the 500-1000 Hz range. The single frequency analysis only aids in determining control trends and serves as a

benchmark for the maximum expected performance that can be achieved with broadband control. Single frequency control at this frequency range would serve no real purpose in an actual flight test since the dominant noise is broadband and not tonal.

Although broadband control brings with it the promise of controlling more than one frequency with random variation, it is slower than a single frequency controller because more FIR filter coefficients are needed. The broadband controller also has difficulties with causality. Unlike single frequency sine waves, random broadband acoustic radiation is non-deterministic in nature. With a single frequency harmonic sine wave it is possible (knowing the frequency) to determine the response at any future time. With broadband random noise this is not possible. This is one of the major hurdles of applying adaptive feedforward broadband control. If the controller does not receive and produce the appropriate control response before the disturbance waves pass the actuators, then the control system is acausal.

The causality issues of adaptive feedforward broadband control systems has been addressed by Vipperman[38]. A system becomes acausal when the propagation time through the control path is longer than the propagation time through the disturbance path (Figure 4-1). For example, to attain proper control the disturbance signal must be sensed by the accelerometer on the skin, be amplified by the accelerometer pre-amplifier, pass through the A/D, be processed by the controller, pass back out through the D/A, proceed through

the filters, amplfierss and transformers and provide a voltage to the PZT's creating noise at the error microphones before the disturbance signal passes from the outer skin to the error microphones.

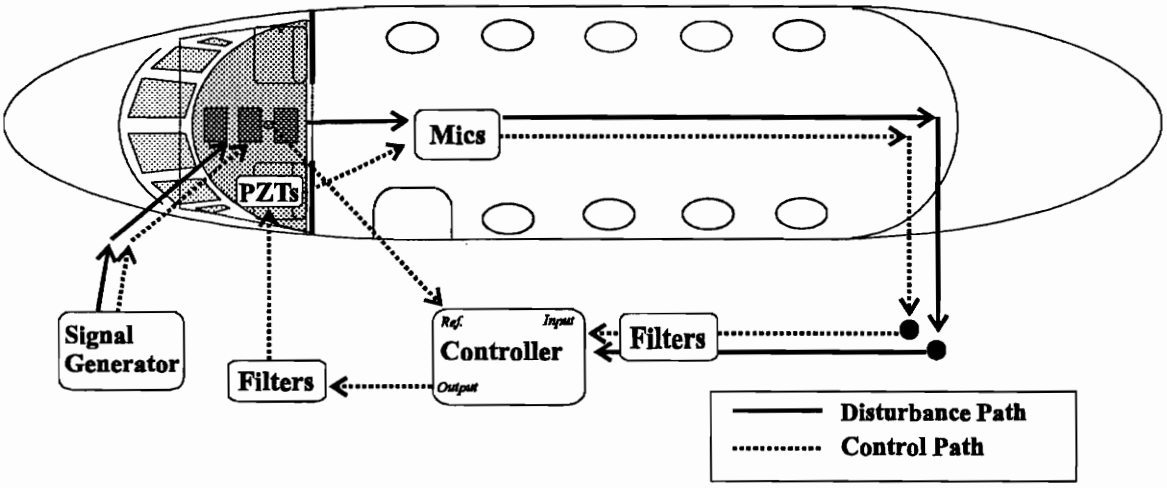

Figure 4-1, Controller Signal Paths

Another problem confronting broadband control is its slow multi-channel A/D sampling rate of current DSP technology. Single frequency control is only required to process two FIR filter coefficients per transfer function to exactly model phase and magnitude. Therefore a 6I3O single frequency controller would possess a total of 36 FIR filter coefficients. The 6I3O single frequency controller could easily operate at a sampling rate of 5000 Hz (5 times the highest operating frequency). However with broadband control, with a complicated system such as the Cessna Citation fuselage, 36 coefficients per transfer function would be the bare minimum for covering the 500-1000 Hz range. In

fact, the fastest the DSP can sample with a 3I3O system with 152 filter coefficients per transfer function is 3300 Hz. This is only slightly more than three times the highest disturbance frequency of 1000 Hz. It is evident that there are significant hardware hurdles standing in the way of the broadband controller for this application.

The specific filtered-X LMS broadband controller used for these experiments is designed so that the user can custom select the number of reference channels, input channels, output channels, sampling speed, and number of filter coefficients. In addition, the controller has a built in white noise signal generator which can be tapped into and delayed to act as a control reference signal. This internal delayed reference signal is helpful for situations in which it is desirable to factor out the affects of causality to better examine how other variables affect control. The controller used in these experiments allows for the online viewing of the filter coefficients and input and output voltages through the computer monitor.

Over 170 individual broadband control tests have been performed. These tests were performed very similarly to the single frequency tests explained earlier. For each of these tests the calibrated microphone levels were recorded both before and after control. The overall SPL was post-calculated by a summation of the auto-spectrum frequency bin levels from 500-1000 Hz. The spectrum responses for each of the sixteen microphones (in the same locations as the single frequency tests) were saved before and after control at a

1.25 Hz resolution up to 2000 Hz. Also saved for analysis were the FIR filter coefficients for both system identifications and control.

4.2 SISO Controller Parametric Studies

The limited maximum sampling speed of the DSP is affected by a number of conditions. These factors are: the number of reference, input, and output channels; the number of FIR filters per reference/input/output; and whether or not the reference signal is sampled externally or internally. Since the controller DSP speed is limited, it is important to determine the best compromise with the numbers of input/output channels, FIR filter coefficients, and sampling rates. Controller performance is also strongly dependent upon the feedforward reference signal. The effects of signal generator delay, and internal verses external referencing should also be examined.

Therefore, three parametric studies are presented which examine the effects of varying the number of FIR filter coefficients, the controller sampling rates, and the reference signal. All tests were performed in a single input-single output (SISO) configuration with microphone #7 (located near the pilot's left ear) as the error sensor and all of the operating PZT's wired in parallel serving as the control output. Except for the experiments testing the control reference, for consistency, all tests were run with a

reference signal being tapped and delayed 20 samples from the signal generator. The delayed reference allows for better overall control, providing more insight into observing other control performance trends. The signal generator and actuator outputs were both band-passed filtered from 500-1000 Hz. The error microphone input, however, was only low pass filtered at 1000 Hz.

The first parametric test was designed to study the effects of the number of FIR filter coefficients. The tests used the previously described microphone #7 as an error sensor with all the actuators running in parallel as control output. The disturbance was 500-1000 Hz random noise created from the three enclosure disturbance speakers described earlier. The sampling rate was 5000 Hz, while the internal signal generator delay was set at 20 samples. Seven tests were performed in which the number of FIR filter coefficients were varied from 20 to the controller maximum of 255. The results of the error microphone reduction and the average response at the global microphones are calculated in the same fashion as the single frequency tests except that the reduction values are integerated over the entire 500-1000 Hz bandwidth. The results can be seen in Figure 4-2.

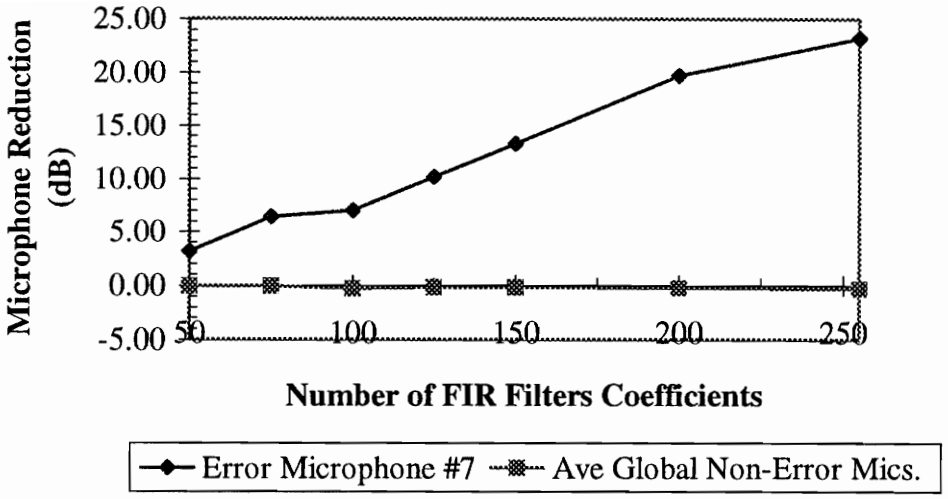

Figure 4-2, Number of FIR Filters SISO Parametric Study

It is shown in Figure 4-2 that the number of FIR filters plays a significant roll in controller performance. The error sensor reduction level steadily decreases as the number of filter coefficients decends. The performance drops 20 dB (from 23.2 to 3.12 dB reductions) when the number of FIR filters is dropped from 255 to 50. As for the effects at the global microphones, their response is generally unaffected by the number of filter coefficients. They show negligible increases ranging from -0.04 to -0.31 dB.

The FIR control filter coefficients for the 255 and 50 coefficient cases are displayed in Figure 4-3 and Figure 4-4. The dashed vertical line on these figures indicate time zero. Time zero is defined as where the start of the filter window would be if there were no signal generator reference delay. It can be clearly seen that the N=255 filter

coefficients are significantly more detailed than the N=50 coefficients. This resolution results in a more detailed control response being sent to the actuators for a given reference input. This explains why better noise control is obtained with more FIR filter coefficients. In fact, because the end coefficients do not taper back down to zero, the N=50 case looks almost unstable even though the controller stabilized. With 255 FIR filter coefficients, the resulting coefficient frequency resolution is approximately 20 Hz wide when sampled at 5000 Hz. This is contrasted with a resolution of 100 Hz when only 50 FIR filter coefficients are used.

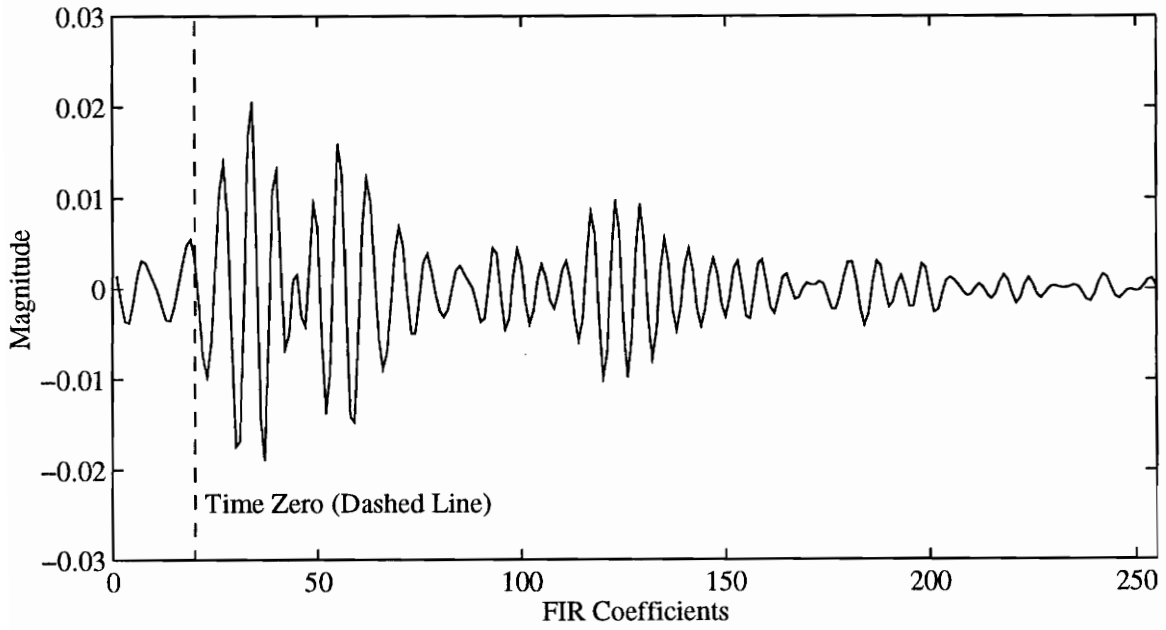

Figure 4-3, Filter Number Parametric Study, FIR Filter Values for 255 Coefficients

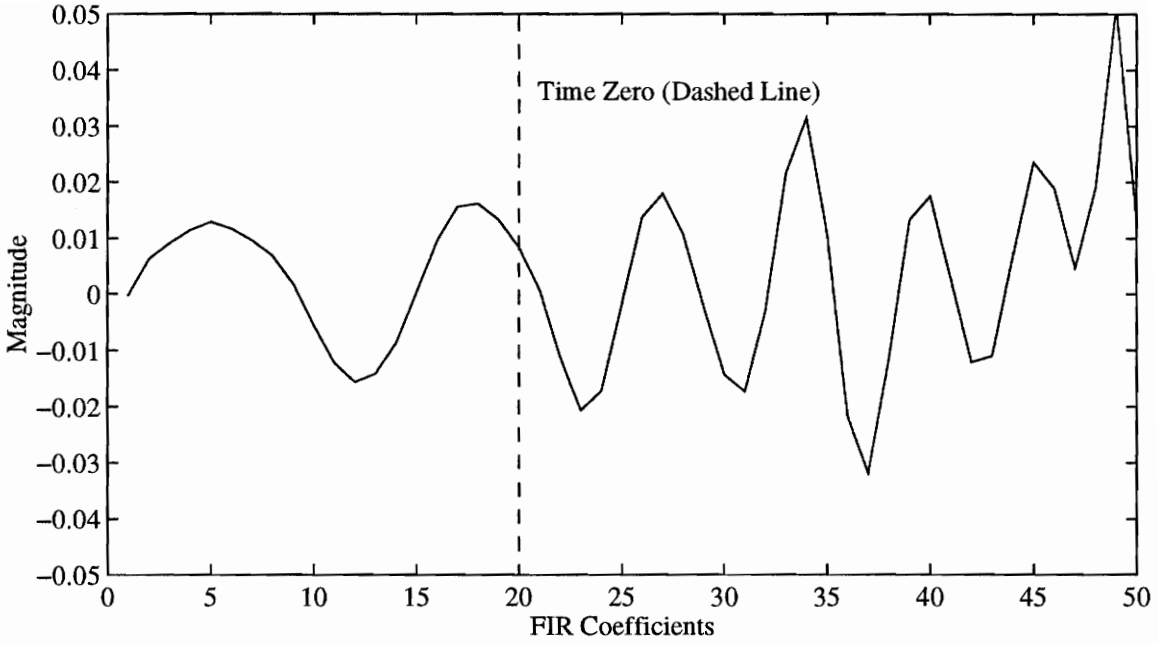

Figure 4-4, Filter Number Parametric Study, FIR Filter Values for 50 Coefficients

The next set of parametric tests was designed to verify what effect the A/D sampling frequency has on control. Tests were again run SISO with the same sensor and actuator configuration as previous parametric tests. The number of filter coefficients was fixed at 255 while the sampling frequency was varied from 5000 down to 2000 Hz. 5000 Hz is the maximum controller sampling rate while 2000 Hz is the theoretical minimum speed required to identify a 1000 Hz signal[39]. In order to maintain consistency, the signal generator delay was varied accordingly with the sampling rate from 20 samples at 5000 Hz to 8 samples at 2000 Hz. The results are shown in Figure 4-5.

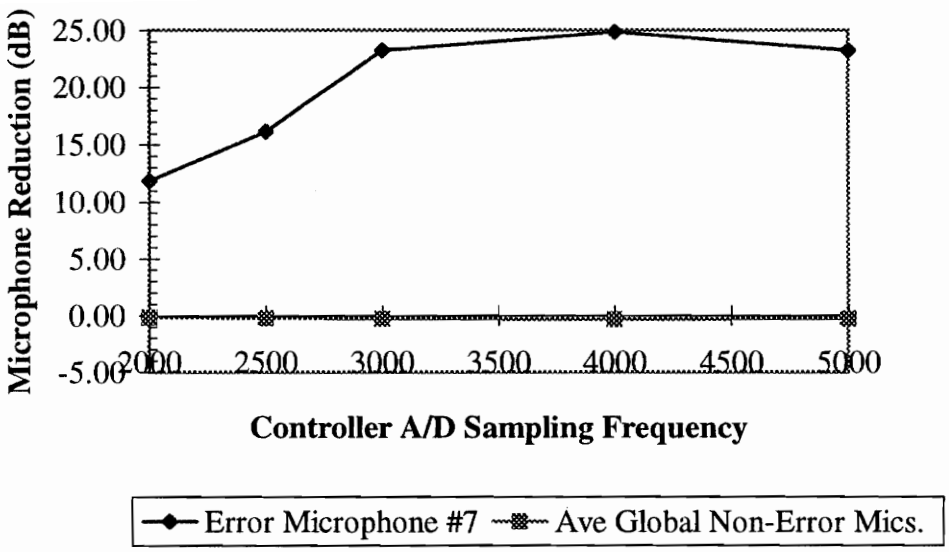

Figure 4-5, Controller A/D Sampling Parametric Study

Figure 4-5 shows that controller performance rolls off dramatically if the sampling frequency drops below 3000 Hz. This is due to the A/D not sampling fast enough to properly identify the 500-1000 Hz disturbance. The noise reduction plateaus in the 3000-5000 Hz sampling range with a slight peak at 4000 Hz. This plateau is a result of the compromise between sampling fast enough to identify the disturbance, and sampling slow enough to create a large time window to record the impulse. For example 3000 Hz is only three times the highest disturbance frequency but has a large time window of 85 ms. Sampling at 5000 Hz is 5 times the highest disturbance frequency however the impulse time window shrinks down to 51 ms. If more FIR filter coefficients then 255 were used then the plateau would most likely shift to a higher frequency because of a larger time

window. As for trends at the global microphones, they again seem to show consistent levels in the -0.1 to -0.4 dB range.

The impulses for the 5000 Hz and 2000 Hz cases can be seen in Figure 4-6 and Figure 4-7. It should be noted that the 5000 Hz sampling impulse is well defined. The waves are individually clearly defined and are somewhat rounded with the impulse tapering to the noise floor towards the 255th coefficient. The 2000 Hz impulse, however, is irregular, lacking resolution with compacted peaks. The filter coefficients from 100 to 255 show nothing but noise. These coefficients would be better used to create more resolution of the main impulse peaks.

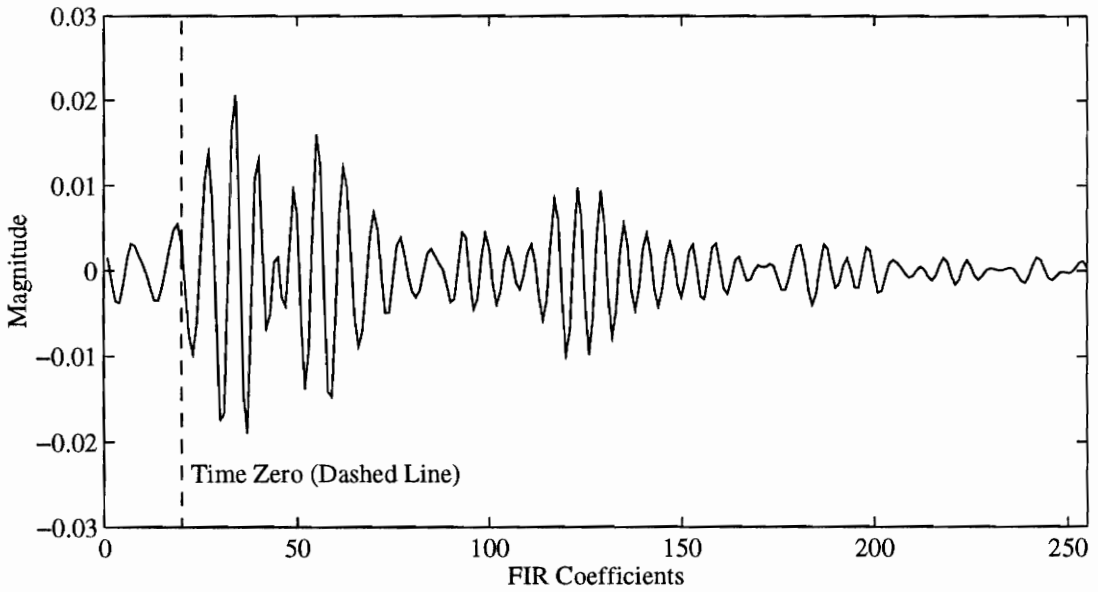

Figure 4-6, Sampling Rate Parametric Study, FIR Filter Coefficients for 5000 Hz Sampling Rate

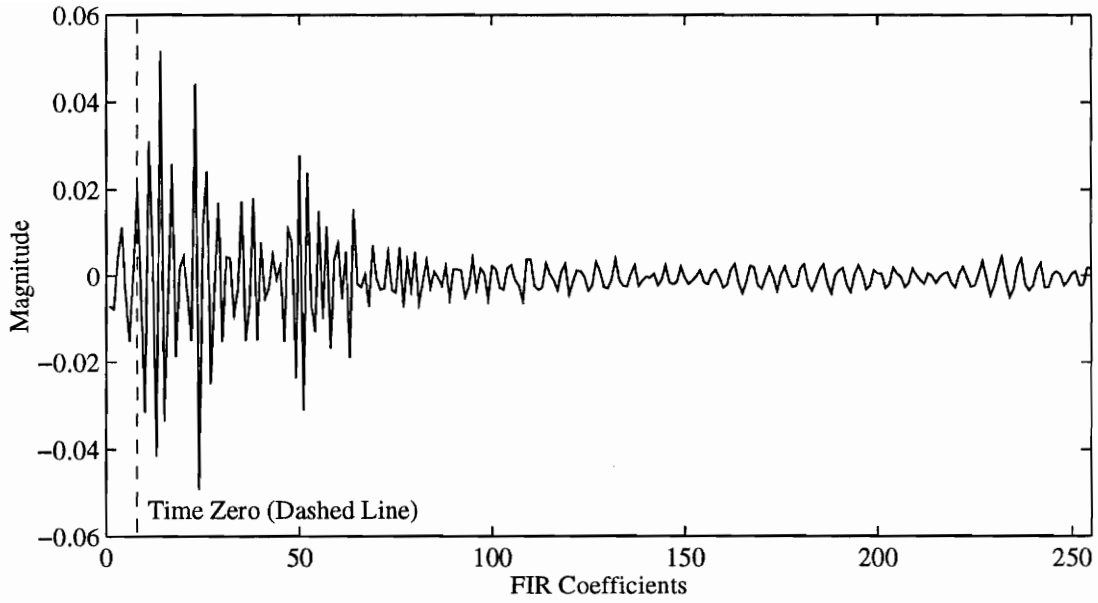

Figure 4-7, Sampling Rate Parametric Study, FIR Filter Coefficients for 2000 Hz Sampling Rate

The final parametric test varied the controller reference signal to investigate the issue of causality. For this study, three types of reference signals were employed: a delayed internal reference signal acquired from the signal generator, an external (non-delayed) reference signal also acquired from the signal generator, and an external reference signal acquired from a accelerometer located on the fuselage skin.

The internal delayed reference signal works by obtaining the reference signal from the controller DSP signal generator. The DSP signal generator sends a signal to both the disturbance and control reference input, however the disturbance signal can be delayed relative to the control reference signal. This delay gives the controller an advantage in

anticipating what signal the disturbance will receive. Varying the delay will give insight into how the controller would react if it was faster, and to what extent does acausality contribute to poor control performance.

The second type of reference signal evaluated is acquiring externally from the signal generator without delay. Here the controller receives the same reference signal as the disturbance at the same time. The third evaluated method of obtaining the reference signal is to draw the signal directly from the vibration of the skin of the aircraft with an accelerometer. This is the most realistic method that would be used in an authentic aircraft application.

An analogy of these different ways of obtaining the reference signal can be drawn to an isolated stock broker in 1917, living far out in the country without any telephone, television, or radio. His main goal is to be able to make as much money as he can based upon information on the stock market. This is analogous to the controller's goal of minimizing noise at the error microphones. However his only form of information is his mail which, by the time it gets to his house, informs him of the market 5 days late. This delay hinders him from reacting fast enough to make a profit. This is equivalent to the controller receiving its reference signal from the external accelerometer so that, by the time the signal passes through all the amplifiers and filters, the controller may not be able to react quickly enough to cancel noise at the error microphones. However, if technology

advances and the stockbroker is able to obtain a telephone, then he can react to the market quickly the same day. Being able to react quickly greatly improves his chances towards making a profit. This is analogous to the controller receiving its signal externally from the signal generator. While this may not break the laws of physics, it is impractical to implement realistically with current technology. The final method of acquiring the control signal with the internal delayed reference signal is analogous to the stock broker having a crystal ball allowing him to see the future of the stock market. This breaks the laws of physics just as the delayed internal reference signal cannot be practically implemented in a in-flight application. However the broker with a crystal ball shows what the maximum amount of money someone can make on the market and it factors out the influence of how quickly the broker receives market information. This provides insight into the market itself which relates to learning more about the control system without worrying about causality.

Tests were performed at with error microphone #7, a sampling frequency of 5000 Hz, 255 filter coefficients, and with the control reference signal varied from 30 down to 2 samples. The resulting error sensor reductions (integrated over the control bandwidth) are shown in Figure 4-8. Since the DSP has to sample an extra channel for the two external reference signal tests, these tests could only be run with a sampling rate of 3000 Hz to maintain the same number of 255 FIR filter coefficients.

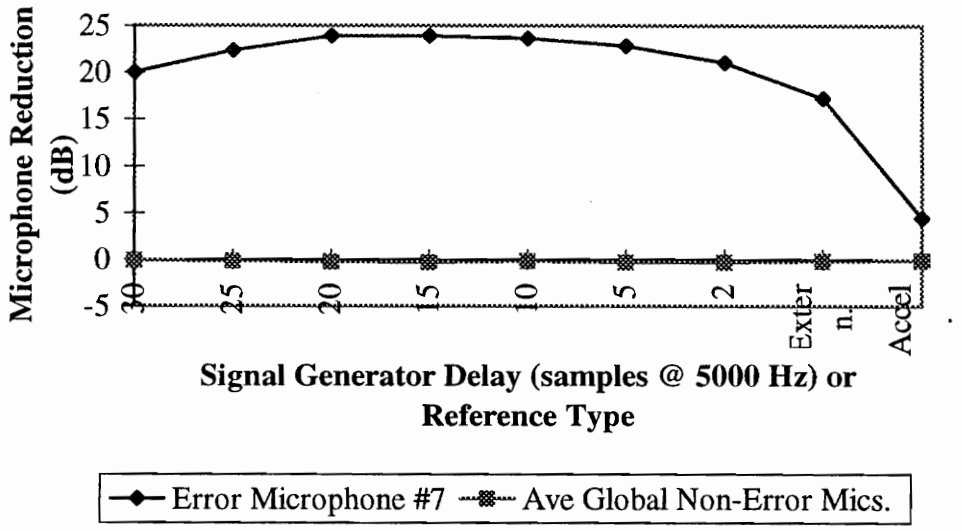

Figure 4-8, Reference Signal Parametric Tests

From these parametric results it is indicated that the performance shows a gradual increase and then decrease in attenuation that peaks at a delay of 15-20 samples. This is probably the result of having to center the impulse in the FIR window. In other words, since the number of FIR filter coefficients is finite, a compromise must be struck between adding more samples before or after main impulse. (If the sampling delay is too long, the end of the impulse is amputated while if the delay is too short, the beginning of the impulse is cut off.)

Looking back at Figure 4-8, a pronounced drop in performance occurs when the signal is tapped externally from the signal generator. (3.8 dB less reduction than with a delay of 2 samples.) This is explained by having a slower sampling rate of 3000 Hz due to

the fact that the A/D is now sampling another channel. Meanwhile, a distinct plunge in performance occurs when the signal is taken from the reference accelerometer mounted on the skin of the aircraft. The FIR filter coefficients for this case, along with the 20 sample delay case can be seen in Figure 4-9 and Figure 4-10.

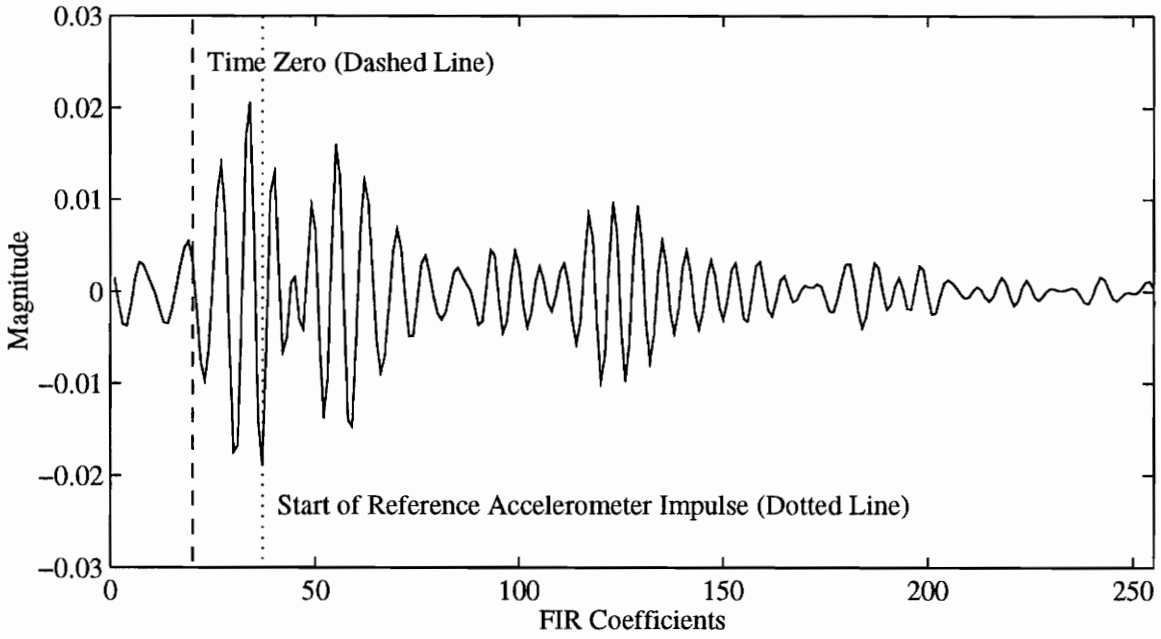

Figure 4-9, FIR Control Coefficients, Internal Reference Delayed 20 Samples

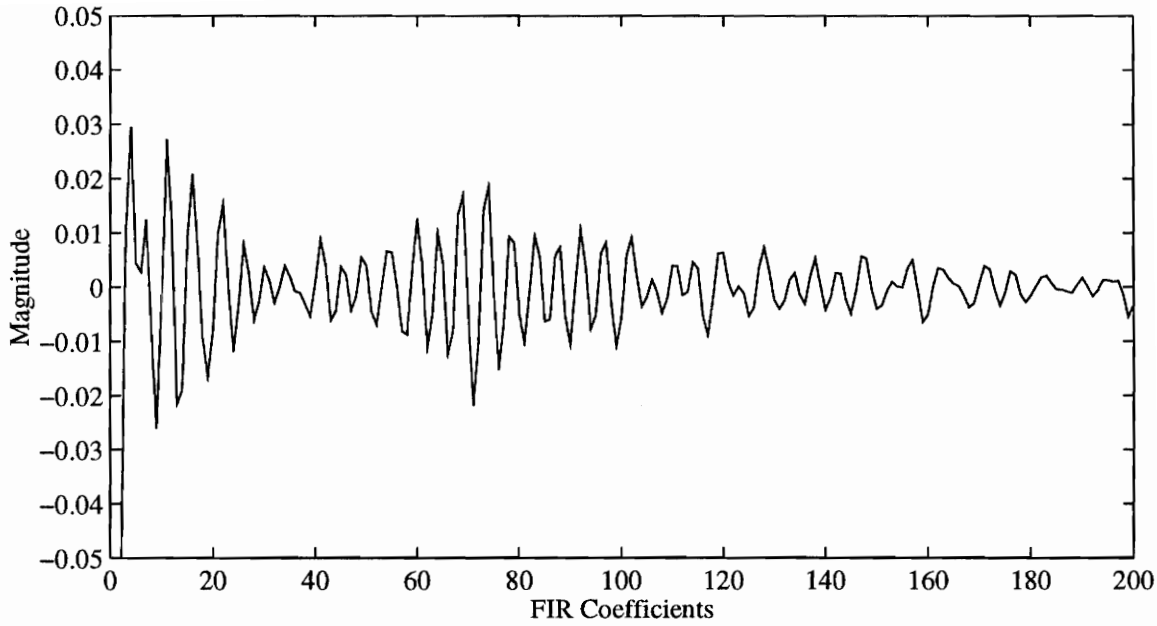

Figure 4-10, FIR Control Coefficients External Accelerometer Reference

4.3 Causality Analysis

The reason for the degradation in controller performance when the reference signal is obtained from the accelerometer may be caused by two reasons. Either the reference signal is not coherent with the error signals, and/or there is a problem with causality. Feedback is not an issue here since there is little coupling between the trim panel and outer fuselage skin. The trim panels vibration has a far greater affect on interior noise levels than the vibration of the outer skin. Tests have verified that the use of electronic feedback removal does not improve system control performance. To investigate the reference

signal quality, the coherence and frequency response function between the error microphone and reference accelerometer was measured. (Figure 4-11). Ideally, the coherence should be one except at the anti-nodes of the frequency response function. From Figure 4-11 it can be seen that the coherence between the disturbance signal generator and reference accelerometer is very good. The few dips that occur correspond with anti-nodes and the coherence is mainly above 0.99 for most of the frequency range. Therefore it can be concluded that the reference accelerometer signal is of good quality.

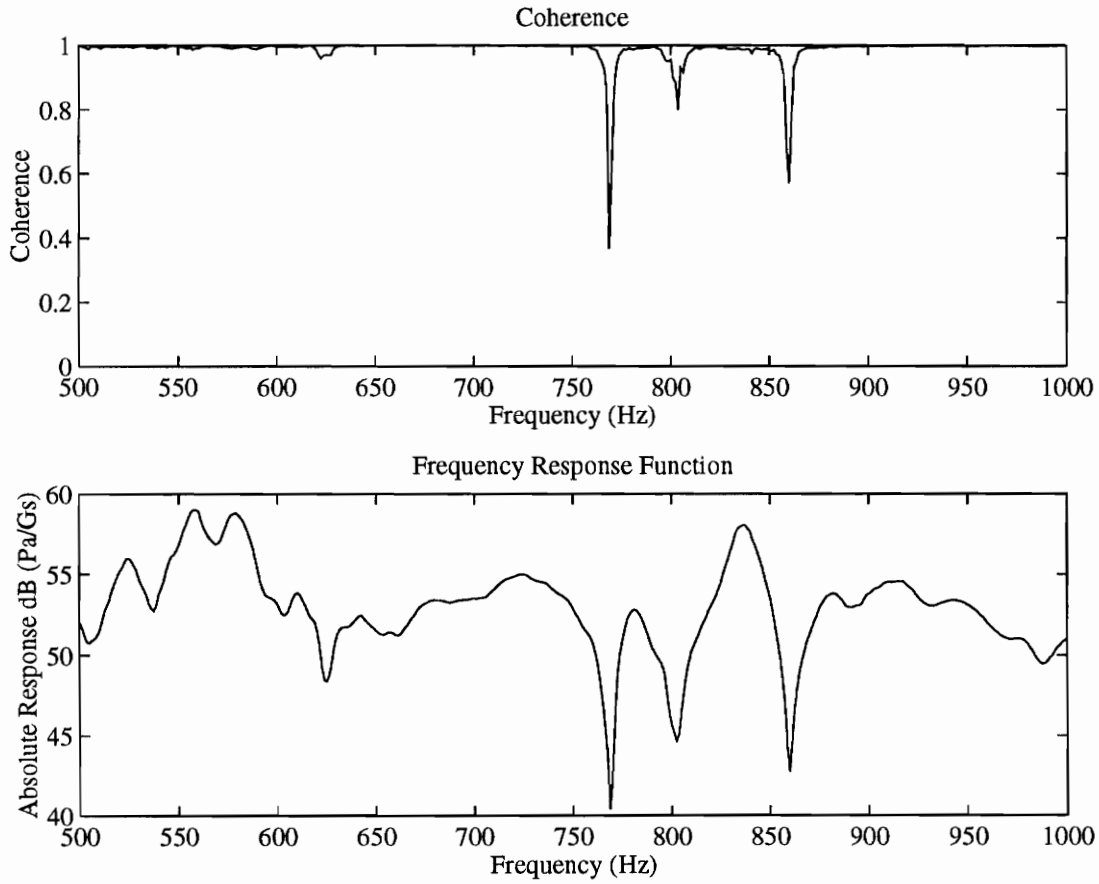

Figure 4-11, Coherence and FRF of Roof Accelerometer Signal to Microphone #7

The next point of investigation over the poor performance of the external reference tests is to investigate the system causality. The first way of checking this is to look at the FIR filter coefficients (Figure 4-9 and Figure 4-10). The external accelerometer FIR control coefficients shows that the control impulse is cut off on the left. This is an indication of acausality since the beginning of the impulse is not captured quickly enough for the controller to react.

To further investigate the system for acausality, the time needed for an impulse to propagate through the disturbance and control paths was measured. This was performed by sending an impulse through the system and measuring the average time delay at microphones #7 & #8 with a cross-correlation analysis. For a system to be causal the time it takes a signal to pass from the signal generator to the error microphones (disturbance path) must be less than the time it takes a signal to pass from the signal generator to the control reference through the control actuators and then to the error microphones (control path). The values shown in Table 4-18 indicate the results.

Table 4-18, System Causality Analysis

Signal Path	Time (Milliseconds)
Disturbance	56
Control	87

Table 4-18 demonstrates that the Cessna fuselage system is acausal by 31 milliseconds. This means that the first part of the disturbance impulse propagates past the active trim panel before the controller has time to react. This is shown visually in Figure 4-10 by the FIR filter coefficient's impulse having its maximum at the first filter coefficient. The impulse doesn't build up like the internal tapped and delayed signal. In other words, the approach to maximum is not gradual but rather occurs abruptly at the left hand edge of the impulse window. The dotted line on the 20 sample delayed test (Figure 4-9) approximates where the accelerometer pulse is first received. (This was calculated by counting the waves from the first lull at about 100 samples on the delayed impulse) Thus the system is acausal and all the information to the left of the dotted line passes to the error sensors before the controller can react and cancel it. This explains the reduction in control attenuation when using the external reference accelerometer

The conclusion of these three parametric tests and causality analysis is that the controller speed is critical with this setup. The controller performance relative to the number of FIR filter coefficients seems to continually increase up to when the maximum 255 filter coefficients are used. The response due to varying the sampling speeds show a plateau from 3000-5000 Hz thus indicating a compromise between slower sampling speeds and too small a impulse time window. The results from varying the reference signal showed a maximum with an internal delay of 15-20 samples. Causality problems

result when the reference signal is acquired from the skin of the aircraft as would be with an flight ready application. The maximum SISO performance seems to be with 255 FIR filter coefficients, a sampling rate of 5000 Hz, and with a internal signal generator delay of 20 samples.

4.4 SISO Experiments

4.4.1 SISO Tests With Internal Delayed Reference Signal

After the parametric studies, the next set of broadband experiments are the single input-single output control tests. Because of the preliminary poor response and causality concerns of using the external reference accelerometer, the strategy here (and throughout the rest of the broadband tests) was to first perform multiple SISO tests with a delayed internal reference signal tapped off the signal generator, then once an acceptable configuration was found, the test was repeated with the external reference accelerometer.

For the following SISO tests control actuation was provided by powering all of the operating PZT's in phase with the same signal. Proper phase orientation of the actuators was checked with an accelerometer before testing. This was accomplished sending a sine

wave signal through the PZT's and measuring the phase of the vibration of the PZT's individually with an accelerometer located next to the actuator. The reason for connecting the PZT's together is to attempt to excite the panel in a distributive fashion so that the actuators will either minimize sound transmission through the panel or serve as an active source to cancel existing noise. For the tests the optimal fastest SISO controller settings were used. This means the A/D was sampling at 5000 Hz, with 255 FIR filter coefficients, and an 20 sample delayed internal reference signal. The results are shown in Table 4-1. Please refer to Figure 2-3 and Figure 2-5 for locations of microphones and PZT actuators.

Table 4-1 shows the four tests illustrating three possible control strategies with the reference signal being acquired and delayed from the signal generator. Using error microphone #3, it is theorized that by placing the error sensor right below the panel in the direct field where the noise enters, the incoming noise will be canceled and the fuselage's overall noise level will be reduced. The second control strategy is demonstrated by the tests with error microphones #7 and #8 in which it is attempted to reduce the noise only at the pilot's ear. The final strategy is to try to reduce noise in the far-field by placing the microphone in the back of the plane.

Table 4-1, SISO Broadband Tests, Delayed Reference Signal

Error Microphone	Error Microphone Reduction (dB)	Global Microphone Reduction (dB)	Ratio of Error Mic Reduction to Global Mics Reduction.	Error Microphone Location
3	13.6	-2.58	-5.3	6 Inches (152 mm) Below Panel
7	23.2	-0.31	-74.8	Left Pilot's Ear
8	14.3	-2.85	-5.0	Right Pilot's Ear
14	3.6	-0.89	-4.0	Rear Center of Cabin

The results of the tests show that good localized reduction is achieved with the error microphones located near the panel or at the pilot's ears. When the error microphone was located in the back of the plane, its reduction was very low at only 3.6 dB. This is most likely caused by two factors. First, since the microphone is much further from the disturbance a larger reference delay is needed to center the impulse because of the longer time it takes for the noise to propagate to the back of the plane. Secondly, although intensity measurements show that most of the noise is radiating through the trim panel, some noise is undoubtedly flanking around the panel and cannot be directly controlled by the active panel. This affect is more pronounced in the rear of the aircraft, away from the direct field affects of the radiating crown trim panel. The spectrum

responses of each of these tests can bee seen in Figure 4-12 through Figure 4-15. Also shown is a typical global microphone spectrum in Figure 4-16.

In the SISO test with the error microphone near the trim panel (microphone #3 Figure 4-12) the acoustic spectrum before and after control shows that the peaks of the spectrums from 500-600 Hz and 750-900 Hz are reduced nicely to provide a good bandwidth reduction of 13.6 dB. This occurs because the high noise levels in these frequency ranges contribute most to the controller cost function and are easier to reduce.

Looking at the before/after spectrums of the error microphones at the pilot's ears (Figure 4-13 and Figure 4-14) it can be seen that with error microphone #7 there is a larger noise reduction (23.2 dB) than with error microphone #8 (14.1 dB). This is explained by the test with error microphone #7 having a higher before-control spectrum than error microphone #8. This is especially evident in the 650-750 Hz range. The reduction of this peak provides a much greater noise reduction for microphone #7 than microphone 8. Also contributing to the differences in reduction is the after-control peak at 525 Hz for microphone #8. This peak most likely results from the actuators inability to couple into the acoustic field at the error sensor for that frequency.

Examining the before and after responses for error microphone #3 located at the back of the plane (3.6 dB reduction), the only region of control is in the 650-750 Hz

range. Here, 10-15 dB of control is achieved while the rest of the frequency range remains unaffected.

Finally, a spectrum response of a typical global microphone from the test with error microphone #8 is shown in Figure 4-16. Here the before/after spectrums of microphone #15 are exhibited. The spectrum increases 5 dB while control is applied. Most of this increase occurs in the 450-650 and 775-825 Hz frequency ranges. Coincidentally, this is where the error microphone (Figure 4-14) shows the most reduction. The control effort that reduced the microphone response at the error microphone directly increases the response at the global microphones. This is typical of other global microphone response spectrums where a net noise increase was observed.

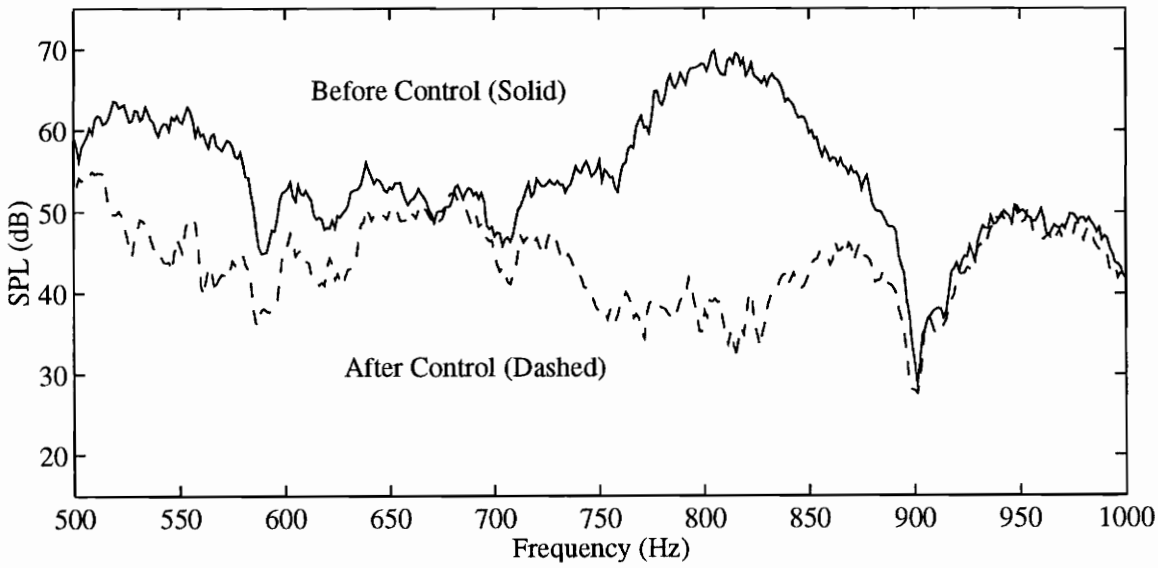

Figure 4-12, SISO Broadband Tests, Internal Ref Sig, Error Mic 3, 13.6 dB Reduction

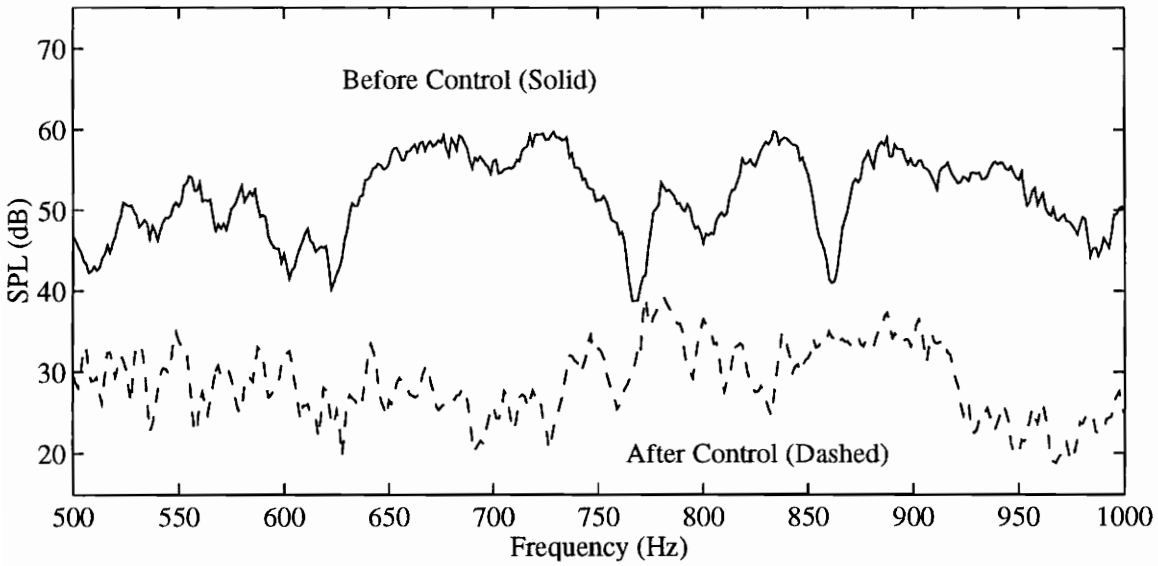

Figure 4-13, SISO Broadband Tests, Internal Ref Sig, Error Mic 7, 23.2 dB Reduction

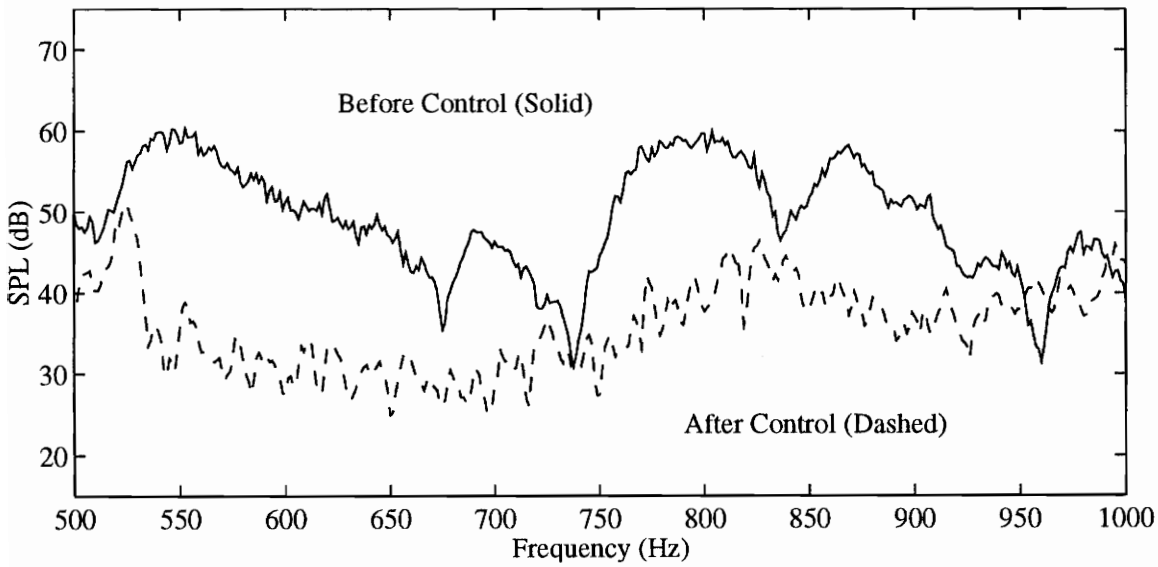

Figure 4-14, SISO Broadband Tests, Internal Ref Sig, Error Mic 8, 14.1 dB Reduction

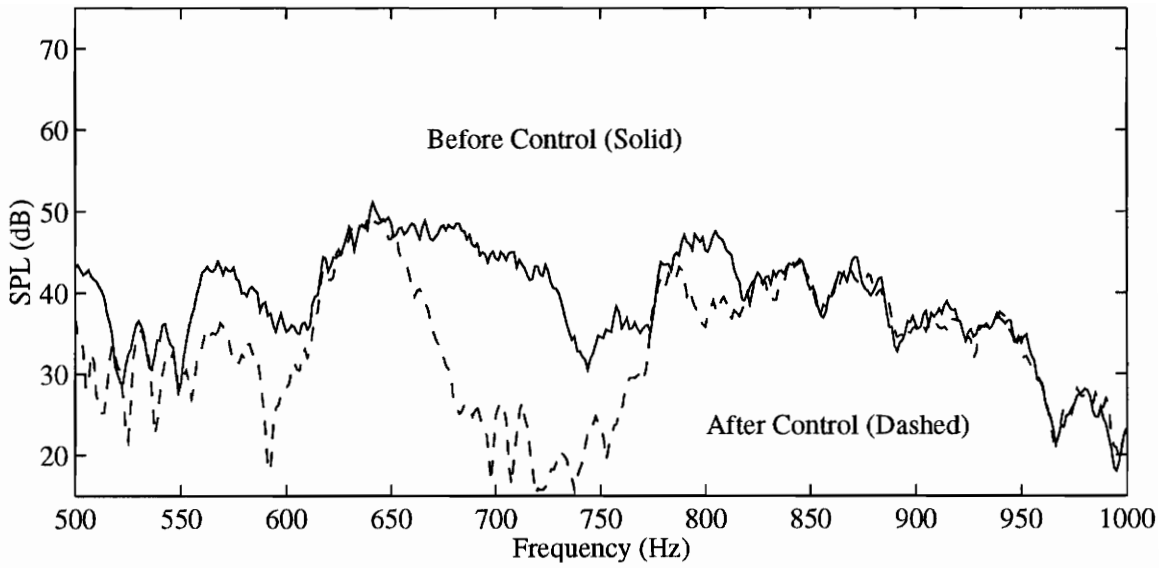

Figure 4-15, SISO Broadband Tests, Internal Ref Sig, Error Mic 14, 3.6 dB Reduction

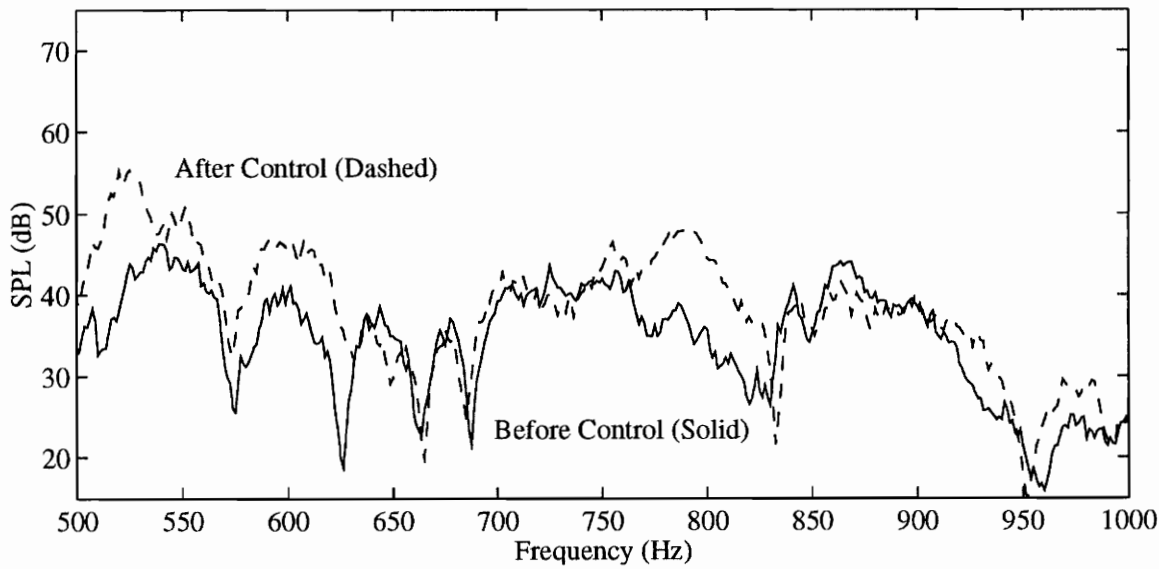

Figure 4-16, SISO Broadband Tests, Internal Ref Sig, Global Mic #15 Spectrum, (Error Mic #8)

When examining the effects of the global microphones, in all four SISO control cases the levels went up. None of the configurations were successful in achieving global attenuation. The cases with error microphones #3 and #8 showed large increases at 2.58 and 2.85 dB while the cases using error microphones #7 and #14 showed only 0.31 and 0.89 dB increases. For all cases except microphone #7 the average ratio of error microphone reduction to global microphone spillover ranges from 4:1 to 5.3:1. The error microphone #7 test has much better ratio at 74.8:1.

4.4.2 SISO with External Reference Accelerometer

Since the tests with error microphones #3 and #14 never achieved any reduction at the global microphones, the only SISO tests of practical merit were the tests with error microphones #7 and #8 which resulted in localized reduction at the pilot's ears. These tests were then repeated with the more realistic setup of obtaining the reference signal externally from an accelerometer on the crown skin of the aircraft. For these tests a small PCB accelerometer (about the size of a pencil eraser) was mounted on the skin of the aircraft with accelerometer wax (Figure 4-17). It was located 5 inches (127 mm) behind the 2nd speaker cone and 5 inches (127 mm) to the right of the centerline of the plane. This location was chosen because it is away from fuselage structural reinforcing ribs yet

near the speaker cones, providing for maximum vibration response. The tests were run with a sampling frequency of 3900 Hz and with 200 FIR filter coefficients. The results of these tests are illustrated in Table 4-2.

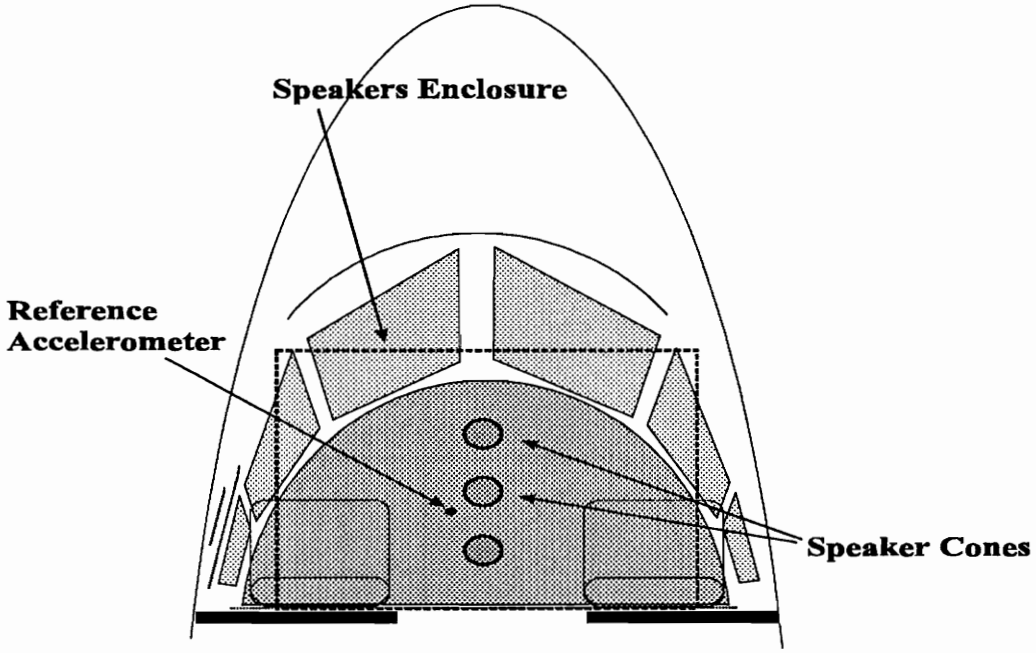

Figure 4-17, Reference Accelerometer Location

Overall, total reductions are much lower than with the internal signal generator reference tap. The before and after control spectrums can be seen in Figure 4-18. These graphs show that good control is obtained in the 850 to 1000 Hz range for the case with microphone #7 and in the 750 to 1000 Hz range for the case with error microphone #8. The controller also seems to show little control in the 500 to 650 Hz range. The poor control performance with the external reference accelerometer can mainly be blamed on system acausality.

Table 4-2, SISO Control Tests, External Accelerometer Reference

Error Microphone	Error Microphone Reduction (dB)	Global Microphone Reduction (dB)	Ratio of Error Mics Reduction to Global Mics Increase	Error Microphone Location
7	5.14	-0.18	28.5	Left Pilot's Ear
8	3.71	-2.45	1.54	Right Pilot's Ear

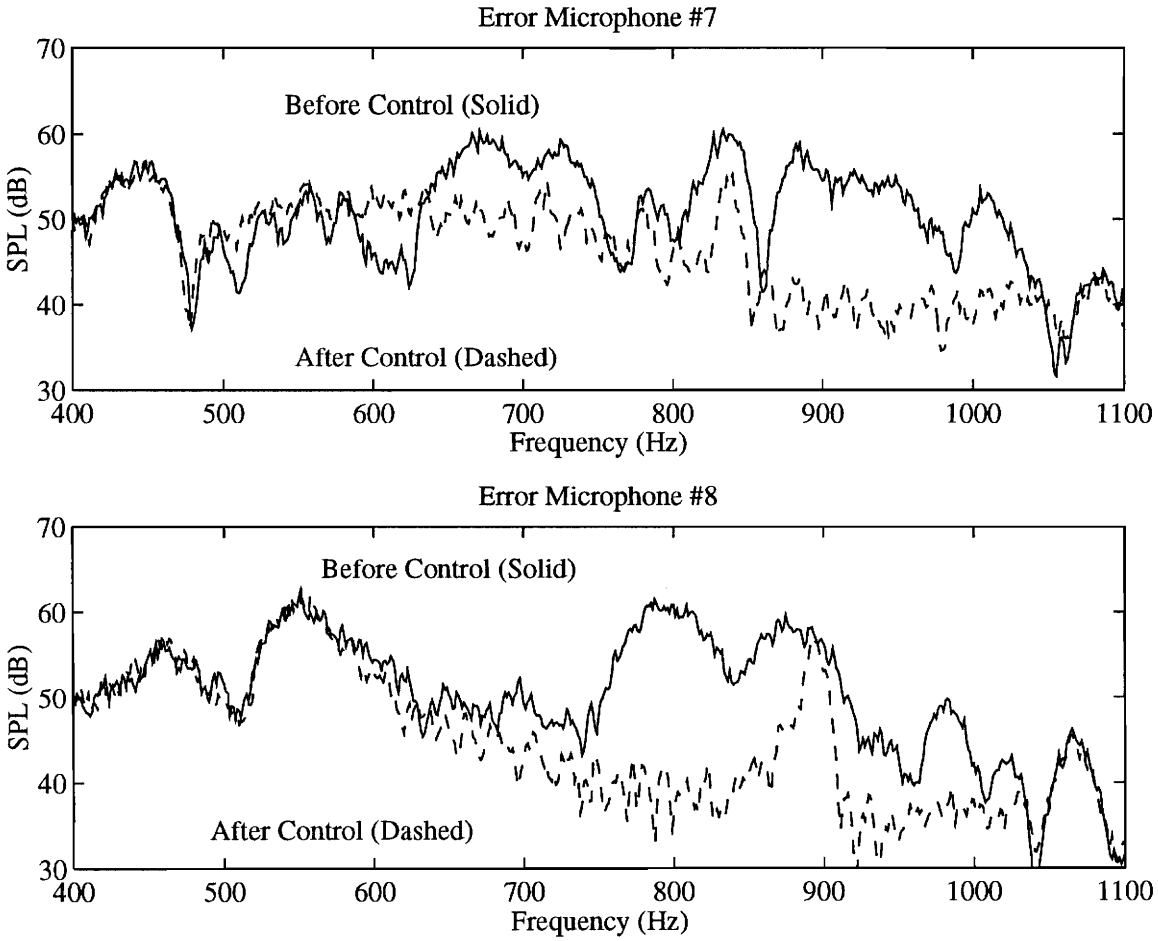

Figure 4-18, Spectrum Responses of SISO Tests with Accelerometer Reference Signal

4.5 Two Input-Two Output Broadband Tests

4.5.1 2I2O Tests With Varying Microphone Positions

From the SISO broadband tests the next set of tests are the 2I2O broadband experiments. The first series of 2I2O tests were designed to again check (by varying microphone positions) if it is possible to obtain a broadband global noise reduction. For control actuation, PZT #3 and #15 were wired together in phase to arbitrarily serve as one control channel while the rest of the PZT's (still wired in phase) served as the other control channel. The controller was operated at a sampling speed of 3800 Hz with 200 FIR filter coefficients per channel and an internal reference signal which was delayed 20 samples. Five different error microphone configurations were used for comparison for these tests. The results of these tests are shown in Table 4-3.

The results show that global control again is not achieved with any of the control setups. The nearest acheivement of any of the setups is an increase of 3.58 dB averaged

over the global microphones, with microphones #3 and #7 serving as error sensors. The average of error sensors reductions range from 8.5 dB with both microphones in the back of the cabin to 25.4 dB with one microphone located at the pilot's ear and one located directly below the crown trim panel.

Table 4-3, 2I2O Broadband Test Results, Microphone Location Varied

Error Microphones	Error Microphone Reduction (dB)	Global Microphone Reduction (dB)	Error Microphones Location
7,8	17.3	-5.45	Left And Right Pilot's Ear
3,7	25.4	-3.58	Below Panel, Pilot's Left Ear
3,14	14.1	-5.71	Below Panel, Back Cabin
3,9*	17.3	-4.21	Both Directly Below Panel
14,16	8.5	-8.99	Both In The Back Cabin

* indicates that microphone 9 was moved from its original location and tacked up near the panel.

4.5.2 2I2O Tests With Varying Actuators

Since none of the configurations came close to yielding global control, the only configuration of practical worth is the test using microphones #7 and #8 located at the pilot's ear. Using these microphones for error sensors creates a localized reduction zone centralized around the head of the pilot. These tests were repeated with a variety of

actuator configurations to determine the best actuation configurations at these microphones. The results are shown in Table 4-4.

It can be seen in Table 4-4 that the reductions fluctuate significantly with differing actuation schemes. The levels varied from a low error microphone reduction of 9.2 dB to 17.3 dB. The global microphone results also differ significantly from 2.63 dB to 5.45 dB. Overall, the actuation scheme with PZT's #2 and #9 wired in phase as one control channel and the rest of the PZT's as the other was judged to have the best compromise of localized reduction and minimized global microphone level increases. This test was then repeated utilizing the external reference accelerometer.

Table 4-4, 2I2O Broadband Test Results, PZT Actuators Varied

PZT Actuators	Error Microphone Reduction (dB)	Global Microphone Reduction (dB)
3&15 In Phase, Rest of Actuators In Phase	17.3	-5.45
3,8	13.2	-4.38
9,10	14.1	-3.21
2&9 Out of Phase, 3 and 8 In Phase	9.2	-2.65
2&9, Rest of Actuators In Phase	12.3	-2.63

The test using the external reference accelerometer was performed at the sampling speed of 3350 Hertz with 150 FIR filter coefficients per channel. This speed is slower then previous tests because more channels are being sampled requiring more filter coefficients and hence a slower sampling rate. The results are shown in Table 4-5. Once again, just as in the SISO broadband cases, the controller performance falls off dramatically when the external reference accelerometer is used. Again this is mainly attributed to the acauaslity of the system and the slow controller speed settings. The spectrum responses of the error microphones for this case can be seen in Figure 4-19. The spectrums show that for both error microphones, most of the measured overall reduction occurs in the 700-1000 Hz range. However, the overall reduction of 1.92 dB is not very significant and ranks as barely perceivable by the human ear.

Table 4-5, 2I2O Broadband Test Results, Accelerometer External Reference Signal, Error Mics 7&8

PZT Actuators	Error Microphone Reduction (dB)	Global Microphone Reduction (dB)
2&9 In Phase, Rest of Actuators In Phase	1.92	-0.43

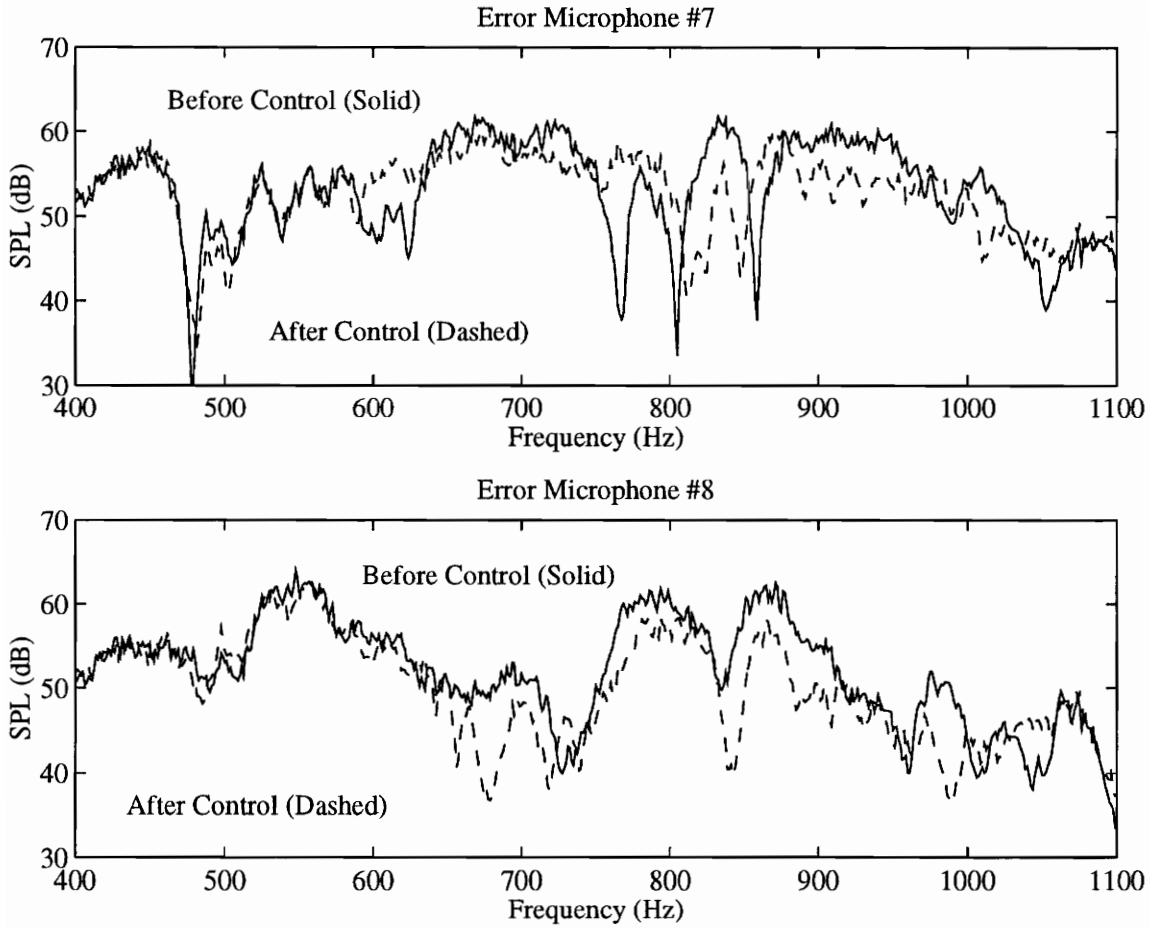

Figure 4-19, Spectrum Responses of Mirophones 7 and 8 with Broadband Control with External Accelerometer Reference

4.5.3 2I2O Tests With Off-Line Optimization

In order to choose the best actuators, an broadband off-line error microphone optimization algorithm similar to the single frequency analysis was performed. The difference between this optimization and the single frequency optimizations is that the total power reduction over the 500-1000 Hz bandwidth for all error microphones was calculated. This optimization was performed holding microphones #7 and #8 as error sensors and cycling through all possible 2I2O actuator arrangements. The top three configurations and their corresponding reductions are shown in Table 4-6

It is shown that choosing actuators with an off-line optimization proved to have little or no performance advantage over selecting actuators by pure intuition. One of the problems is that the off-line optimization is just a summation of single frequency control. It does not take into account the problems of causality or any of the ill effects of sampling frequencies or number of FIR filter coefficients. Therefore an intuitive approach towards actuator selection provides actuator configurations that perform just as well as the optimally selection configurations.

Table 4-6, 2I2O Broadband Optimizations With Error Microphones #7 & #8

Test Number	Actuator Configuration	Theoretical Reduction (dB)	Actual Error Microphone Reduction (dB)	Actual Global Microphone Reduction (dB)
1	12,15	25.14	9.55	-3.96
2	3,15	25.11	12.16	-5.84
3	2,8	25.09	11.63	-5.02

4.5.4 Reduction Zone Mapping

The next area of investigation deals with the size of the zones of reduction at the pilot's head. It is important to map out the zones of reduction to see if the localized reduction occurs over a large enough region to cover the size of a human head and yet allow for some movement. To perform this analysis 16 microphones were calibrated and mounted on a rod at a spacing of every 1.5 inches (38 mm). This rod was mounted horizontally on a microphone stand and measurements were taken to map out the acoustic field in a horizontal plane parallel to the floor, passing through the pilot's ears. Measurements were taken at 4 longitudinal positions. These measurements ranged from 3 inches (76 mm) behind the error microphones to 6 inches (152 mm) in front of the error microphones at 3 inch (76 mm) measurement spacing.

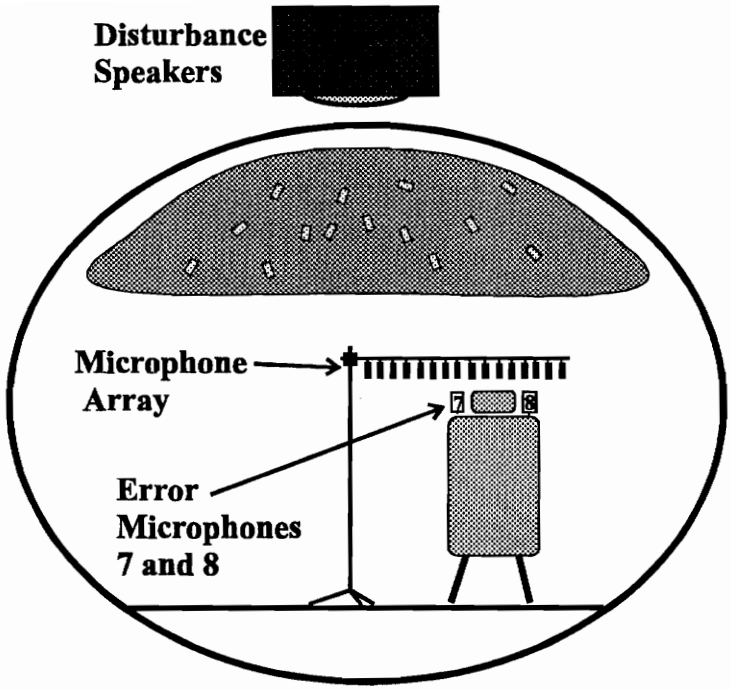

Figure 4-20, Microphone Array

Three control tests were performed with the 2I2O broadband configuration utilizing error microphones #7 and #8. One of the tests used the external reference accelerometer with the actuator arrangement of #2 & #9 in phase as control channel 1, and the rest of the actuators in phase as control channel 2. Another test was performed with the same actuation configuration but with a 20 sample delayed internal reference signal, while the final test was performed using internal delayed reference signal with the control output provided by speakers located at the pilot's seat and the co-pilot's window (speakers #3 and #5 in Figure 3-14). The speaker reduction zone contour plotting was intended to provide an comparison between active structural acoustic control of the interior trim panels, and traditional active noise control.

For the PZT configurations (Table 4-7), the levels of control for these tests were not identical to what was found experimentally previously. Differing conditions such as a bumped microphones or varying amplifier settings probably account for this, particularly with the delayed PZT case in which a reduction of only 8.44 dB was obtained compared with 12.3 dB as measured earlier.

Table 4-7, 2I2O Broadband Reduction Contour Zone Mapping Configurations and Control Levels

Test Number	Actuator Configuration	Reference Signal	Error Microphone Average Reduction (dB)	Global Microphone Average Reduction (dB)
1	2&9, Rest	External Accelerometer	2.07	-0.89
2	2&9, Rest	Internal Delayed 20 Samples	8.44	-2.83
3	Speakers 3 & 5	Internal Delayed 20 Samples	7.57	-3.41

The contour plots detailing overall bandwidth integrated reductions are shown in Figure 4-21 through Figure 4-23. Each contour indicates 1 dB of reduction. Positive contour values represent a noise reduction while negative contours indicate a noise increase ("spillover"). The first contour plot (Figure 4-21) is the test with PZT actuation

and an external accelerometer control reference signal. It shows a very low overall level of reduction around the two error microphones but this reduction zone is large enough to cover a human head. It also shows that the peak noise level spillover away from the error microphones does not get above 2 dB.

The second contour plot (Figure 4-22) is the same control configuration as the first PZT test except that the internal delayed reference signal was utilized. This test showed overall larger levels of localized reduction with contour peaks at each error microphone. However the increase in localized reduction comes at the price of having greater increases in noise levels away from the error microphones. This increase peaks out at -4 dB in the upper right corner of the plot. It should also be noticed that overall, the zero contour line tends to cover the same area as the with test 1. The zero line does close in on the top of the plot but on the bottom and left side of the error microphones it follows the same trace as test 1 while actually moving further out on the right side of the plot. This means delaying the reference signal creates roughly the same area of reduction, except with greater magnitudes of control and spillover.

The third contour plot corresponding with the speaker actuation case shows dramatically different results. The reduction levels are highly asymmetrical and skewed giving a much greater reduction at microphone #7 than microphone #8. The zone of reduction at the left ear (microphone #7) drops off steeply away from the error

microphone. This is in contrast with the area of reduction around the right ear which drops off more gradually. The zero contour line is drawn in much closer to the error microphones and spillover away from the error microphones reaches a increase of over 9dB.

When comparing the zones of reductions between tests 2 and 3 it is clearly evident that the ASAC configuration with its PZT actuators created a much better zone of reduction than the Active Noise Control case with its speaker actuation. This is because the control output noise waves from the PZT's of the ASAC system more realistically duplicated the disturbance waves than the output produced with just two ANC speakers.

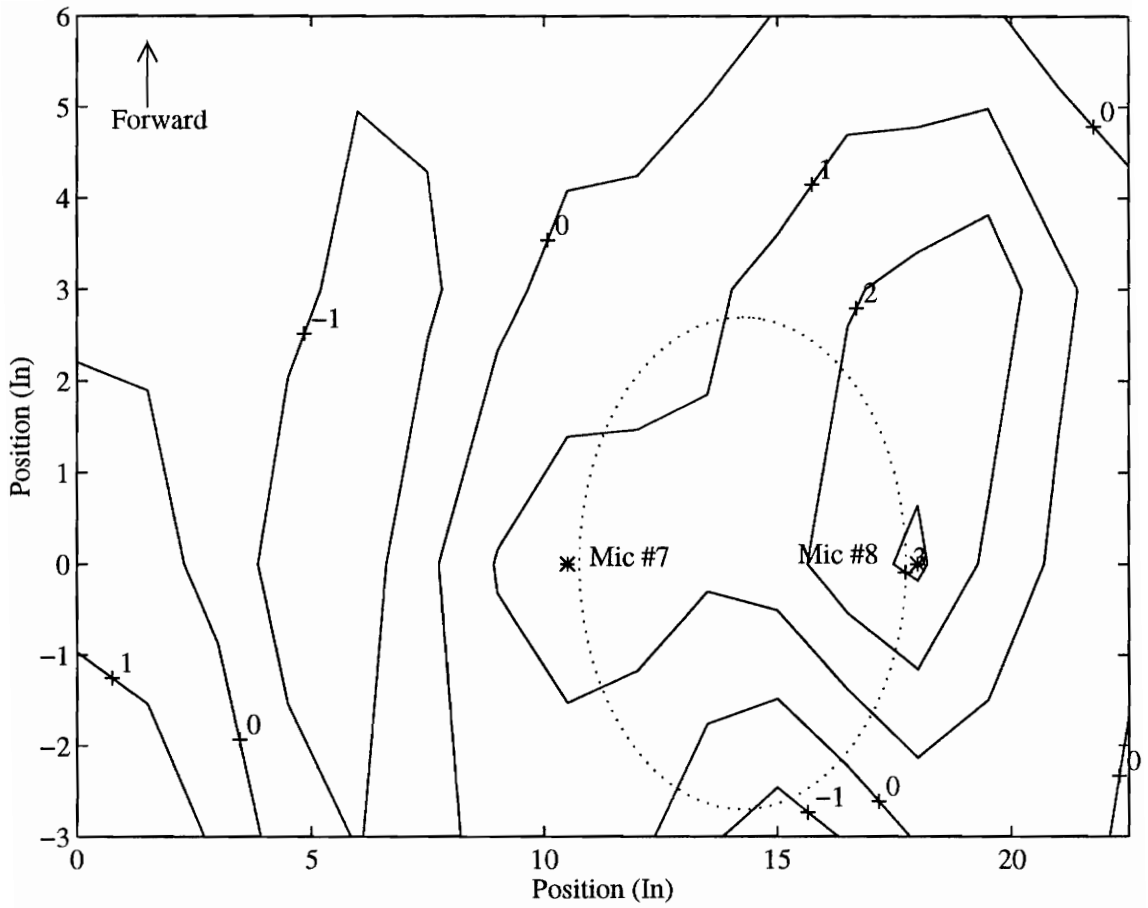

Figure 4-21, Contour Test #1, PZT Actuation, External Reference Signal

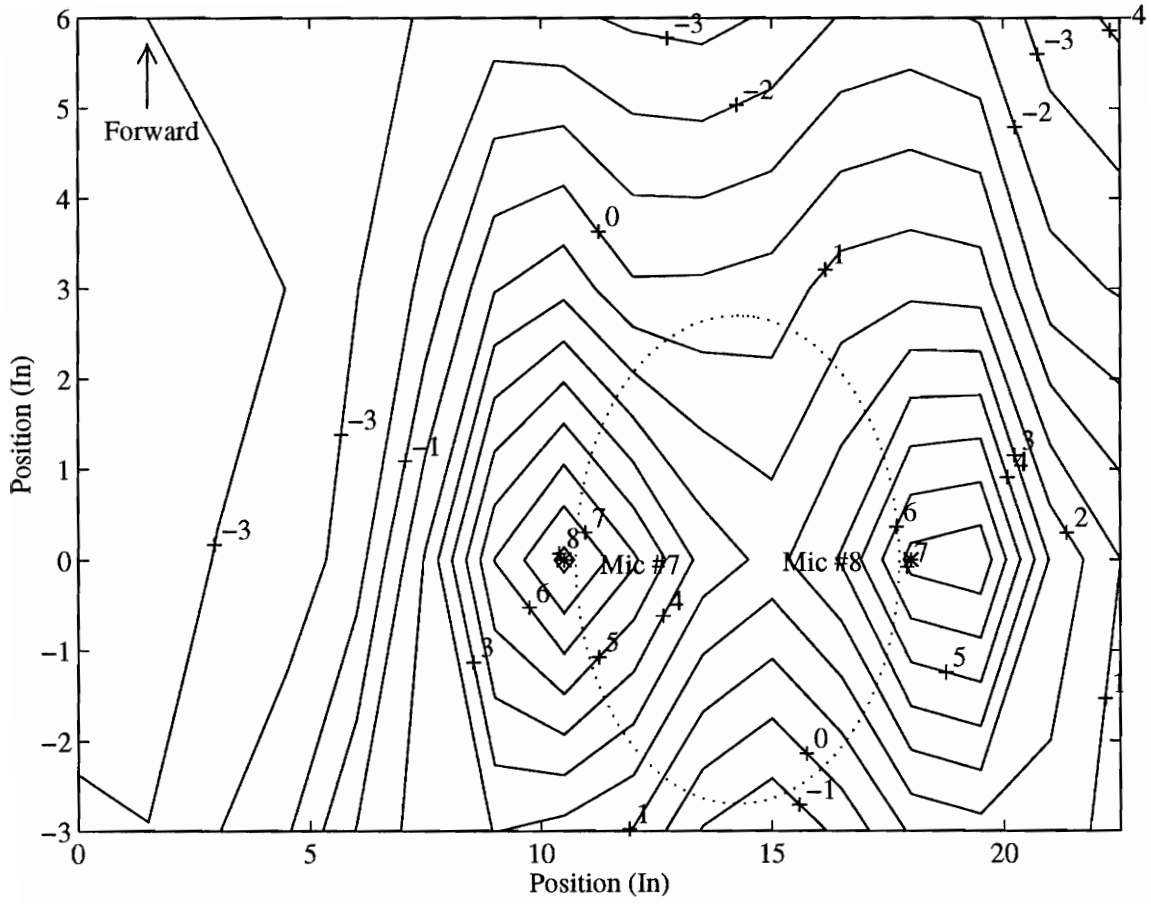

Figure 4-22, Contour Test #2, PZT Actuation, Internal Reference Signal

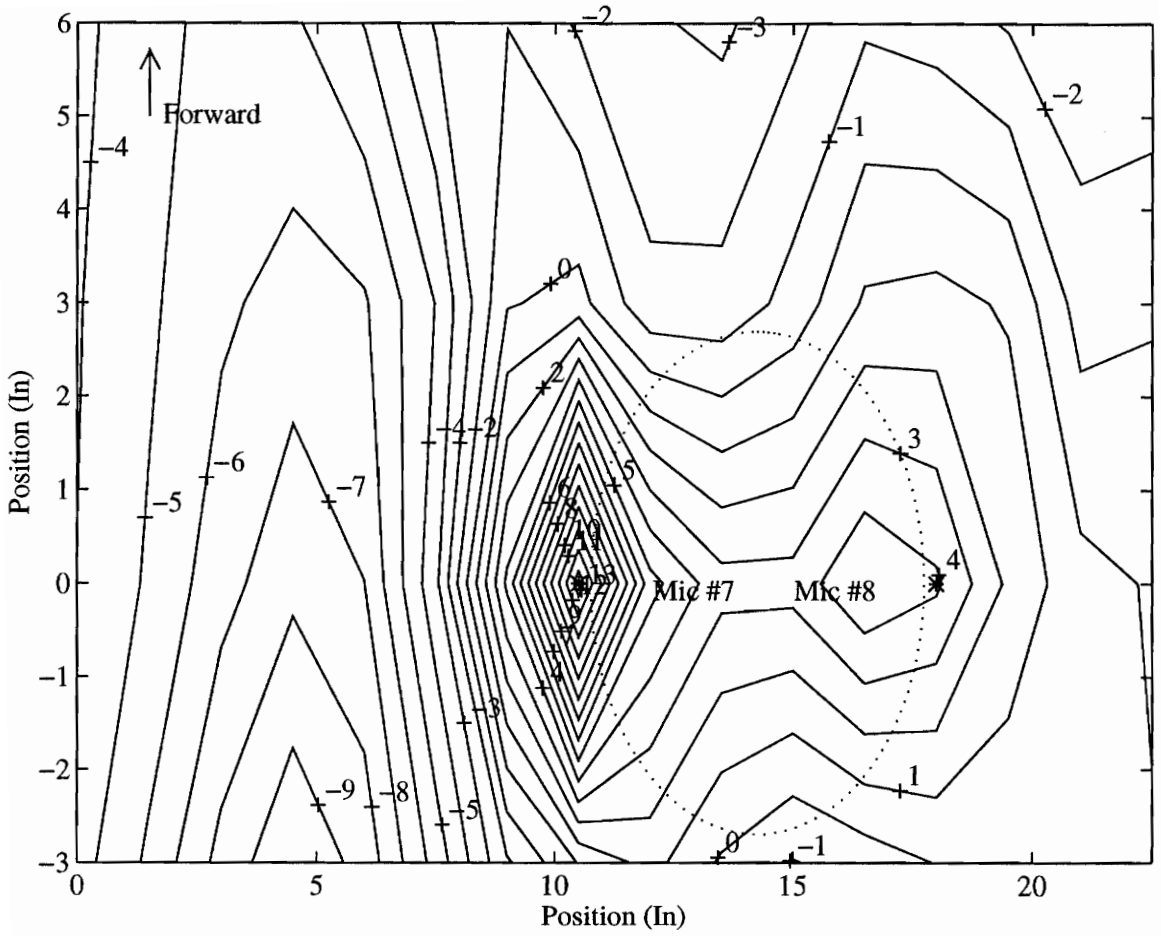

Figure 4-23, Contour Test #3, Speaker Actuation, Internal Reference Signal

4.6 Three Input-Three Output Broadband Tests

The final set of broadband tests were performed with 3I3O configurations. Due to the number of input and output channels, these tests were executed with only 152 FIR filter coefficients sampling at 3300 Hertz with an internal delayed reference signal. A multitude of different testing configurations were first attempted to understand the overall effectiveness of control. These are shown

Table 4-8.

The 3I3O results are disappointing. In most cases, the average levels of the global microphones increased more than the reduction levels of the error microphones. During tests, the controller often would not stabilize and the control outputs would drift. The control output levels kept growing, never reaching stability. It is believed that the PZT's output were fighting each other: some of the actuators output were being canceled by another so they both increase their voltage levels to overcome this in an infinite loop until control is either halted or until one of the PZT's burns out. This has the effect of raising the noise levels of the global microphones and creates low levels of control at the error sensors. Since the number of FIR filter coefficients per channel is down to 152 the controller FIR frequency resolution is hampered. This contributes to the PZT's fighting each other.

Table 4-8, Initial 3I3O Broadband Results

Test Number	Error Microphones	Actuators	Actual Error Microphone Reduction (dB)	Actual Global Microphone Reduction (dB)
1	3,7,8	3&15 out of Phase, 7&9 in Phase, Rest of PZT's	4.10	-6.69
2	7,8,14	3&15 out of Phase, 7&9 in Phase, Rest of PZT's	0.79	-8.14
3	2,7,11	3&15 out of Phase, 7&9 in Phase, Rest of PZT's	4.69	-5.11
4	2,6,8	3&15 out of Phase, 7&9 in Phase, Rest of PZT's	1.31	-8.74
5	2,7,8	3&15 out of Phase, 7&9 in Phase, Rest of PZT's	0.17	-9.16
6	3,7,8	2&9 in Phase, 3,8	2.93	-3.23
7	2,7,8	2&9 in Phase, 3,8	2.82	-0.55

To help improve 3I3O control performance, off-line optimizations were performed. For this two of the three error microphones were fixed at positions #7 and #8. The optimization routine then solved for the third error microphone and the three control channel PZT's that give the best power reduction at the error microphones when summed over the frequency range from 500-1000 Hertz. The results are shown in Table 4-9.

Table 4-9, 3I3O Broadband Optimizations

Test Number	Microphones	Actuators	Theoretical Error Microphone Reduction (dB)	Actual Error Microphone Reduction (dB)	Actual Global Microphone Reduction (dB)
1	7,8,9	9,10,12	25.05	4.27	-3.2
2	3,7,8	7,10,12	24.99	3.16	-3.93
3	3,7,8	2,11,12	24.98	4.85	-3.06

From the results it can be seen that the optimization slightly improved controller performance. The global microphone levels do not spill over as much as before. Nevertheless, the levels of global microphone spillover still almost equals the amount of attenuation at the error microphone. Because of the poor error microphone reductions and the high global microphone increase in noise levels with an internal delayed reference signal, experiments using the external reference accelerometer fared much worst and are not worth presenting here.

Altogether, the poor results of the 3I3O broadband tests show that the 3I3O controller configuration may be at the limits of the present DSP speed and technology, especially with this frequency range and complexity of the fuselage structure.

5. Discussion of Results

The goal of this thesis was to further develop active noise reduction technology toward the point where it can be applied to actual noise problems. The project objective was to develop a system which could minimize broadband flow noise inside an business jet resulting from flow separation over the crown of the aircraft. Overall the experiments show mixed results. Although it was initially hoped that an global reduction of noise could be achieved, this never occurred. The noise control strategy then shifted towards trying to create a localized zone of reduction at the pilot's head.

The single frequency experiments were a prelude to the broadband tests by providing a trail of control feasibility. While the tests themselves do not serve a practical purpose for controlling the broadband noise phenomenon, they do provide insight for such

issues as optimization algorithms, overall system dynamics, and maximum achievable controller performance.

The 6I3O single frequency tests show good control potential with reduction levels of 10-20 dB when averaged over the 6 error microphones, but with this control came an 3-5 dB increase of noise at the global microphones. Differing types of off-line optimizations were applied to these tests to improve controller performance. The PZT actuator grouping algorithm provided error microphone reductions of lesser levels (10-15 dB reductions) than the straight error microphone reduction optimization. However both had similar global microphone increases in noise levels of around 2-5 dB. The routines that optimize noise reductions at the global microphones showed overall global experimental reductions at the global microphones. Nonetheless when investigated more closely it is seen that reductions only occur at the loudest 2-4 (out of 9) global microphones.

The broadband adaptive feedforward tests provide noise reductions over a large frequency range, but this is very much a double edged sword. While the single frequency tests have no problem running at a 6I3O configuration with a sampling rate above 5000 Hertz, the broadband controller suffers severely with speed deficits. The 3I3O configuration is only able to run at a maximum sampling rate of 3300 Hz using only 152 FIR filter coefficients per channel. Having 152 coefficients is inadequate to properly

control the dynamics of the Cessna fuselage in the modally dense, wide 500-1000 Hz range. The parametric tests show that compared with 255 FIR filter coefficients, 152 coefficients gives only about half the attenuation performance. The parametric tests also show the importance of centering the impulse in the FIR filter coefficients "window" and they displayed the first signs of system acausality.

The SISO broadband tests show that when the multiple PZT actuators are wired together and run in parallel with an delayed internal tap on the signal generator, reductions of just over 20 dB are obtainable over the 500-1000 Hertz spectrum. Unfortunately, the same problem as the single frequency experiments of increasing noise at global microphones plagues the broadband controller. The global microphones typically increase in levels in the range of 1 to 5 dB for most all the tests.

When obtaining the control reference signal from the skin mounted accelerometer, performance again dropped dramatically showing only 3-5 dB of SISO reduction with a slight increase in noise levels at the global microphones. Tests show that causality is a major problem with the controller working with a time deficit of 31 milliseconds. This means that the accelerometer has to sense the signal on the skin of the aircraft, pre-amplify the signal, filter the signal, sample the signal with the A/D, process the signal with the controller and send out a control output signal through the D/A, filters, amplifier, PZT

transformers and out to the PZT's in the time that it takes the noise to propagate approximately 3 inches (76 mm) from the skin of the aircraft to the crown trim panel.

From the SISO broadband tests the next step was performing 2I2O broadband experiments. Again, none of the configurations provided any overall reductions at the global microphones. Their levels typically rose an average of 4-6 dB. The strategy then shifted towards trying to reduce noise levels localized at the pilot's left and right ears. Reduction levels of 10-17 dB at the left and right ears are obtainable with the internal signal generator tap. When the external reference accelerometer was used, levels of reductions at the error microphones of only 2 dB are obtained with an half a dB increase at the global microphones. Broadband off-line optimization routines that try to optimize the reductions at the pilot's left and right ears were also tried. However their results proved to be no more of an improvement over intuitive selections of the actuators due to inefficient off-line optimizations.

The 3I3O broadband tests results showed little attenuation. The lack of FIR filter coefficient and sampling resolution results in the actuator's fighting each other. This causes controller instabilities. This results in less control at the error microphones with an equal increases of spillover noise at the global microphones.

Examining the experimental results, the main problems preventing application of this technology into a aircraft is causality and controller speeds. The controller can not react quickly enough to produce the proper actuator output for a given accelerometer reference. Delays in the controller and filters are the major contributors to this.

However, there are some other important issues not yet discussed in this thesis. One of these issues is the durability of the actuators. While running control experiments at realistic SPL levels, 4 PZT's actuators burnt out during the experiments. Several others now show visible signs of wear but their output levels seem unaffected. For commercial application thicker, stronger PZT's with a higher breakdown voltage should be used so that the voltage levels the actuators need to receive do not eventually destroy them. Another consideration for in-flight applications is the coherency of the reference signals. With a aircraft, external flow noise at one location is not typically coherent with flow noise six inches (152 mm) away. Therefore the disturbance is spatially incoherent and it would be much more difficult obtaining a proper control reference than the single reference accelerometer on the skin of the aircraft used in these experiments.

6. Conclusions and Recommendations

Overall, the active trim panel system is not yet ready for in-flight applications. Laboratory reduction levels of 2 dB at the pilot's ears (with the external reference accelerometer 2I2O broadband tests) do not yet justify the costs of the system. In order to successfully apply this concept future work must be performed dealing with the issues of control speeds, causality, and incoherency of airflow as a disturbance. However, overall the concept shows promise; the trim panel mounted PZT actuators can produce noise at in-flight levels and the system would be light and compact enough for flight applications. The results also show, that if the causality problem is resolved, then good attenuation in the cockpit around the pilots' head are possible.

Although this project may have not succeed in fully developing a flight-ready workable active noise system for the aerospace industry it does contribute to overall ASAC knowledge for this problem. For the first time, ASAC was attempted in a real fuselage in the higher "mid" frequency range of 500-1000 Hz. This is well into the highly damped modally dense noise zone of the fuselage. The project is also one of the few applications of double panel systems, and is one of the few cases of multiple input/output broadband controllers. It also attempts to perform off-line optimizations and it draws a comparison of ASAC with traditional Active Noise Control.

An overall summary of the main conclusions obtained for these experiments follows:

1. Single frequency control of the flow disturbance using microphones as error sensors and trim panel mounted PZT's as actuators was demonstrated on a real aircraft fuselage. Control attenuation's of over 20 dB at the error sensors were obtained in an 6I3O controller configuration.
2. In a realistic setting with this control configuration, noise reductions of 2 dB can be developed at the pilot's left and right ear with a 2I2O broadband controller.
3. MIMO Broadband ASAC has been applied on a real structure to control mid-frequency noise with a large frequency bandwidth of 500 Hz for localized control.

4. Causality plays a primary role in diminishing controller performance when the reference signal is taken realistically from the skin of the aircraft.
5. The effects of varying the number of FIR filter coefficients and sampling speed was examined in parametric tests. It was proven to be very influential in overall system performance.
6. ASAC is proven measurably superior in controller performance than traditional ANC for this arrangement.
7. Noise levels generated by the active trim panel are comparable to typical in-flight cockpit levels.

However, no experimental investigation is truly complete and there is always further work to be performed. What follows is a recommended listing of future work that will further the development of the system:

1. In order to be able to better control the mid frequency range flow noise, more ASAC studies should be done on complex structures in disperse noise fields with modally dense highly damped systems.
2. There should be more work developing off-line actuator/sensor optimization routines, especially with broadband controllers and the inherent problems that they bring. This will help more effectively locate the actuators and error sensors

3. Faster DSP boards to support faster controllers are needed. The MIMO broadband experiments here are on the threshold of controller speed inadequacies within the 500-1000 frequency range.
4. Tests with an incoherent noise source better simulating realistic flow noise should be evaluated with the use of multiple reference sensors.
5. Possible control solutions and developments to remedy causality ill effects with adaptive feedforward control should be investigated. Such examples might be investigating faster DSP's, simpler filters, or using a reference signal from an external fuselage mounted microphone.
6. Tests with more actuator channels (requiring a faster DSP) should be performed to better control the mid-frequency noise and the complicated noise fields in order to not increase noise at the global microphones or achieve global reductions.

APPENDIX: Comparison of the Performance of Permanent and Removable PZT Actuators

All the control experiments presented in this thesis utilize PZT actuators mounted in a removable manner. The PZT's were mounted this way because the original PZT's positions were not fully optimized and future relocation may be required. Mounting PZT's in an removable fashion allows for possible removal of the actuators without destroying the expensive actuator itself. An initial investigation into removable PZT's has been performed by McCray[26].

Creating removable actuators is accomplished by mounting the PZT with adhesive to an aluminum shim which in turn is mounted to the trim panel surface with accelerometer wax (Figure A-1). The wax seal can be melted away if the PZT needs to be removed. This is in contrast to the traditional mounting approach where the PZT is fixed directly to the structure with adhesive and must be destroyed and chipped away for removal.

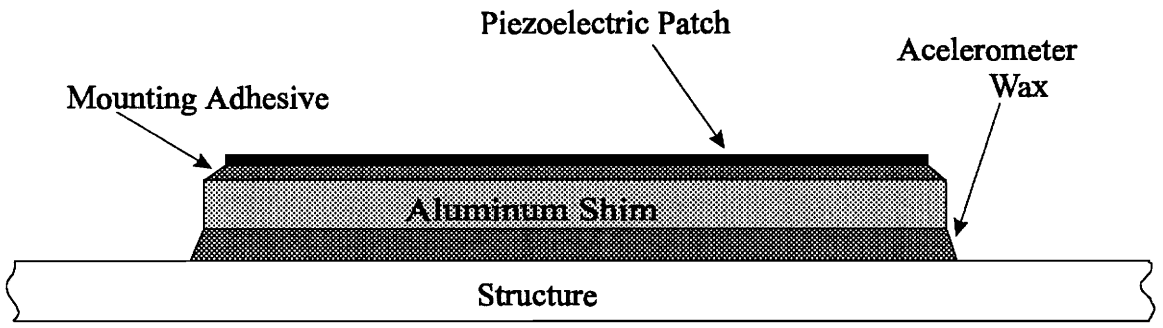

Figure A-1, Removable PZT Actuator

Since removable PZT's are unconventional, justification of their effectiveness is required. For this, three permanent PZT's (P8, P9, P12) were mounted besides three existing removable PZT's (#8, #9, #12). This is shown in Figure A-2. Six pairs of broadband control tests were performed comparing control cases with permanent and removable PZT actuation.

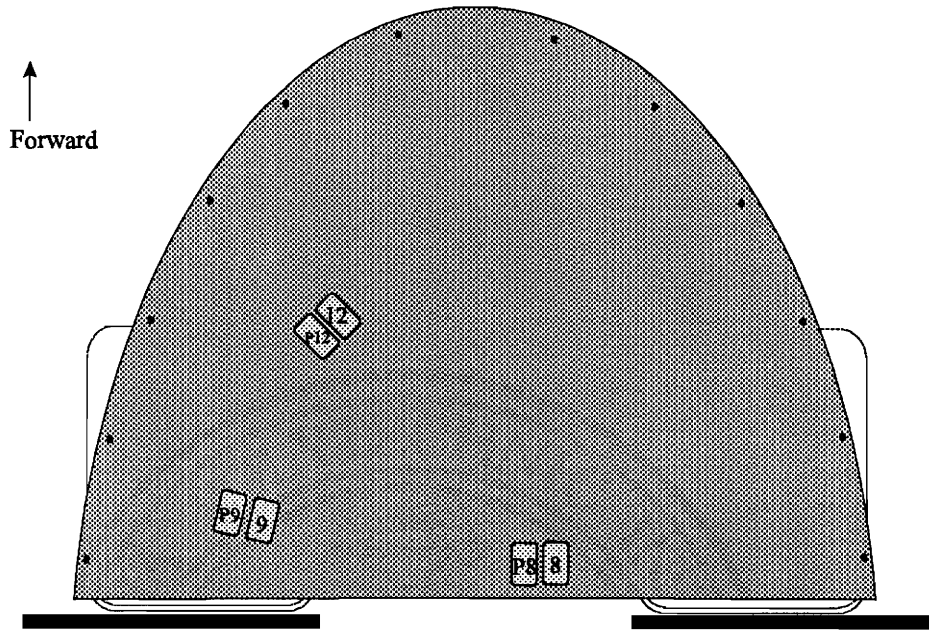

Figure A-2, Permanent and Removable Comparison PZT Locations

For comparison, three SISO and three 2I2O pairs of tests were performed. These tests were executed in the same fashion as previous SISO and 2I2O broadband experiments with a 20 sample delayed reference signal acquired from the signal generator. The SISO tests utilize microphone #7 as an error sensor with each PZT as an individual actuator. The 2I2O tests utilize error microphones #7 and #8 with three combinations of removable or permanent PZT's as actuator channels. The testing configurations and control attenuations are shown in Table A-1 and Table A-2.

Actuators:	Error Sensor Reduction With Permanent Actuators (dB)	Error Sensor Reduction With Removable Actuators (dB)
8 or P8	4.8	12.9
9 or P9	6.4	3.1
12 or P12	4.3	5.4

Table A-1, SISO Permanent Verses Removable PZT Control Comparison Tests

Actuators:	Error Sensor Reduction With Permanent Actuators (dB)	Error Sensor Reduction With Removable Actuators (dB)
8&9 or P8&P9	10.1	5.9
8&12 or P8&P12	5.1	8.2
9&12 or P9&P12	5.4	7.8

Table A-2, 2I2O Permanent Verses Removable PZT Control Comparison Tests

The results show large discrepancies between control cases. However, the error microphone noise reductions with permanently mounted actuators approximately equals the noise attentions obtained with removable actuators. Since equal noise reductions occur with either permanent or removable actuators, the use of removable PZT actuators is validated for this system.

However it should be noted that although the two types of actuators provide the same levels of control attenuation, the permanent actuators have a stronger acoustic output level than the removable PZT's. The use of removable PZT's in these experiments results in 3-5 dB loss in control authority. Despite this loss in authority, all experiments presented in this thesis were still performed at in-flight noise levels.

References

[1] P. Lueg, "Process of Silencing Sound Oscillations", U.S. Patent 2 043 416 1934.

[2] Olson, H.F. and May, E. G., "Electronic Sound Absorber", J. Acoust. Soc. Am., Nov 1953, 25, 1130-1136

[3] Conover, W.B., "Fighting Noise With Noise", Noise Control, 1956, pp. 78-92.

[4] Jessel, M., Mangiante, G., "Active Sound Absorbers in an Air Duct", Journal of Sound And Vibration, Vol.23, No. 3, pp. 383-390, 1972.

[5] Swinbanks, M.A., "The Active Control of Sound Propagation in Long Ducts", Journal of Sound and Vibration, Vol 27, No. 3, pp. 411-436, 1973.

[6] G.E. Warnaka, "Active attenuation of noise - The state of the art," Noise conrol Eng. 18(3) pp100-110, 1982.

[7] J.E. Ffowcs-Williams, "Anti-sound," Proc. R. Soc. London; Ser A 395, pp63-88, 1984

[8] C. Deffayet and P.A. Nelson, "Active control of low frequency harmonic sound radiated by a finite panel," J. Acoust. Soc. Am. 84(6), pp2192-2199, 1988.

[9] C.R. Fuller and R. J. Silcox, "Active Structural Acoustic Control," J. Acoust. Soc. Am. 91(1), p519, 1992.

[10] C.R. Fuller, "Apparatus and method for global noise reduction," U.S. Patent No. 4,715,599; 1987.

[11] C.R. Fuller "Active Control of Sound Transmission/Radiation From Elastic Plates By Vibration Inputs : I. Analysis," J. Acoust. Soc. Am. 136(1), pp1-15, 1990.

[12] V.L. Metcalf, C.R. Fuller, R.J. Silcox, D.E. Brown, "Active control of sound transmission/radiation from elastic plates by vibration inputs, II: experiments", J. Acoust. Soc. Am. 153(3), pp387-402, 1992.

[13] H.C.Lester and C.R. Fuller, "Active control of propeller induced noise fields inside a flexible cylinder," AIAA Paper 86-1957, 1986.

[14] C.H. Hansen, S.D. Snyder, and C.R. Fuller, "Reduction of noise radiated by a Vibrating Rectangular Panel by use of Active Sound Sources and Active Vibration Sources," Proceedings of the 1989 International Conference on Noise and Vibration, Singapore, pp E50-E57, August 1989.

[15] E.K. Dimetriadis, C.R. Fuller and C.A. Rogers, "Piezoelectric Actuators for Distributed Vibration Excitation of Thin Plates," J. of Vib. and Acoustics, Vol 113, Jan. 1991

[16] J.S. Vipperman, R.A. Burdisso, and C.R Fuller, "Active Control of Broadband Structural Vibration Using the LMS Adaptive Algorithm", J. Sound and Vibration. 166(2), pp283-299, 1993.

[17] J.P. Smith, "Active Control Of Broadband Acoustic Radiation From Structures," Masters Thesis, Virginia Tech, 1993

[18] H.C. Lester and C.R. Fuller, "Active Control of Propeller Induced Noise Filelds Inside a Flexible Cylinder," American Institute or Aeronautics and Astronautics Paper 86-1957, 1986.

[19] C.R. Fuller, J.P. Maillard, M. Mercadal and A.H. von Flotow, "Control of Aircraft Interior Noise Using Globally Detuned Vibration Absorbers",

[20] C.R. Fuller and J.D. Jones, "Experiments on Reduction of Propeller Induced Interior Noise by Active Control of Cylinder Vibration", Journal of Sound and Vibration, 112(2), pp389-395, 1987.

[21] C.R. Fuller and R.J. Silcox, "Active Control of Interior Noise in Model Aircraft Fuselages Using Piezoelectric Actuators", AIAA Paper 90-3922, 1990.

[22] R.J. Silcox, S Lefebvre, V.L. Metcalf, T.B. Beyer, and C.R. Fuller "Evaluation of Piezoceramic Actuators for Control of Aircraft Interior Noise", AIAA Paper 92-02-091, 1992.

[23] M.A. Simpson, T.M. Long, C.R. Fuller and J.D. Jones, "Full-Scale Demonstration Tests of Cabin Noise Reduction Using Active Vibration Control", AIAA Paper 89-1074, 1989.

[24] I.U. Borchers et al, "Advanced Study for Active Noiser Control in Aircraft", DGLR/ AIAA-92-02-092, 1992.

[25] J.P.Carneal and C.R. Fuller, "Active Structural Acoustic Control of Noise Transmission Through Double Panel Systems", AIAA paper 94-4421, 1993

[26] T.W.McCray, "Construction and Characterization of Removable and Reusable Piezoelectric Actuators", Masters of Science Thesis, Virginia Tech, 1994.

[27] B.J. Widrow and S.D. Stearns, *Adaptive Signal Processing*, Prentice-Hall, Englewood Clifts, New Jersey 07632, 1985.

[28] S. Haykin, *Adaptive Filter Theory*, 2nd ed., Prentice-Hall, Englewood Clifts, New Jersey 07632, 1991.

[29] S.J. Elliot, I.M Stothers and P.A. Nelson, "A Multiple error LMS algorithm and its aplication to the Active Control of Sound and Vibration", IEEE Transactions on Acoustics Speech and Signal Processing, ASSP-35, 1423-1434, 1987.

[30] R.L. Clark and C.R. Fuller, "Experiments on Active Control of Structurally Radiated Sound Using Multiple Piezoelectric Actuators," J. Acoust. Soc. Am.91(6), pp. 3313-3320, 1991.

[31] J.S. Vipperman, "Adaptive Feedforward Control of Broadband Structural Vibration", M.S. Thesis, Virginia Tech, 1992.

[32] J.S. Vipperman, R.A. Burdisso, and C.R. Fuller, "Active Control of Broadband Structural Vibration Using the LMS adaptive Algorithm", J. Sound Vib., 1991.

[33] J.P. Smith, "Active Control of Broadband Acoustic Radiation from Structures", M.S. Thesis, Virginia Tech, 1993.

[34] G.P. Gibbs, B. W. Mahnken and C.R. Fuller, "System Identification and Preliminary Active Control of the Interior Acoustic Field of a Cessna Citation III Fuesalage", Year One Anual Report, VAL Technical Report Number VAL-9401, August 1994

[35] J.P.Carneal and C.R. Fuller, "A Biologocally Inspired Controller for Sound and Vibration Applications", American Institute of Aeronautics and Astronautics, AIAA-94-1785, 1994.

[36] M.P. Waser and M.J. Crocker, "Introduction to the Two Mocrophone Cross-Spectral Method of Determining Sound Intensity", Noise Control Engineering Journal, May-June 1984.

[37] R.H. Cabell, G.C. Smith and C.R. Fuller, "Experimental Investigation of Actuator Grouping for Active Structural Acoustic Control", Proceedings of Active '95, Newport Beach, California, p347-358, July 1995

[38] J.S. Vipperman, "Adaptive Feedforward Control of Broadband Structural Vibration", M.S. Thesis, Virginia Tech, 1992.

[39] Julius S. Bendat and Allan G. Piersol, "Random Data, Analysis and Measurement Procedures", Second Edition, John Wileys & Sons, Inc., 1986.

Vita

The author was born on July 7th 1971 in Syracuse, New York. In 1986 he moved to Bloomfieled Hills, Michigan and completed high school there in 1989. That same year he began his undergraduate studies at Michigan Technological University in Houghton, Michigan and graduated with his Bachelors of Science in Mechanical Engineering in 1993. Later that year he began his graduate studies at Virginia Polytechnic Institute and State University in Blacksburg, Virginia in the Mechanical Engineering Master of Science Program. Upon completion of his Masters Degree he plans to begin work with General Motors in their Noise and Vibration Lab in Milford, Michigan.